Master's Thesis

UNIVERSITY *of the*
WESTERN CAPE

A study of the nearby interacting galaxy pair NGC 1512/1510

Xola Ndaliso

A dissertation submitted in partial fulfillment of the requirements
for the degree Magister Scientiae
in the

Faculty of Natural Sciences

Department of Physics and Astronomy,
University of the Western Cape

Supervisors:

Dr E. Elson, Dr. M. Glowacki, Prof. R. Maartens

September 1, 2020

http://etd.uwc.ac.za/

Declaration of Authorship

I, **Xola Ndaliso**, declare that this thesis titled, '**A study of the nearby interacting galaxy pair NGC 1512/1510**' and the work presented in it are my own. I confirm that:

- This work was done wholly or mainly while in candidature for a research degree at this University.
- Where any part of this thesis has previously been submitted for a degree or any other qualification at this University or any other institution, this has been clearly stated.
- Where I have consulted the published work of others, this is always clearly attributed.
- Where I have quoted from the work of others, the source is always given. With the exception of such quotations, this thesis is entirely my own work.
- I have acknowledged all main sources of help.
- Where the thesis is based on work done by myself jointly with others, I have made clear exactly what was done by others and what I have contributed myself.

UNIVERSITY of the
WESTERN CAPE

Signed:

Date:

http://etd.uwc.ac.za/

"Space isn't remote at all. It's only an hour's drive away, if your car could go straight upwards."

— Sir Fred Hoyle

http://etd.uwc.ac.za/

Acknowledgements

This thesis presents work that was carried out at the Department of Physics and Astronomy of the University of Western Cape between June 2019 and June 2020. This work was fully funded by the Square Kilometer Array (SKA) Masters Grant with additional funding from the Center for Radio Cosmology (CRC).

I would like to express my gratitude to my supervisor, Dr Ed Elson. I might not have been the best student to work with, but I really appreciate your patience. Thanks for the endless guidance you have given me, this project would've been horrific without your support. To my co-supervisors, Dr M. Glowacki thanks for teaching me useful tricks about data imaging and always willing to help. I appreciate you holding my hand through the 'write-up' route, I will always be thankful. *"I'll do it your style!"*. I would like to thank Prof. Roy Maartens for his substantial kindness and always willing to help. You have just been nothing but a FATHER away from home. To Dr Honjiswa Conana, thanks for being a mother away from home. To the Department of Physics and Astronomy, 'the HOME', I would like to thank everyone for making the environment so welcoming and conducive. Special thanks to Prof. Delia Marshall, Prof. Nico Orce, the HoD, and last but not least Dr. Mark Herbert.

To my parents and siblings, your prayers have brought me this far. Thanks for being patient and always wishing the best for me. May the good lord keep you, for there's better days coming. Special thanks goes to Sihle Thembeni, thanks for being a sister, thanks for always willing to listen in good and in bad times, I'm enormously beholden to have met you. *"It's a personal decision!"*. I'm deeply indebted to my very best friend Wanga Mbabe, bro thanks for keeping me sane throughout the period of this project. *"You've been real man!"*. To Siyambonga Matshawule, Siyanda Matika and Sibonelo Ngobese, brothers I'm never grateful enough for your guidance/mentorship, ndiyabulela boBhuti. To the boys, Xola, Kholekile and Avuzwa, thanks gents for the discussions we had from time to time about life in general and about the science. It's really been a pleasure having you by my side, it's the smallest things that matter a lot in this world. *"Nibe mnandi braz!"*

To my day one colleague, Junaid Townsend, I'm deeply grateful for the useful discussions, the jokes and laughter we always had. I won't say a lot but hopefully you know how I feel. *"Someone has to work!"* To my partner in research, Narusha Isaacs, I sincerely appreciate the coding sessions, science discussions and the bomb of jokes we always shared. Thanks for everything, I hope we can be again together in the future.

To my office mates, Brandon Engelbrecht, Eliab Malefahlo and many others in the office, I sincerely appreciate the discussions we had from time to time. I wish you all good progress in your research work.

http://etd.uwc.ac.za/

Contents

UNIVERSITY of the WESTERN CAPE

http://etd.uwc.ac.za/

UNIVERSITY of the
WESTERN CAPE

http://etd.uwc.ac.za/

List of Figures

UNIVERSITY of the WESTERN CAPE

http://etd.uwc.ac.za/

UNIVERSITY of the WESTERN CAPE

http://etd.uwc.ac.za/

http://etd.uwc.ac.za/

List of Tables

UNIVERSITY of the
WESTERN CAPE

http://etd.uwc.ac.za/

This Thesis is dedicated to my parents, No-Amen Ndaliso and Mntundini Ndaliso...

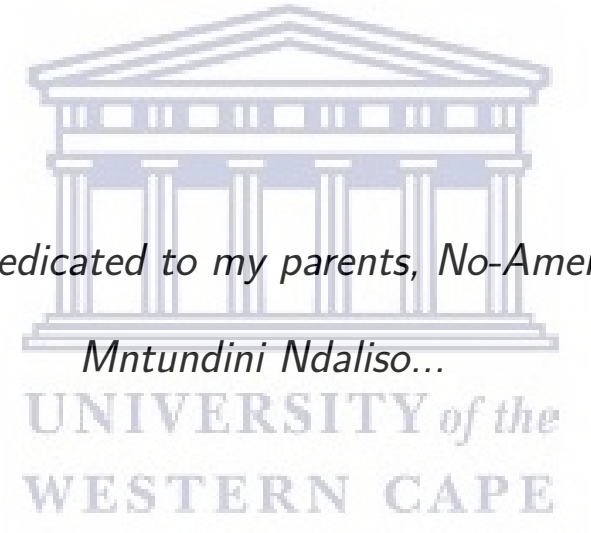

http://etd.uwc.ac.za/

Abstract

This work focuses on generating a new dynamical model of the nearby (9.5 Mpc) interacting galaxy system NGC 1512/1510. Neutral hydrogen (H I) observations from the Australia Telescope Compact Array (ATCA) are used to model the dynamics of the main H I disk using two routines, the two and three-dimensional modeling techniques. For the two-dimensional modeling technique, we adopt ROTCUR which is based on fitting a tilted ring model onto the 2D velocity field of the galaxy. The three-dimensional modeling routine used is ^{3D}Barolo, which is a recently developed algorithm of fitting 3D tilted ring model to the full data cube. We note that the 2D approach fails to model the inclination profile of NGC 1512. Thus, a new rotation curve is generated using the three-dimensional modeling routine only i.e. by fitting a 3D tilted ring model to the H I line data cube of NGC 1512/1510. This technique models the inclination profile of this galaxy system without incurring significant problems. This rotation curve compares favorably with existing results from the literature. To test the accuracy of our model we directly compare it to the H I line data cube. We note that the new model agrees well with the data. This proves that the three-dimensional modeling routine is not affected by any instrumental effects or processes linked to the ongoing interaction between NGC 1512 and NGC 1510. Furthermore, the modeled rotation curve of this galaxy is a fairly straight line, starting at r = 30″ to r = 480″, with the innermost rotation velocity of $V_{rot} \sim 140$ km s^{-1} and maximum rotation velocity of $V_{rot} \sim 159$ km s^{-1}. The new rotation curve is used to model the distribution of the mass in NGC 1512. However, due to its flat nature, a sensible fit is not achieved. Thus, we generate a new rotation curve that has inner points from the major-axis ($PA = 260^{\circ}$) position-velocity (PV) slice. We then parameterize this rotation curve with a polyex curve. This new rotation curve is used to model the distribution of mass in NGC 1512. To study the contribution of the stellar component in the observed rotation curve we used 3.4μm imaging of NGC 1512/1510 from the Wide-field Infrared Survey Explorer (WISE). To model the distribution of the dark matter halo mass we used both the observationally-motivated pseudo-isothermal sphere (ISO) and the theoretically-favored Navarro-Frenk and White (NFW) halo models. Both of these models were able to produce a good fit for the observed rotation curve of NGC 1512. A dynamical mass of $M_{dyn} = 9.43 \times 10^{10}$ $M_{\odot}$ is inferred for NGC 1512. Furthermore, the mass-model results show that the dark matter halo mass of NGC 1512 is dominant over the baryonic mass (i.e. $M_{halo}/M_{baryons} > 1$ for most modeled cases). The results of the mass-model of NGC 1512 were compared to literature results, the comparisons suggest that the fitted halo parameters of NGC 1512 are well within the range of the literature results.

UNIVERSITY of the WESTERN CAPE

http://etd.uwc.ac.za/

Chapter 1

Introduction

The space around us is occupied by the stunning objects called galaxies. As such, galaxies are known to be the building blocks of the universe. A galaxy is a collective combination of stars, gas, dust and cold dark matter, bound together by their self-gravity. These objects serve as good probes to gain insights about the universe on cosmological scales. However, even though galaxies provide such information, there is still a lot of unanswered questions such as the 'unknown' dark matter and the 'elusive' dark energy (Houjun Mo (2010)).

1.1 Dark matter in galaxies

The standard model of cosmology or the LCDM model of the universe (Scott, 2018; Hack, 2013) suggests that atomic matter and standard-model fundamental particles in the universe constitute only about $\sim 5\%$ of the total mass-energy density of the universe. LCDM stands for Lambda Cold Dark Matter, where Lambda represents the cosmological constant, which is the simple model of dark energy, i.e. dark energy as vacuum energy. In LCDM, $\sim 70\%$ of the total-mass energy density is contributed by dark energy. Dark energy has strongly negative effective pressure and therefore counteracts the decelerating effect of ordinary matter and cold dark matter - leading at late times to the accelerating expansion of the universe (Nielsen et al. (2016); Rezaei (2020)). The remaining quarter in the mass-energy budget of the universe is that of another mysterious type of matter, dark matter (Einasto (2009)). There is strong evidence from Cosmic Microwave Background (CMB) observations (Planck-Collaboration et al. (2018)) that dark matter is cold and non-baryonic. This evidence is further strengthened by the fact that galaxies could not form in the time available and in the numbers observed without a dominant cold dark matter component. Some studies have shown that dwarf galaxies are dominated by dark matter at all radii (Carignan & Beaulieu (1989); Côté et al. (2000)). This fact has prompted detailed studies of the dark matter distribution in these galaxies, in order to constrain galaxy evolution models.

Observational astronomers have resorted to defining this type of matter as any matter that is too 'dark' to be observed. More accurately, dark matter appears either to not interact at all, or only very weakly, with light, baryons, or itself. Instead, it appears to primarily interact through gravity. Studies have shown that galaxies are enveloped by dark matter, these envelopes have become to be known as the dark matter halos. However, this matter has not been observed.

http://etd.uwc.ac.za/

1.1.1 Observing dark matter

Various detector experiments, at the Large Hadron Collider (CERN), in deep mines or under water have so far failed to detect CDM particles. One of the leading ways to probe the existence of dark matter in galaxies is to indirectly infer its gravitational influence. This has been done successfully in the past using galaxy rotation curves (De Blok et al. (2008a); Oh et al. (2008)). Freeman (1970) came up with the idea that there has to be unobserved matter beyond the optical extent of NGC 300. This idea was controversial at first because previous studies of rotation curves based on optical spectroscopy showed that rotation curves of spiral galaxies could be well-fit without any dark matter component. However, it was later found that rotation curves generated from neutral hydrogen (H I), extending well beyond the stellar light, supported the existence of this mysterious matter (Freeman (1970)).

1.1.2 Rotation curves

A rotation curve is a representation of how the total mass at a given point from the center of the galaxy rotates. There are various ways in which rotation curves of galaxies are modeled. One traditional way of doing this is fitting the tilted ring model onto the two-dimensional velocity field of the galaxy (see Begeman (1989); Sofue & Rubin (2001); De Blok et al. (2008a)). The tilted-ring model was introduced by Rogstad et al. (1974) to possibly explain the H I disk of Messier 83 (M83). There are several software packages that have been developed to achieve this exercise: GIPSY task ROTCUR[1] (Begeman (1989)), rewsri[2] (Schoenmakers et al. (1997)), diskfit[3] (Spekkens & Sellwood (2007)), kinemetry[4] (Krajnović et al. (2006)). These are known as the 2D modelling approaches because they are based on the galaxy's velocity field, which is a 2D map that contains its kinematics information. To model the rotation curve, this work used the ROTCUR algorithm.

Even though several studies have applied these modeling routines successfully, they are still highly affected by effects such as beam smearing, non-circular motions of gas in the galactic plane, etc. Thus these effects lead to less accurate rotation curves of galaxies, which results in less realistic mass modeling. To account for such effects new three-dimensional tilted-ring model fitting algorithms have been developed. Instead of fitting the tilted-ring model to the velocity field of the galaxy, it is fitted to the 3D data cube. One good example of these is the newly developed ^{3D}Barolo algorithm (di Teodoro & Fraternali (2015)). This algorithm has been applied successfully to high and low-resolution data sets of galaxies (Fraternali et al. (2004); Di Teodoro et al. (2016)) and it has proven to work better than the 'traditional' 2D tilted-ring model algorithms.

Different types of galaxies have different shapes of rotation curves. Dwarf galaxies are known for their slowly rising rotation curves and that they are dominated by dark matter at all radii

[1] ROTCUR
[2] REWSRI
[3] DISKFIT
[4] KINEMETRY

UNIVERSITY of the WESTERN CAPE

http://etd.uwc.ac.za/

(Carignan & Beaulieu (1989); Côté et al. (2000)). For this reason, dwarf galaxies have been studied intensively to gain insights on the properties of dark matter. However, Swaters (1998) later found that late-type dwarf galaxies have similar rotation curves to those of spiral galaxies (i.e. steeper in the inner parts) and with dark matter dominance on the outer parts only.

Spiral galaxies on the other hand have rotation curves that rise steeply on the inner parts followed by a flat outer part (Rubin (1983)). Rotation curves of spiral galaxies serve as an important laboratory to investigate how the mass is distributed in these objects (Sofue & Rubin (2001)). Previous studies to determine the rotation curves of spiral galaxies have proved the existence of dark matter (Bosma (1981); Sofue et al. (a); Sofue & Rubin (2001); Carignan & Freeman (1987)). In the Newtonian paradigm of gravity, this is explained by a considerable amount of mass that cannot be observed (Freeman (1970)). Figure 1.1 below presents a generic example of an H I rotation curve of the spiral galaxy NGC 3198 taken from the work done by Begeman (1989). This Figure shows that an extra component besides the stellar and gas component is indeed needed to account for the flat part of the observed rotation curve of this spiral galaxy.

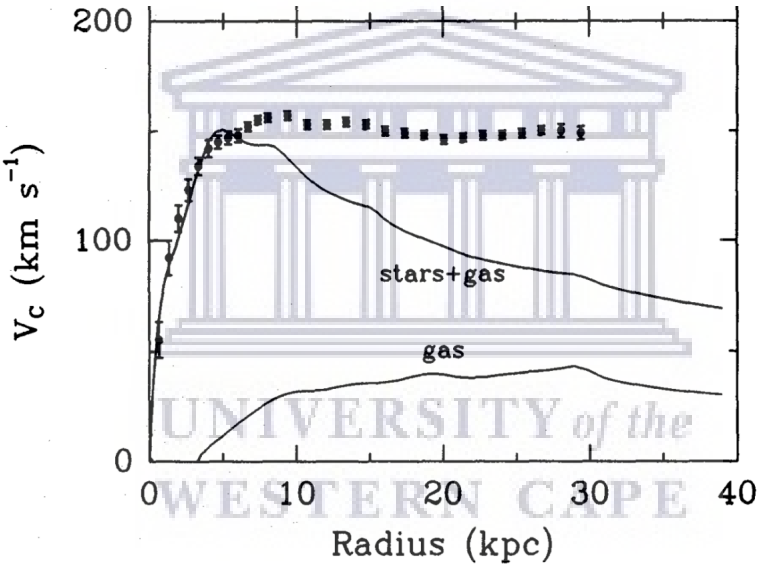

Figure 1.1: H I rotation curve of the spiral galaxy NGC 3198 (Begeman (1989)). Black rectangles show the observed rotation curve of the galaxy. This is a good example to show that the total mass of the galaxy is not only made up of stars and gas only but also of dark matter.

UNIVERSITY of the WESTERN CAPE

http://etd.uwc.ac.za/

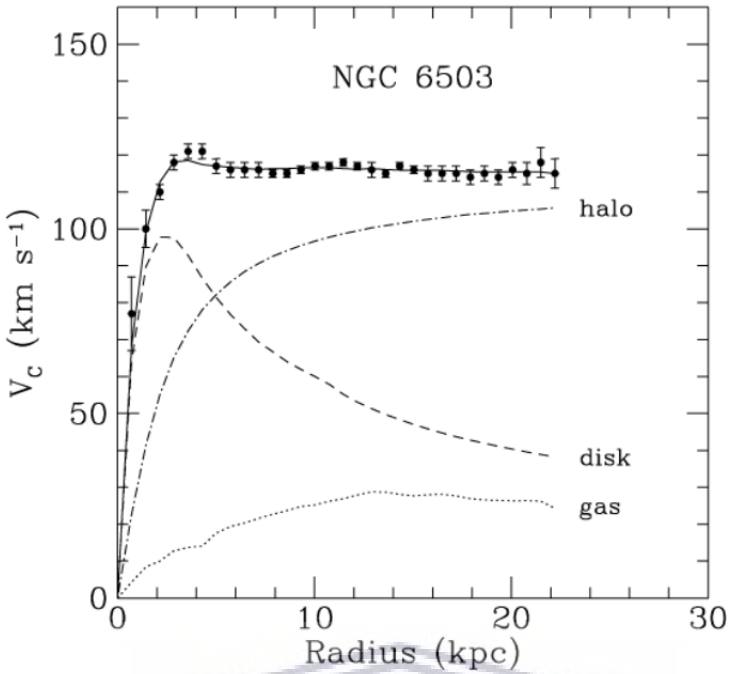

Figure 1.2: Rotation curve of NGC 6503. Black rectangles show the observed rotation curve of the galaxy.

Studies have also shown that when the dark matter is included, then the total rotation curve matches fairly well with the observed rotation curve. Figure 1.2 is another example of a rotation curve that highlights this (Rubin et al. (1980)). In this Figure, the 'halo' component presents the dark matter halo distribution.

The contribution of the halo in galaxies is modeled by dark matter halo models. In this work we will focus on two dark matter halo models, the pseudo-isothermal sphere distribution (hereafter `ISO`) and the Navarro-Frenk and White dark matter halo model (hereafter `NFW`) (Navarro et al. (1996)). Several studies have been conducted to investigate which dark matter halo model is more dominant in galaxies (De Blok et al. (2008a)); Swaters et al. (2011); Oh et al. (2015); Korsaga et al. (2019)). Observational studies have shown to strongly support the `ISO` halo model, whilst theoretical studies suggest the `NFW` halo model.

1.1.3 Dark matter distributions

Observational evidence shows that the mass-density distribution of the dark matter halos is well modeled by a constant density inner core (Broeils (1992), De Blok et al. (1996), Begeman (1989)). The `ISO` dark matter halo model seem to be well described by the observations. The core-density is often given as:

$$\rho(r) \sim r^{\alpha}, \tag{1.1}$$

where $\alpha \approx 0$. However, theoretical predictions suggested otherwise. In the theoretical framework, numerical simulations are used to model the distribution of dark matter in galaxies (Navarro et al. (1996), Springel et al. (2008)). This is done by generating mock halos of cold dark matter in galaxies by using high-resolution N-Body simulations. These predictions suggested that the equilibrium density of the halo varies with the radius as:

http://etd.uwc.ac.za/

$$\rho(r) \propto r^{\alpha}, \tag{1.2}$$

with $\alpha \approx$ -1 (Navarro et al. (1997)).

This notable discrepancy between observations and cold dark matter simulations on the distribution of the dark matter density at inner parts was reported first, by Navarro et al. (1997), who realized a steep rise in the density profile with an increase in radius. Similar deviations were found by Efstathiou et al. (1990), in their simulations of free-scale hierarchical clustering. They also reported that this discrepancy was more pronounced in the well-resolved simulated halos. Similarly, Dubinski & Carlberg (1991) were plagued by the same problem.

This is known as the 'famous' cusp-core problem in the field of extra-galactic astronomy. It remains one of the unsolved questions in small-scale ΛCDM cosmology (Oh et al. (2008)). These terms. i.e. cusp and core were invented following the behavior of the density profiles produced from these two dark matter halo models. The NFW dark matter halo model is called cusp-dominated due to the increase in the density profile towards the center (Navarro et al. (1996)). On the other hand, observations were seen to favor a constant central density core, hence ISO came to be referred to as a core-dominated dark matter halo (Oh et al. (2008), De Blok et al. (1996)).

Researchers have largely used these two dark matter models to probe the distribution of dark matter in galaxies (De Blok et al. (2008a); Swaters et al. (2011); Oh et al. (2015); Korsaga et al. (2019)). Swaters et al. (2011) used the ISO halo model to study the distribution of the dark matter in 18 late-type dwarf galaxies. These galaxies were observed as part of the Westerbork H I Survey of Spiral and Irregular Galaxies (WHISP). In using the ISO dark matter halo model they, found that most of the galaxies with more extended observed rotation curves have dark matter rotation profiles that show a solid body appearance. They claim that this showcases dark matter halos with constant density cores.

UNIVERSITY of the WESTERN CAPE

Oh et al. (2015) studied the mass distribution in 26 dwarf galaxies. These galaxies form part of Local Irregulars That Trace Luminosity Extremes, The H I Nearby Galaxy Survey (LITTLE THINGS). The rotation curves of the dark matter halo for all of these galaxies were compared with those of the dwarf galaxies from The H I Nearby Galaxy Survey (THINGS) (see De Blok et al. (2008a)) and ΛCDM Smoothed Particle Hydrodynamic Simulations (SPH) (Hayashi et al. (2007)) with baryonic feedback. Most of the LITTLE THINGS galaxies used in this study showed rotation curves that are consistent with dwarf galaxies from THINGS and SPH simulations. These rotation curves show a uniform increase in the inner regions, making the dark matter density profiles of these galaxies to have shallower logarithmic inner slopes.

1.2 NGC 1512/1510

NGC 1512 is a barred, double ring spiral galaxy which is interacting with the blue compact dwarf (BCD) galaxy NGC 1510, making a system called NGC 1512/1510 (Hawarden T. G. (1979)). This minor merger is estimated to have started about ~ 400 Myr ago (Koribalski & López-Sánchez (2009)). According to the Hubble's classification scheme, NGC 1512 is classified as an SBab galaxy, making it an intermediate-type spiral galaxy. Koribalski &

http://etd.uwc.ac.za/

López-Sánchez (2009) claims that the H I disc of NGC 1512 is much more extended than the optical diameter by a factor of ~ 4 (see Figure 1.5).

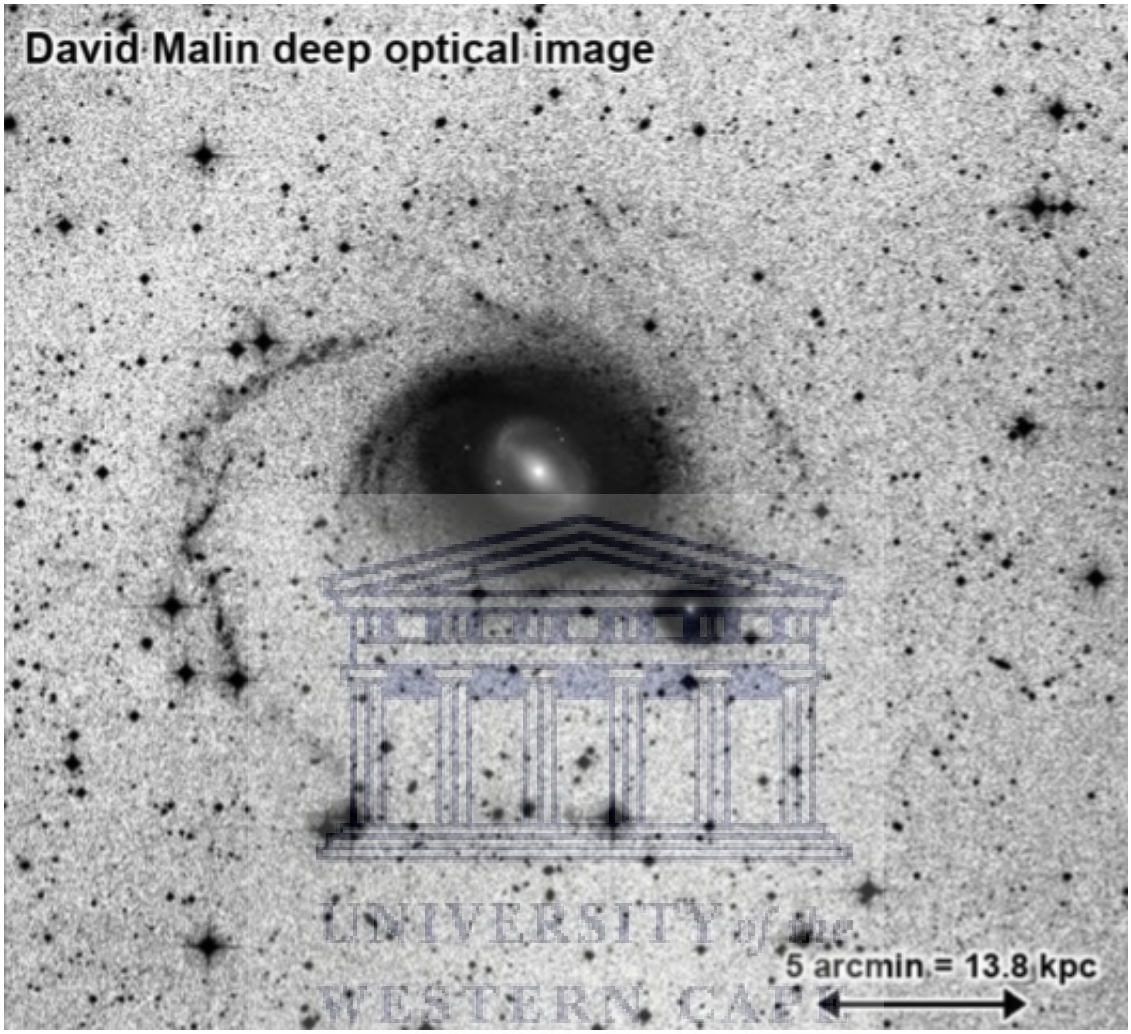

Figure 1.3: The deep optical image of NGC 1512 taken from Koribalski & López-Sánchez (2009). This image was obtained by David Malin from combined UK Schmidt Telescope plates. To emphasize the faintest stellar structure of the system this image was saturated. A non-saturated R-band image of the pair, obtained as part of the SINGS project, is overlaid onto the central region.

This galaxy (i.e. NGC 1512) has been observed and studied in multiple wavelengths. Buta (1988) generated the first rotation curve of NGC 1512 using ionized hydrogen (Hα) data, Koribalski & López-Sánchez (2009) used H I data observed with the Australia Telescope Compact Array (ATCA) to regenerate the rotation curve of this galaxy and also studied its star-formation properties. Hawarden T. G. (1979) conducted a study of the optical and H I properties of NGC 1512/1510 and López-Sánchez et al. (2015) studied the ultra-violet (UV) properties of this system. The far-ultraviolet image of NGC 1512/1512 is presented in Figure 1.4 below.

http://etd.uwc.ac.za/

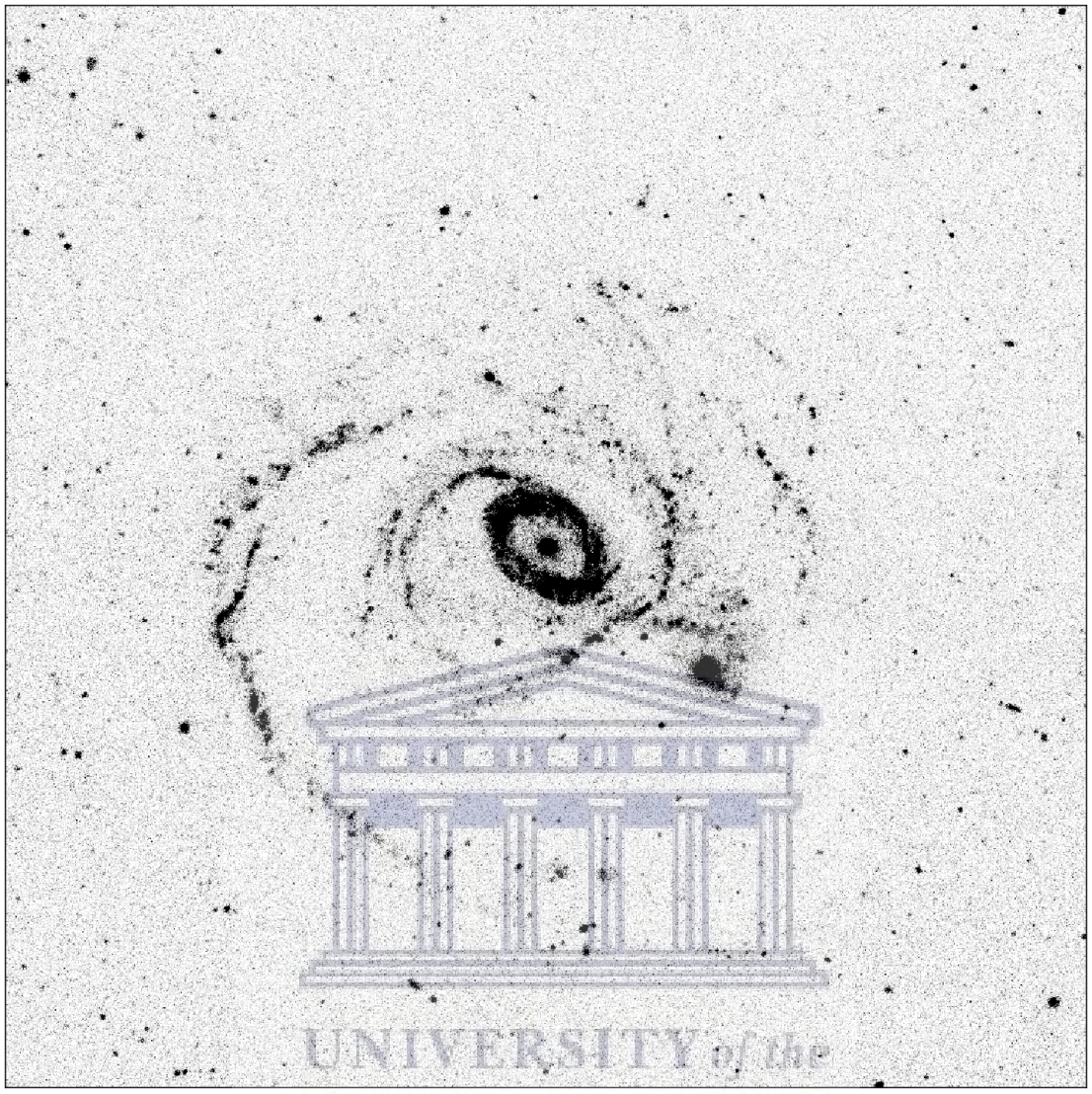

UNIVERSITY of the
WESTERN CAPE

Figure 1.4: The far-ultraviolet image of NGC 1512/1510.

Even though Buta (1988) and Koribalski & López-Sánchez (2009) generated the rotation curves of NGC 1512, the mass model of this galaxy has not been done. This work aims at filling this gap i.e. generating a new accurate dynamical model and studying the dark matter distribution of this galaxy.

In the study of Buta (1988), ionized hydrogen (Hα) observations from the McDonald Observatory Mark II Fabry-Perot interferometer together with observations from the TAURUS Fabry-Perot interferometer of the Anglo-Australian Observatory were used. This study only modeled the rotation curve of the inner ring (i.e. out to $\sim 100''$) of NGC 1512. The rotation curve of Buta (1988) was generated from the position-velocity slice of the galaxy following the iterative procedure discussed in Warner et al. (1973). In this work an inclination angle of $i = 35^{\circ}$ was used, however, they claim that a reliable inclination angle of NGC 1512 could not be achieved. The maximum rotation velocity achieved from this work is ~ 210 km s^{-1}.

Koribalski & López-Sánchez (2009) studied the gas dynamics and the star formation rate of NGC 1512 using neutral hydrogen (H I) observations from the Australia Telescope Compact

http://etd.uwc.ac.za/

Array (ATCA). ATCA is a radio interferometer of 6 dishes, each with a 22-meter diameter. The main focus of their work was to model the kinematics of the gas component of NGC 1512. H I data were used because it is a good tracer of the kinematics of the gas component in galaxies (Sofue et al. (b), De Blok et al. (2008a)). This is often due to its extended radial extent as compared to ionised hydrogen (Hα), which is often patchy (De Blok et al. (2008b)). To generate the rotation curve of NGC 1512, Koribalski & López-Sánchez (2009) fitted a tilted-ring model onto the velocity field of this galaxy using ROTCUR.

The final H I rotation curve produced by Koribalski & López-Sánchez (2009) shows that the inner disk of NGC 1512 has regular rotation velocities. However, there are notable deviations along the outer arms and close to the position of NGC 1510. Koribalski & López-Sánchez (2009) modeled the rotation curve of NGC 1512 out to r $\sim$ 1200″. The resulting rotation curve of NGC 1512 rises slowly to a maximum rotational velocity of $\sim$ 225 km s^{-1} at r $\sim$ 300 ″. Beyond this point there is a drastic decline to a rotational velocity of $\sim$ 110 km s^{-1} till the last measured point. Koribalski & López-Sánchez (2009) claims that the inclination angle of NGC 1512 increases from i = 30° to 50°, however, a fixed inclination of 35° (same as Buta (1988)) was used to generate the final rotation curve of NGC 1512. Table 1.1 provides basic properties of NGC 1512.

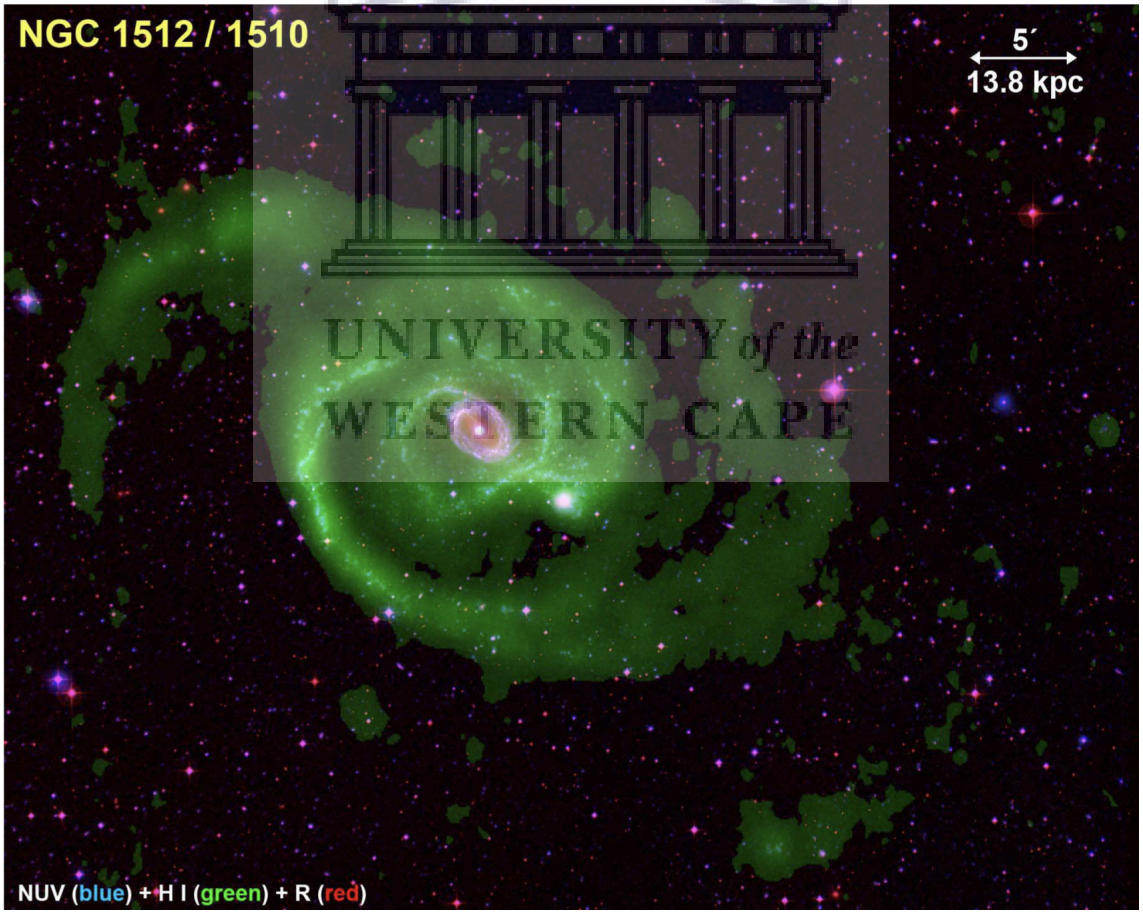

Figure 1.5: A multi-wavelength color-composite image of the galaxy pair NGC 1512/1510 obtained using the DSS R-band image (red), the ATCA H I distribution (green) and the GALEX NUV - band image (blue). The Spitzer 24 μm image was overlaid just in the center of the two galaxies. This images was taken from Koribalski & López-Sánchez (2009).

UNIVERSITY of the WESTERN CAPE

http://etd.uwc.ac.za/

Table 1.1: Basic properties of NGC 1512.

	NGC 1512	Ref
α(J2000)	-43° 21′ 03″	(1)
δ(J2000)	-43° 24′ 01″	(1)
Distance [Mpc]	9.5	(2)
$V_{H\,I}$ [km s^{-1}]	898	(3)
Position angle	260°	(3)
Inclination	50°	(3)
$M_{H\,I}$ [10^9 $M_\odot$]	4.72	(3)
$F_{H\,I}$ [Jy km s^{-1}]	221.6	(3)
W_{20} [km s^{-1}]	264	(3)
W_{50} [km s^{-1}]	224	(3)

UNIVERSITY of the WESTERN CAPE

Refs: (1) de Vaucouleurs et al. (1991), (2) Koribalski & López-Sánchez (2009), (3) This thesis

1.3 This thesis

In this thesis we study a system of nearby interacting spiral NGC 1512/1510 at a distance of D = 9.5 Mpc (Koribalski & López-Sánchez (2009)), in an attempt to understand galaxy evolution, and extend the work of Koribalski & López-Sánchez (2009). We use neutral hydrogen (H I) to probe the dynamics of the system and thus to infer the gravitational influence of dark matter in the system.

To model the dynamics of NGC 1512 this work uses both the 2D dynamical modeling technique (i.e. ROTCUR, Begeman, 1989) and the 3D approach (i.e. ^{3D} Barolo, di Teodoro & Fraternali, 2015) of fitting tilted-ring models to H I line observations. Using this new approach, i.e. the 3D modeling routine, a new rotation curve is generated. This new dynamical model is rigorously compared to data to test the accuracy of the modeling routine. The new dynamical model matches the data well. However, the new rotation curve is fairly flat at all radii. This poses some difficulty in modeling the dark matter distribution of NGC 1512. This was accounted

http://etd.uwc.ac.za/

for by regenerating a new rotation curve from the major-axis PV slice. To account for the contribution of the stellar component to the total rotation curve, 3.4 μm infrared imaging from WISE was used.

1.3.1 Thesis outline

Chapter 2 gives insights into the nature of the data. It also presents all the high-quality H I data products generated and the methods used in deriving these.

Chapter 3 gives a detailed description of the dynamical procedures followed to model the dynamics of NGC 1512/1510. A new dynamical model of NGC 1512/1510 is presented. A set of position-velocity diagrams at different angles is also presented, showing how well the data matches the current model.

Chapter 4 discusses in detail the approach used to model the dark matter distribution of NGC 1512. Mass-models are presented here as well.

Chapter 5 presents a summary of the results obtained in this work as well as future prospects.

UNIVERSITY of the
WESTERN CAPE

http://etd.uwc.ac.za/

Chapter 2

H I data of NGC 1512/1510

This work presents H I spectral line observations and data products of the nearby interacting galaxy system NGC 1512/1510. We then adopt a method of parameterizing the H I data cube of this system. We show how this method improves the signal-to-noise and in turn provides a more accurate representation of the H I kinematics of the galaxy system.

We use the H I spectral line observations of the interacting galaxy pair NGC 1512/1510 which was observed as part of the Local Volume H I Survey (LVHIS) using the Australia Telescope Compact Array (ATCA) Koribalski & López-Sánchez (2009).

The details of each observation are summarised in Table 2.1. The ten observations were undertaken in different telescope configurations between September 1996 and November 2005. Four overlapping pointings were also used (Koribalski & López-Sánchez (2009)). During the observations of this interacting galaxy system, multiple configurations of the ATCA array were used (Koribalski & López-Sánchez (2009)). The different amounts of the observing times were spent on different configurations to achieve better spatial and spectral resolutions. An excellent *uv*- coverage was achieved by combining the data from different telescope configurations. The range of baselines during the time of observations is from 30 m to 6 km.

UNIVERSITY of the WESTERN CAPE

http://etd.uwc.ac.za/

Table 2.1: ATCA radio observations of NGC 1512/1510.

1 Config.	2 Date (yyyy-mm-dd)	3 Time (hrs)	4 Primary Calibrator	5 Flux (Jy)	6 Phase Calibrator	7 Flux (Jy)	8 Bandwidth (MHz)
H168	2005-11-05	7.5	1934-638	14.95	0438-436	4.55	8
210	2000-07-06	5.3	1934-638	14.95	0438-436	4.55	8
	2000-07-08	5.1	1934-638	14.95	0438-436	4.55	8
375	1996-09-23	8.3	1934-638	14.95	0438-436	4.55	8
	1996-09-24	8.4	1934-638	14.95	0438-436	4.55	8
	1996-12-3	5.1	1934-638	14.96	0438-436	4.55	8
750A	1996-11-6	10.9	1934-638	14.95	0438-436	4.55	8
1.5A	1996-10-20	10.1	1934-638	14.95	0438-436	4.55	8
6A	1997-02-05	4.7	1934-638	14.95	0438-436	4.55	8
6B	1996-09-14	10.5	1934-638	14.95	0438-436	4.55	8

Column Notes. Columns 1: Configuration used; Column 2: date of the observation; Column 3: time spent on source; Column 4/5: name of primary calibrator and its flux-density; Column 6/7: name of phase calibrator and its flux density; Column 8: bandwidth

UNIVERSITY of the WESTERN CAPE

Following the observations of NGC 1512/1510, this dataset was reduced and imaged by Koribalski & López-Sánchez (2009). Upon request a robust (r = 0, where *r* is called the robust sub-parameter) weighted cube in `fits` format was received. The value of this parameter i.e. *r* ranges from -2.0 (which is close to uniform weighting which boosts the resolution) to +2.0 (which is close to natural weighting which boosts the sensitivity), thus robust-weighting is the weighting of the data visibilities which creates a point-spread function (PSF) that changes between uniform and natural weighting making it to have both good sensitivity and resolution. Thus, robust weighting of the data boosts the sensitivity to even faint emission i.e. diffuse emission. The spatial resolution of this data cube is 62.11″. Table 2.2 below summarizes the main properties of the ATCA data cube. The H I data cube was used to produce a new set of H I maps that are used in this work. These maps were generated by parameterizing the H I line profiles of the ATCA data cube. Discussions on how each of these maps were generated is detailed below in subsection 2.1.4 for the H I surface density map and subsection 2.1.5 for the H I velocity field.

http://etd.uwc.ac.za/

Table 2.2: Characteristics of the ATCA data cube of NGC 1512/1510.

1	2	3	4	5	6	7
B_{maj}	B_{min}	BPA	noise	size	pixel	width
//	//	○	mJy beam^{-1}	pixels	//	km s^{-1}
62.11	55.31	10.15	2.13	778 × 779	5	4

Column Notes. Columns 1 and 2: Major and minor axis of the synthesized beam in arcseconds; Column 3: Beam position angle in degrees; Column 4: rms noise per channel map in mJy beam^{-1}; Column 5: image size in pixels; Column 6: pixel scale in arcseconds; Column 7: channel width in km s^{-1}

http://etd.uwc.ac.za/

2.1 H I data products

This section presents the H I data products of the interacting galaxy pair NGC 1512/1510 produced from the ATCA data cube as well as how these maps were generated.

2.1.1 Channel maps

Figure 2.1 presents individual channel maps of the interacting galaxy pair NGC 1512/1510 based on the ATCA data cube.

http://etd.uwc.ac.za/

Figure 2.1: H I channel maps of NGC 1512/1510 based on the robust-weighted ATCA data cube (greyscale range: –0.02σ to 10σ, where σ = 2.13 Jy/beam). Each channel spans a velocity width of 4 km/s, and the velocity of each channel is shown in the upper right corner of each panel. H I flux density contours are shown in black at levels of $\sigma 2^n$, where n = 1, 2, 3,....8. The synthesized beam of size 62″.11 × 55″.31 is shown in black at the bottom left of each panel.

UNIVERSITY of the WESTERN CAPE

http://etd.uwc.ac.za/

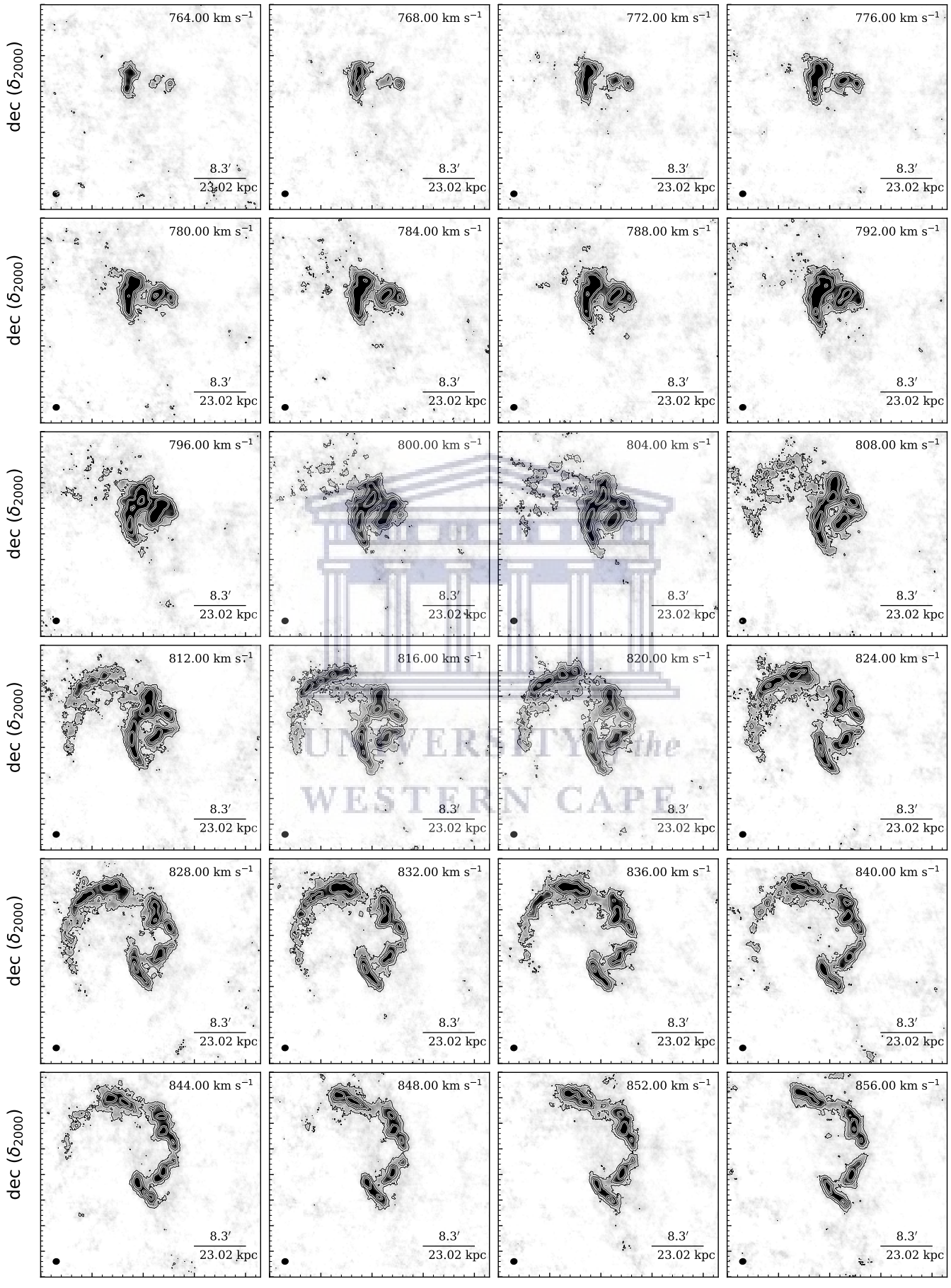

UNIVERSITY of the WESTERN CAPE

http://etd.uwc.ac.za/

Figure 2.1: Continued

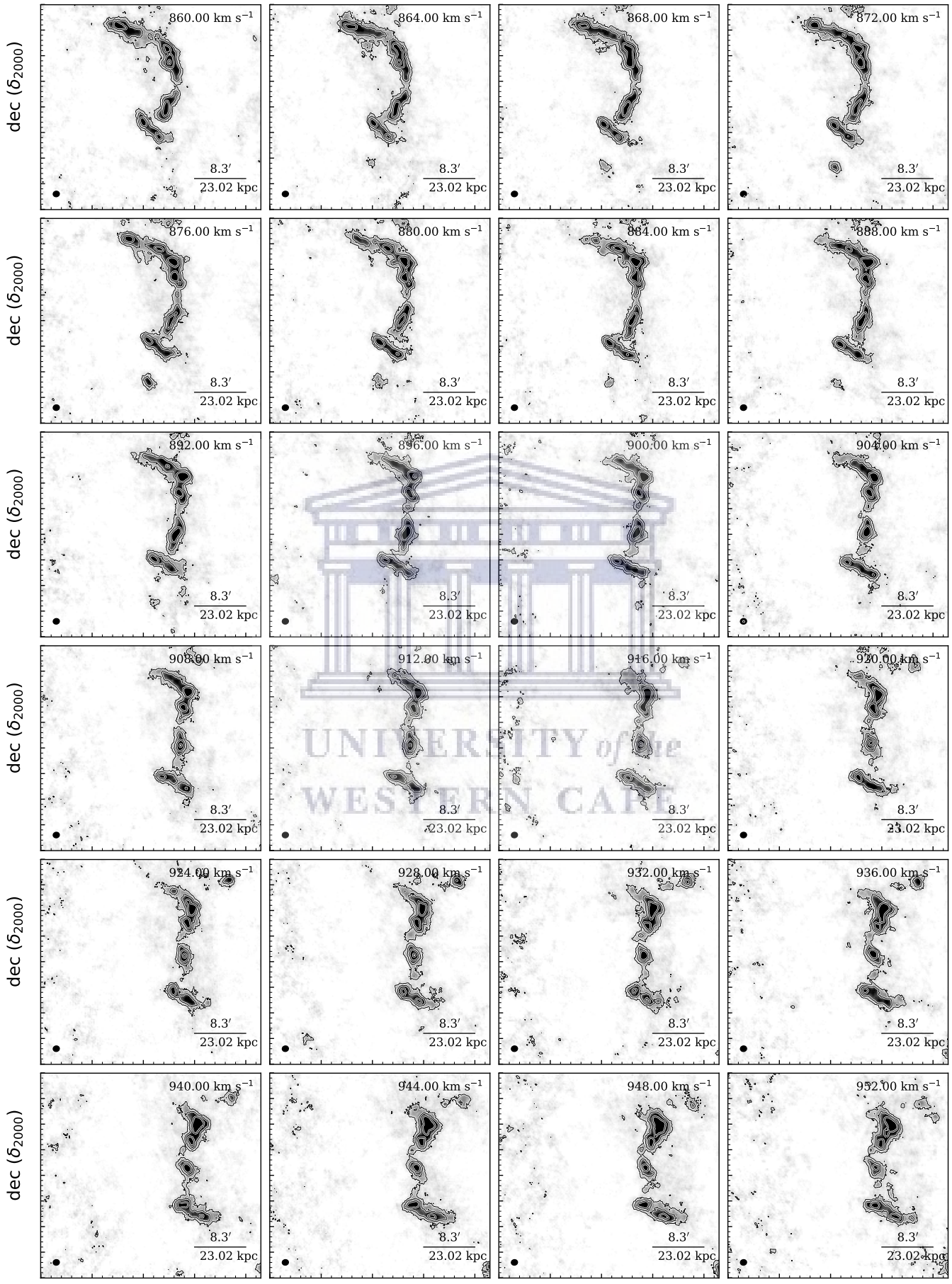

UNIVERSITY of the WESTERN CAPE

http://etd.uwc.ac.za/

Figure 2.1: Continued

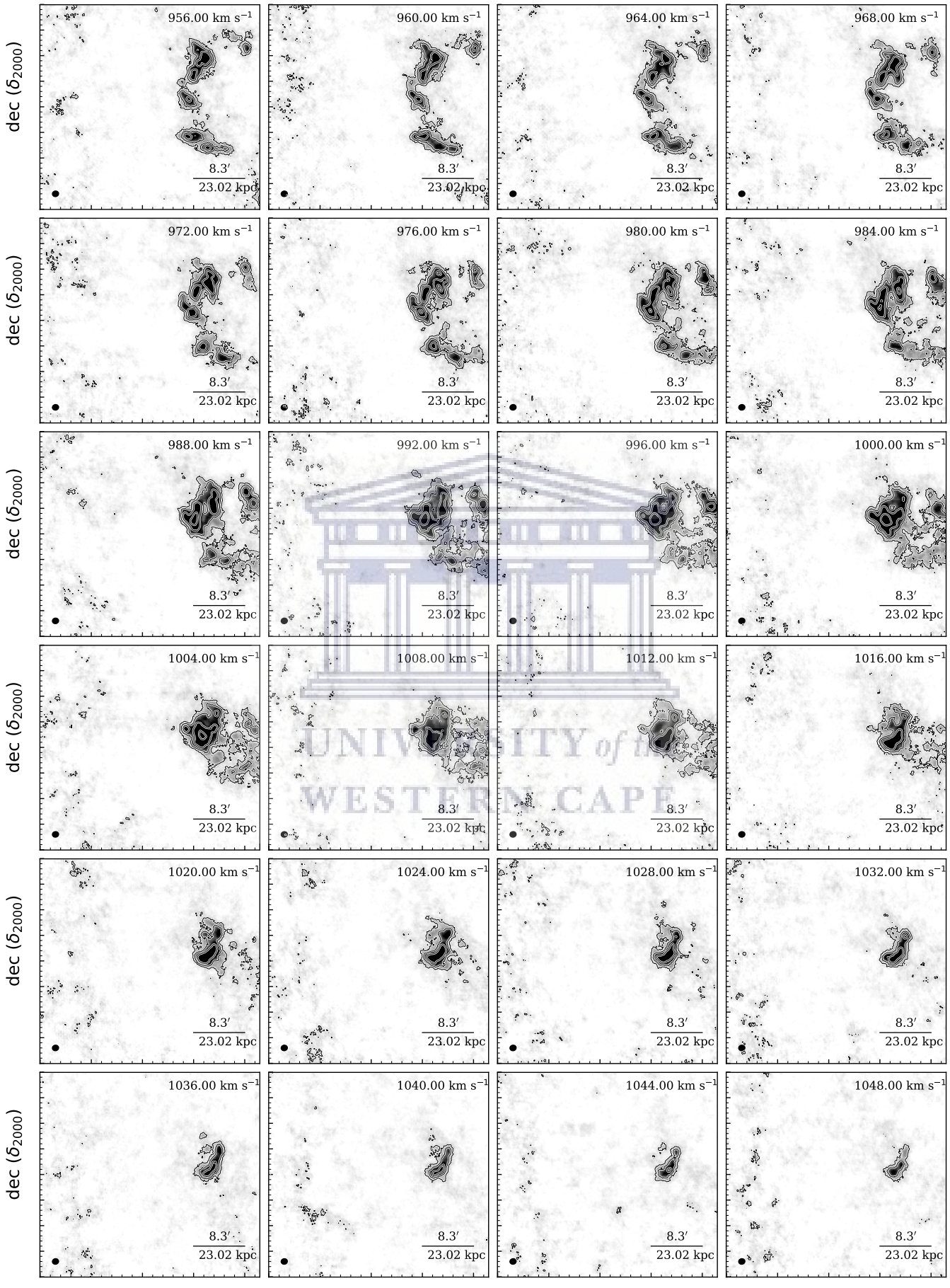

UNIVERSITY of the WESTERN CAPE

http://etd.uwc.ac.za/

Figure 2.1: Continued

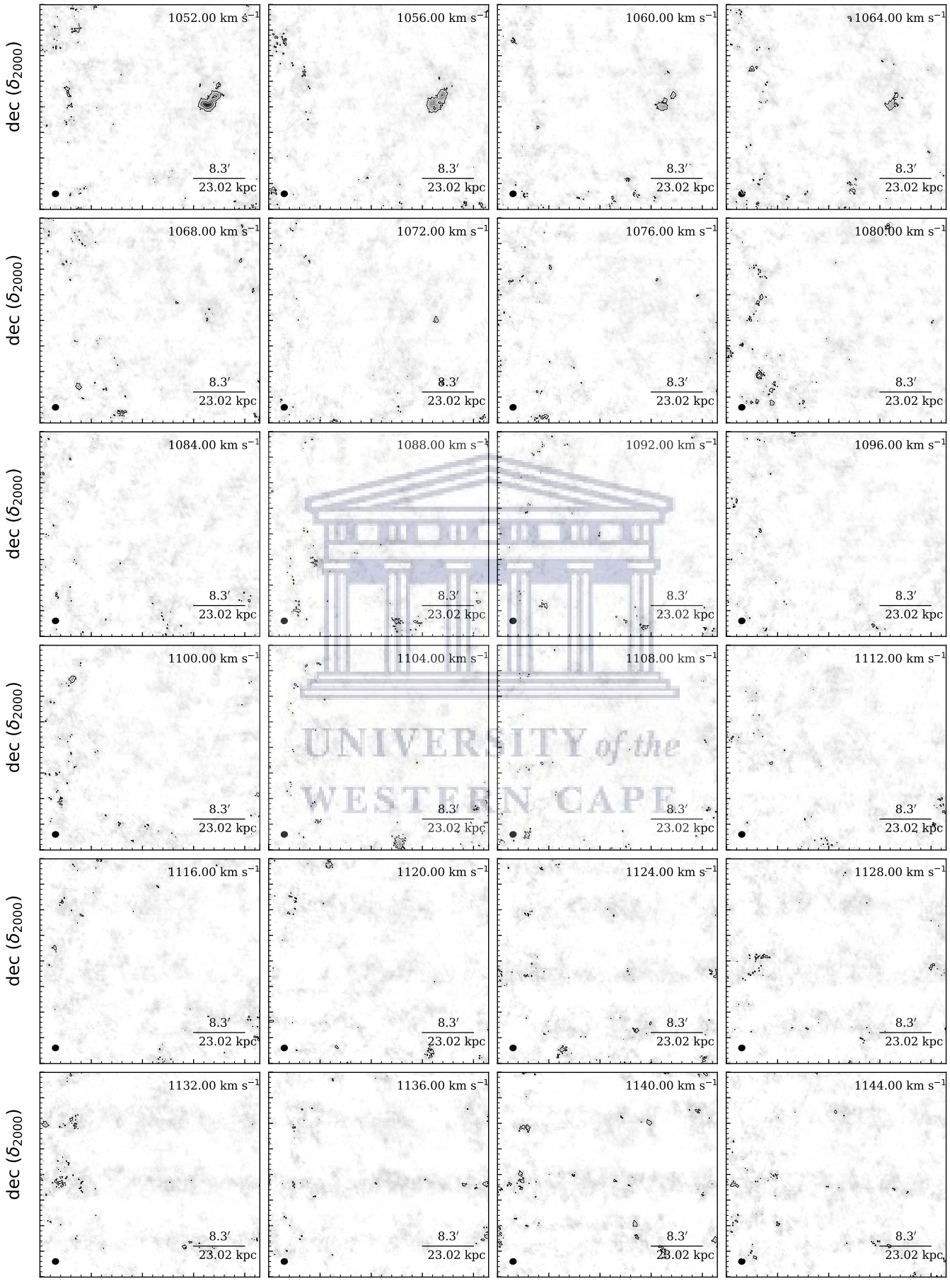

UNIVERSITY of the WESTERN CAPE

http://etd.uwc.ac.za/

Figure 2.1: Continued

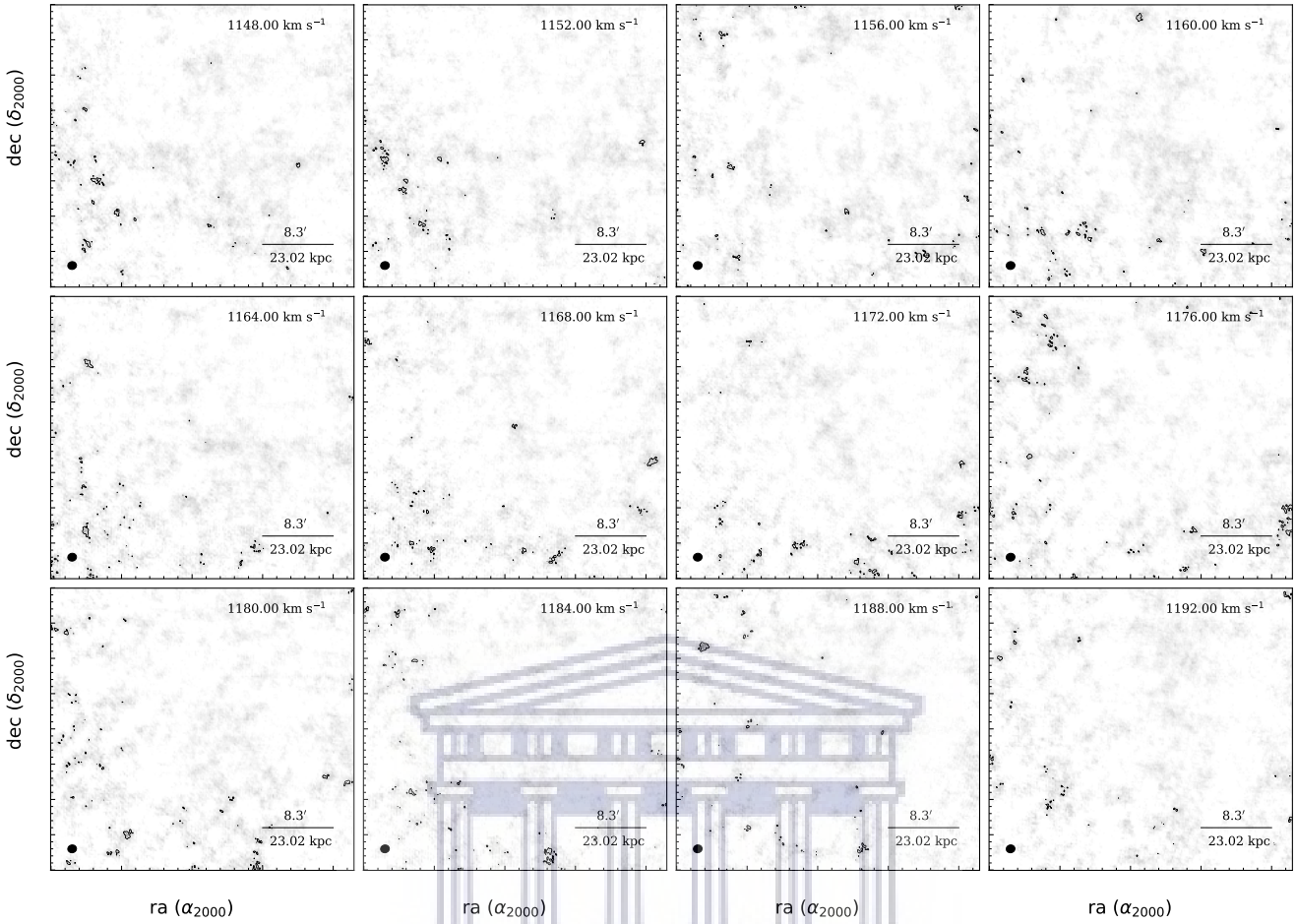

Figure 2.1: Continued

UNIVERSITY of the
WESTERN CAPE

http://etd.uwc.ac.za/

2.1.2 Global profile

The global profile is produced by taking the sum of H I emission in each channel of the data cube. For this work, the global profile was created by adding all the emission above 3σ ($\sigma = 2.13$ mJy/beam) in each channel of the ATCA data cube. The global profile of NGC 1512/1510 based on the ATCA data cube is presented below in Figure 2.2. On the same Figure, we also present the global profile of the NGC 1512/1510 based on HIPASS data (Hawarden T. G. (1979)). The two global profiles do not differ significantly except for the global profile based on the HIPASS data having much lower right horn as compared to the one produced in this work. This difference might be largely due to the fact HIPASS data was observed using a single dish telescope which is the Parkes 64 m dish.

From the global profile generated in this work, the value of the width at 20% level of the maximum flux is $W_{20} = 264$ km s^{-1} and at the 50% level the velocity width is $W_{50} = 224$ km s^{-1}. The values found by Koribalski & López-Sánchez (2009) are $W_{20} = 270 \pm 9$ km s^{-1} and $W_{50} = 234 \pm 6$ km s^{-1}. The values derived from this work are close to the ones found by Koribalski & López-Sánchez (2009). The integrated H I flux measured from our H I spectrum is $F_{H\,I} = 346.35$ Jy km s^{-1} which translates to an H I mass of $M_{H\,I} = 7.38 \times 10^9$ $M_\odot$, adopting a distance of 9.5 Mpc. Through equation 2.1, the systemic velocity of NGC 1512/1510 is $V_{sys} = 898.0$ km s^{-1}. This value agrees well with the one found by Koribalski & López-Sánchez (2009).

$$V_{sys} = 0.25 \times (V^{20\%}_{high} + V^{20\%}_{low} + V^{50\%}_{high} + V^{50\%}_{low}), \tag{2.1}$$

where ($V^{20\%}_{high}$, $V^{20\%}_{low}$, $V^{50\%}_{high}$, $V^{50\%}_{low}$) are the high and low velocities in km s^{-1} at 20% and 50% peak flux levels respectively.

UNIVERSITY of the WESTERN CAPE

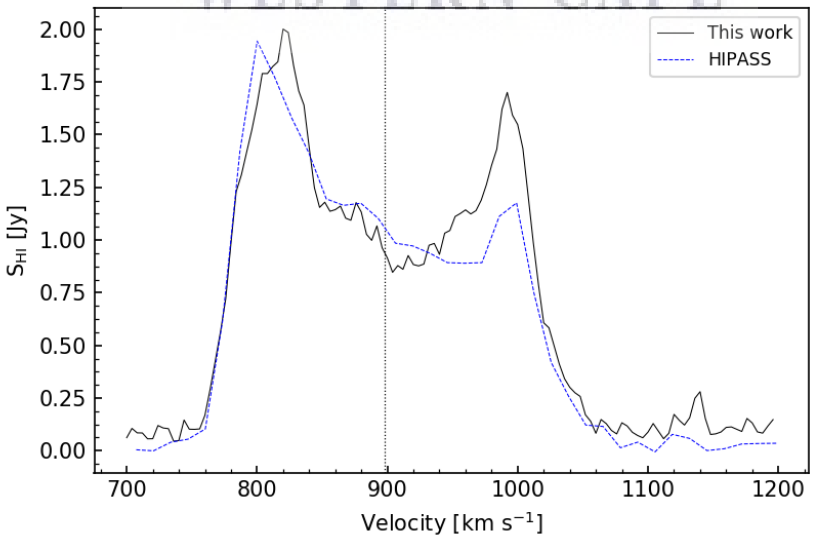

Figure 2.2: The global profile of NGC 1512/1510 based on the ATCA data cube (black) compared to the one based on the HIPASS data (blue). The vertical dotted line marks the systemic velocity of the galaxy at $V_{sys} = 898.0$ km s^{-1}.

http://etd.uwc.ac.za/

2.1.3 Parameterization

The traditional way of generating H I maps from the H I data cube is potentially affected by noise, especially in the outer parts of the galaxy where there is a low signal-to-noise (S/N) ratio. In this work, to minimize the effects of noise we parameterize the ATCA H I data cube on a line-by-line basis. This was done by fitting a 3rd order Gauss-Hermite polynomial at each RA-Dec pixel position in the ATCA data cube. The mathematical form of a third-order Gauss-Hermite polynomial is given below by equation 2.2,

$$\phi(x) = a \exp\left(\frac{-1}{2}y^2[1 + \frac{h_3}{\sqrt{6}}(2\sqrt{2}y^3 - 3\sqrt{2})]\right). \quad (2.2)$$

It is noticeable that for $h_3 = 0$, equation 2.2 reduces to a Gaussian function. Thus, the parameter h_3 is described as signifying the deviation of a Gauss-Hermite polynomial from a Gaussian function. The parameter y on equation 2.2 is given as $y = \frac{x-\mu}{c}$, where μ is the mean and c is the standard deviation as it is the case with a Gaussian function. The h_3 is very important for this study as it tracks the asymmetries of the H I line profiles which helps in producing high quality data products of NGC 1512/1510. The H I line profiles based on the ATCA data cube of NGC 1512/1510 are asymmetric rather than purely Gaussian, this arises from the interaction of the two galaxies hence the need to parameterize the data cube with third-order Gauss-Hermite polynomials.

This method of parameterization was introduced by van Der Marel & Franx (1993). It since has been employed successfully in previous studies to create H I maps (van Der Marel & Franx (1993); De Blok et al. (2008a)). The third order Gauss-Hermite polynomial parameterization is a good method to create reliable and high-quality H I maps since it is not largely affected by asymmetries in H I line profiles (De Blok et al. (2008a)) which is usually the case with a system of interacting galaxies like NGC 1512/1510. To ensure high-quality data products i.e. data products with high signal-to-noise ratio, the third-order Gauss-Hermite polynomial was only fitted to H I line profiles (extracted along individual pixels) having at-least three consecutive channels with peak flux above the level of 3σ, where $\sigma = 2.13$ mJy beam^{-1} is the root mean square (rms) noise in the line-free channel of the ATCA data cube. Selected few H I line profiles that met this strict criterion are shown below in Figure 2.3. In their work, De Blok et al. (2008a) discuss in great detail several other methods that can be used when creating H I maps from galaxy data cubes.

UNIVERSITY of the WESTERN CAPE

http://etd.uwc.ac.za/

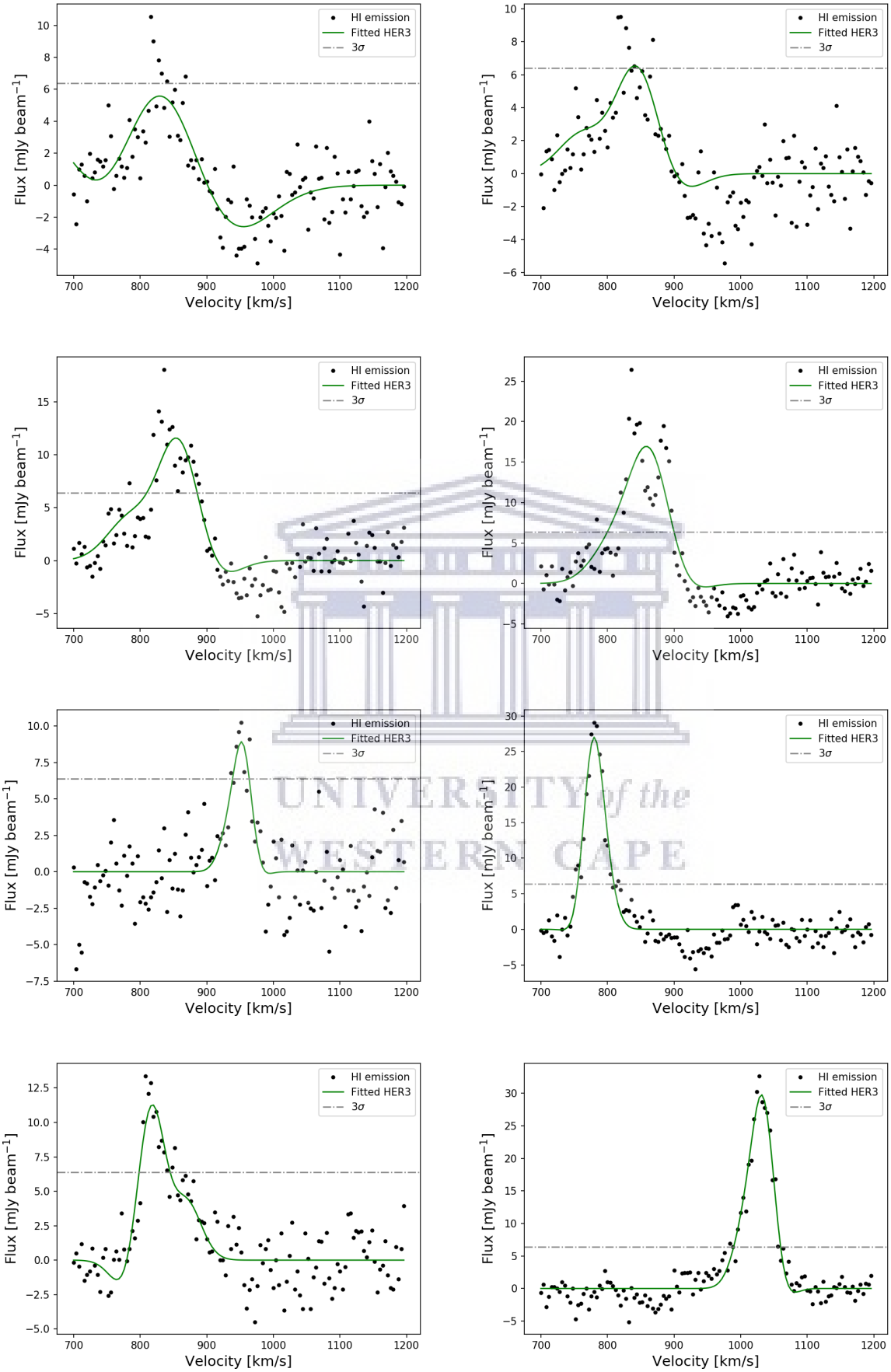

Figure 2.3: Selected H I line profiles with fitted third order Gauss-Hermite polynomial (green curve). The asymmetries in the H I line profiles are well accommodated by the Gauss-Hermite polynomial.

http://etd.uwc.ac.za/

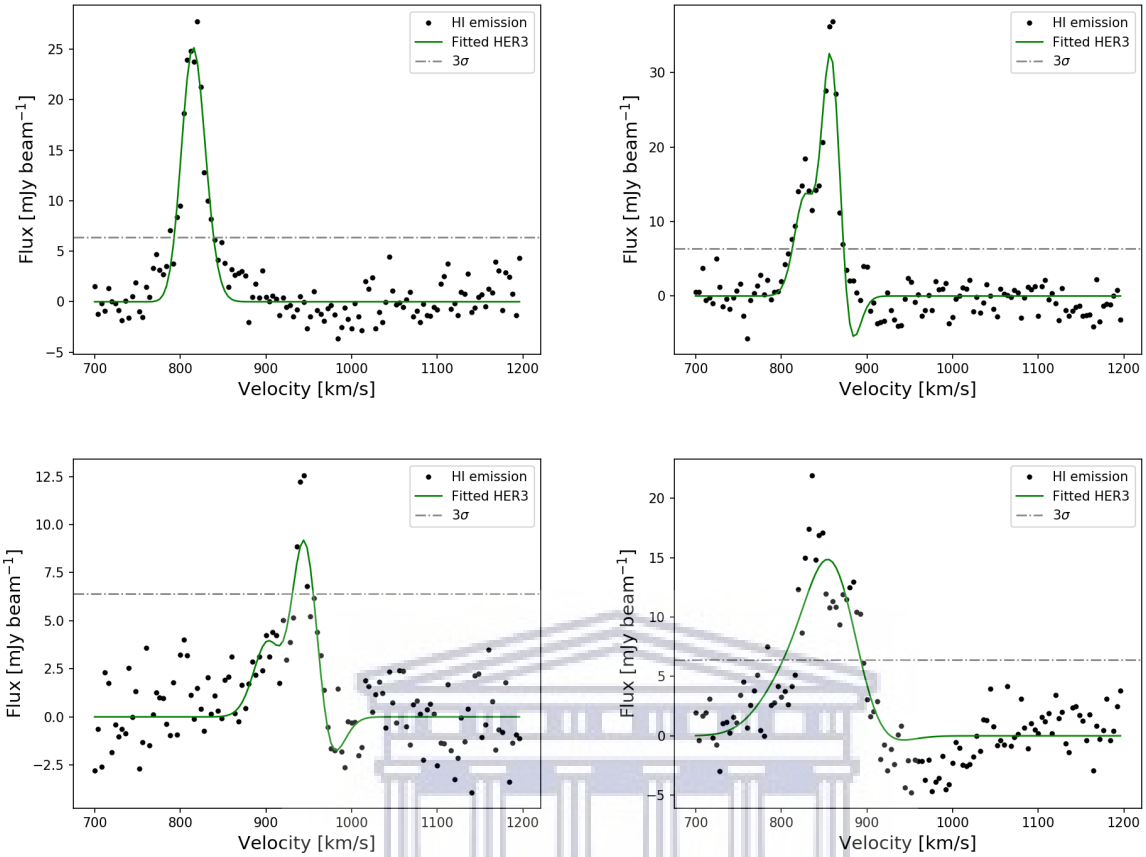

Figure 2.3: Continued

UNIVERSITY of the
WESTERN CAPE

2.1.4 H I total intensity map

The H I total intensity map was generated by calculating the area under each of the fitted third-order Gauss-Hermite polynomials. The H I total intensity map was converted from units of Jy/beam to $M_\odot$ pc^{-2}, which makes it an H I surface density map. The H I surface density map of NGC 1512/1510 generated by parameterizing the ATCA data cube is presented in Figure 2.4. For comparison, we present the WISE 3.4 µm image of NGC 1512 in Figure 2.5. The 3.4 µm photometry is a sensitive tracer of the main stellar component of the galaxies.

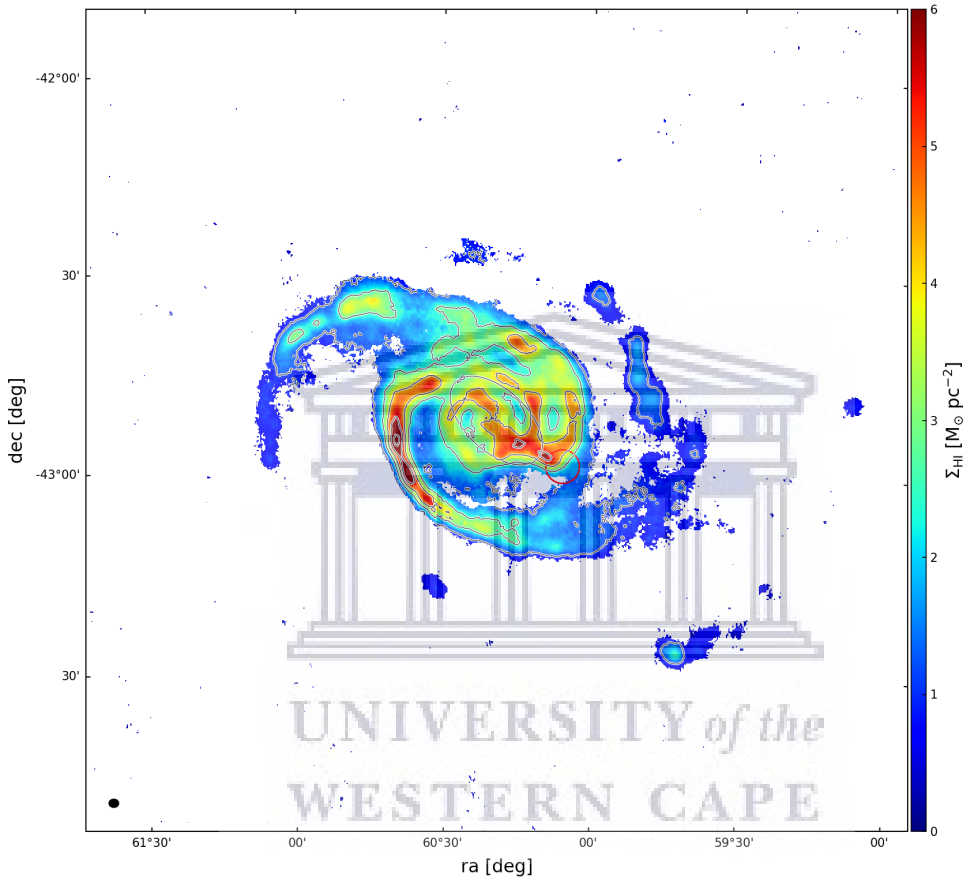

Figure 2.4: The H I surface density map of NGC 1512/1510 generated by parameterising the data cube with Gauss-Hermite polynomials. The contours levels range from 1.1 to 10 $M_\odot$ pc^{-2} spaced by 1.5 $M_\odot$ pc^{-2}. The synthesized beam of size 66.11″ × 55.35″ is shown on the bottom left corner. The black ellipse marks the inner infrared disk of NGC 1512 (see Figure 2.5). The red circle marks the position of NGC 1510.

From the H I total intensity map of NGC 1512/1510 we calculated the total amount of mass stored in the gas component of the galaxy i.e. the H I mass ($M_{H\,I}$) and the total H I flux ($F_{H\,I}$) of the galaxy. The H I mass of the galaxy is calculated by using equation 2.3 and the total H I flux is calculated by taking the sum of the H I total intensity map in units of Jy km s^{-1},

$$\frac{M_{H\,I}}{[M_\odot]} = \frac{2.13 \times 10^5}{1+z} \frac{D^2}{[\mathrm{Mpc}]} \frac{\Sigma_i S_i \Delta v}{[\mathrm{Jy\ km\ s^{-1}}]}, \tag{2.3}$$

http://etd.uwc.ac.za/

where D is the distance to the galaxy in Mpc. This work adopts the distance D to the system of galaxies to be 9.5 Mpc as used by Koribalski & López-Sánchez (2009). The last term in this equation (i.e. $\Sigma_i S_i \Delta v$) is the H I total intensity map in units of Jy km s^{-1}.

Table 2.3 below presents the values of the H I mass ($M_{H\,I}$) and the total H I flux ($F_{H\,I}$) NGC 1512/1510 as derived from the Gauss-Hermite H I total intensity map together with the values found by Koribalski & López-Sánchez (2009).

Table 2.3: The H I mass and the total H I flux as derived from the Gauss-Hermite H I total intensity map compared to the values found by Koribalski & López-Sánchez (2009).

Study	$M_{H\,I}$ [10^9 $M_\odot$]	$F_{H\,I}$ [Jy km s^{-1}]
This work	7.16	336.03
Koribalski & López-Sánchez (2009)	5.51 $\pm$ 0.37	259.3 $\pm$ 17.4

The values of the H I mass and the H I flux derived in this work disagree significantly from the values found by Koribalski & López-Sánchez (2009). This work extracts more H I flux and H I mass as compared to the work of Koribalski & López-Sánchez (2009). The differences between the values found in this work and that of Koribalski & López-Sánchez (2009) are largely due to the fact that effects such as low signal-to-noise ratio arising from the H I line profiles of NGC 1512/1510 were accounted for in this work by parameterizing the ATCA data cube with Gauss-Hermite polynomials.

UNIVERSITY of the WESTERN CAPE

http://etd.uwc.ac.za/

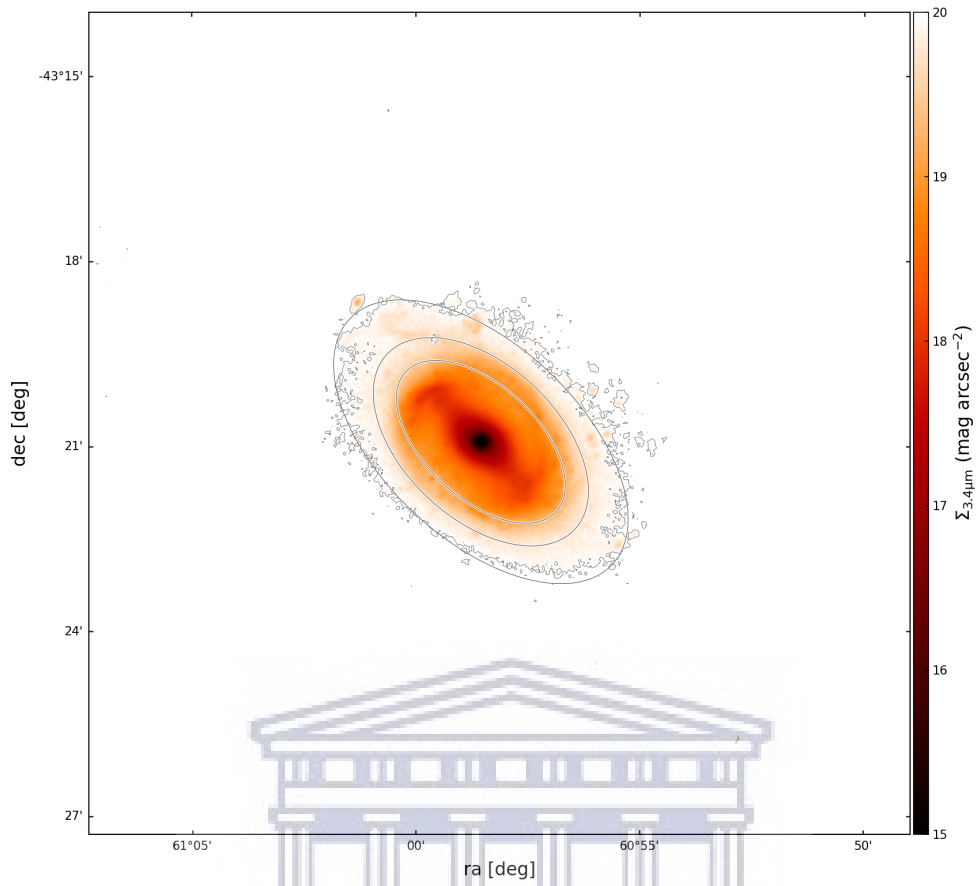

Figure 2.5: The WISE 3.4μm infrared image of NGC 1512. The three ellipses overlaid on the image to get an initial estimate of the inclination angle of the galaxy, used later in Chapter 3 of this work. The outermost ellipse traces the isophote with the least flux at a level of 20 mag arcsec^{-2}. The innermost ellipse is shown in Figure 2.4 to compare the size of the H I disk to that of the infrared disk.

UNIVERSITY of the WESTERN CAPE

The H I surface density map of a galaxy depicts the morphology of the galaxy as it shows in detail the spatial distribution of the emission. H I surface density maps also show signatures of activities taking place around the galaxy e.g. features of tidal tails due to gravitational interactions as is the case with NGC 1512/1510, ram pressure stripping within a cluster of galaxies and the position of the companion in most cases e.g. in the M81/82 system. This is primarily due to the H I gas extending well beyond the stellar radius of the galaxy and thus revealing features that are usually hidden from the optical. The H I surface density map (Figure 2.4) of NGC 1512/1510 shows two prominent arms emerging from the main HI disc of NGC 1512. We notice the absence of these features from the WISE 3.4 μm shown in Figure 2.5. This controversy suggests that these two features are tidal tails or tidal debris rather than the spiral arms of NGC 1512. These are largely due to the ongoing interaction of NGC 1512 with the blue compact dwarf galaxy NGC 1510.

http://etd.uwc.ac.za/

2.1.5 Velocity Field

The velocity field was generated by taking the fitted mean velocity of each Gauss-Hermite polynomial. The velocity field of NGC 1512/1510 based on the parameterized ATCA data cube is presented in Figure 2.6.

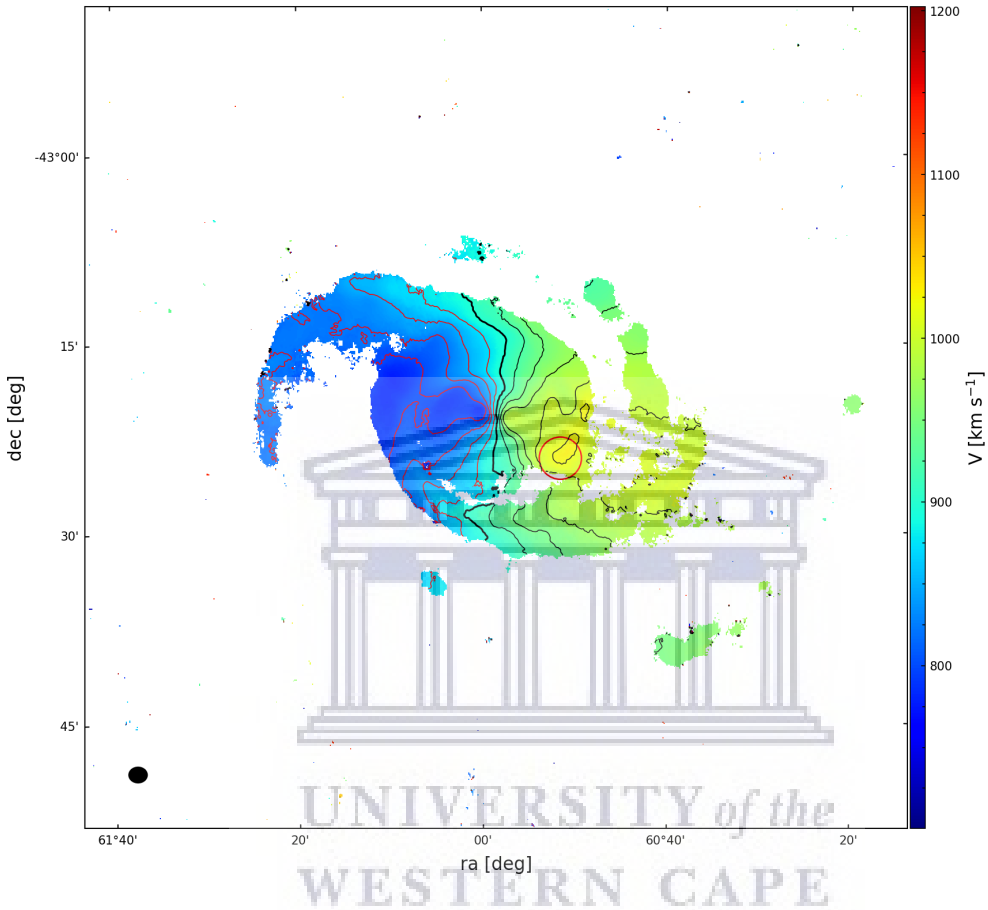

UNIVERSITY of the WESTERN CAPE

Figure 2.6: The velocity field of NGC 1512/1510 based on fitting Gauss-Hermite polynomials to each H I line profile of the ATCA data cube . The red contours mark the approaching side and the black contours mark the receding side of the galaxy with a spacing of 25 km s^{-1}. The bold, black contour marks the systemic velocity at 898 km s^{-1}. The red cirle marks the position of the interacting companion NGC 1510. The synthesized beam of size 66″.11 × 55″.35 is shown in the bottom left corner.

Using the traditional method detailed in Walter et al. (2008), the intensity weighted mean velocity field of NGC 1512/1510 was also generated from the ATCA data cube. The intensity weighted mean velocity field is presented in Figure 2.7.

http://etd.uwc.ac.za/

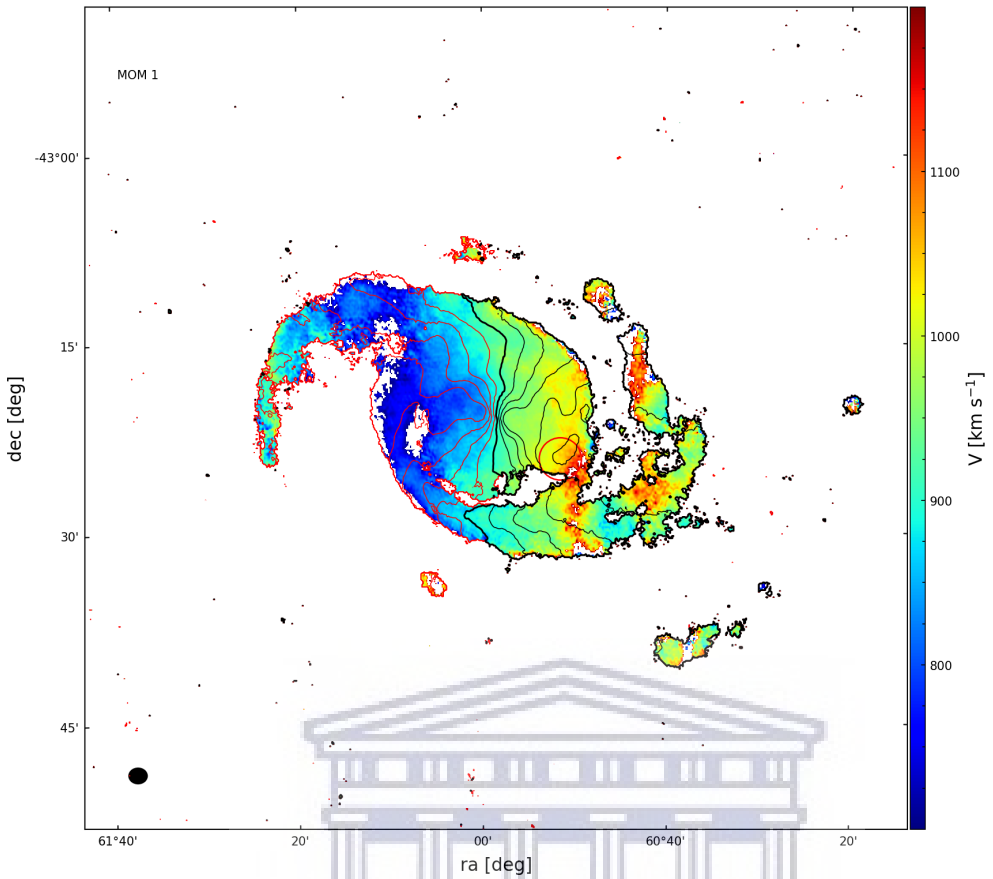

Figure 2.7: The intensity weighted mean velocity field of NGC 1512/1510 as derived from the ATCA data cube by using the traditional method. The contour levels are spaced by 25 km s^{-1}. The bold, black contour marks the systemic velocity at 898 km s^{-1}. The red circle marks the position of the interacting companion NGC 1510. The synthesized beam of size 66″.11 × 55″.35 is shown in the bottom left corner.

UNIVERSITY of the WESTERN CAPE

The two maps i.e. the intensity weighted mean and the Gauss-Hermite velocity field were compared against each other to investigate which one best portrays the true kinematics of NGC 1512/1510. The method in generating each of these maps is different. The intensity weighted mean velocity field is generated through equation 2.4:

$$\langle v \rangle = \frac{\Sigma_i S_i \Delta v}{\Sigma_i S_i}, \tag{2.4}$$

where S_i is the flux in channel i of the data cube in units of Jy beam^{-1} and Δv is the channel width (i.e. 4 km s^{-1}).

The Gauss-Hermite velocity field is based on the parameterization of the ATCA data cube with third order Gauss-Hermite polynomials. The Gauss-Hermite velocity field was subtracted from the intensity weighted mean velocity field. The resulting map is called the residual map, shown in figure 2.8. This was done to investigate how much the two maps deviate from each other.

http://etd.uwc.ac.za/

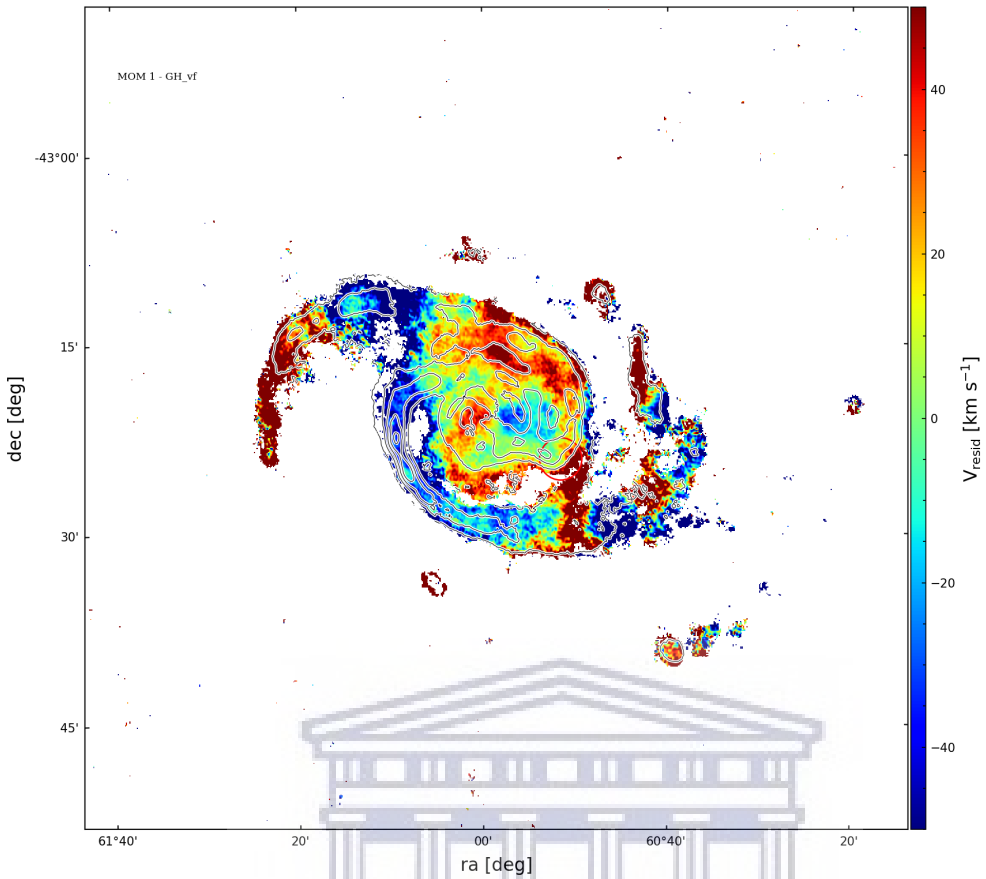

Figure 2.8: The residual map, i.e. the difference between the Gauss-Hermite velocity field and the intensity weighted mean velocity field based on the ATCA data cube of NGC 1512/1510. The overlaid contours are the same as those of the H I surface density map in Figure 2.4.

The residual map shows that there are huge variations between these two maps i.e. the residuals are greater than $|v_{resid}| = 40$ km s^{-1}. A statistical way of quantifying the difference was performed by fitting a Gaussian function to the histogram showing the distribution of the residuals. From this check, we noticed that the residuals produce a non-Gaussian distribution (see Figure 2.9) due to the huge value of the fitted standard deviation $\sigma = 39.03$ km s^{-1}. The choice was made to continue with the Gauss-Hermite velocity field because it accounts for effects such as asymmetries in the H I line profiles.

UNIVERSITY of the WESTERN CAPE

http://etd.uwc.ac.za/

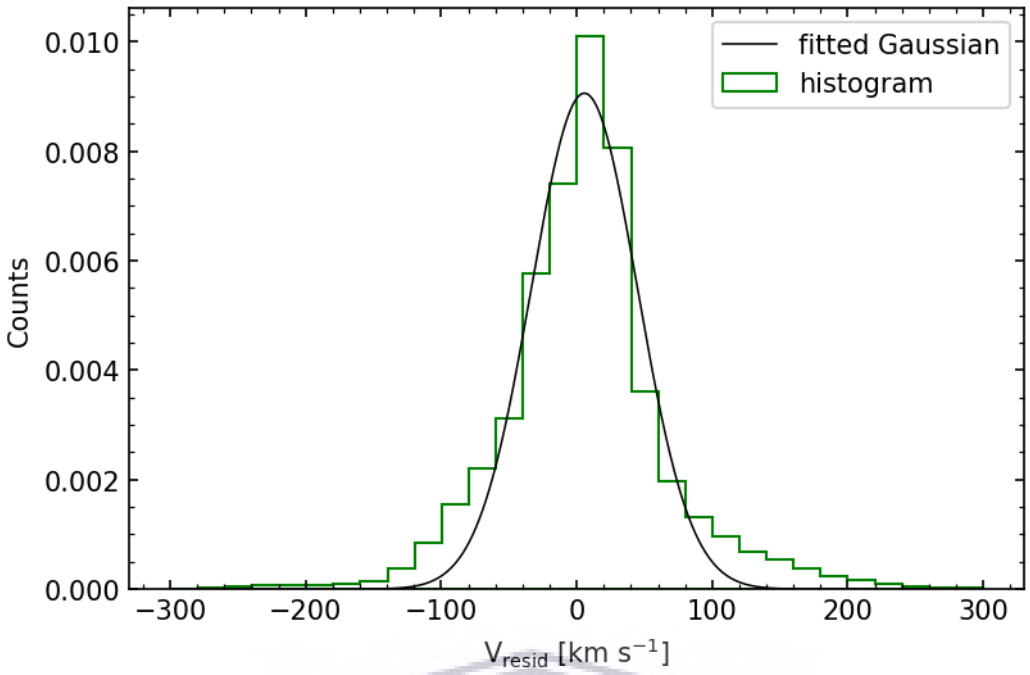

Figure 2.9: The histogram shows the distribution of the residual velocities between the intensity weighted mean and the Gauss-Hermite velocity field of NGC 1512/1510 both based on the ATCA data cube.

UNIVERSITY of the
WESTERN CAPE

http://etd.uwc.ac.za/

2.1.6 H I line profile asymmetries

The intensity weighted mean velocity field is expected to be highly affected by asymmetries in H I line profiles as there was no parameterization involved when producing this map, i.e. the mean velocity of the H I line profile is taken to be the velocity of the galaxy at that specific spatial position, as opposed to the fitted mean velocity of the third-order Gauss-Hermite polynomial fitted to single H I line profiles. To investigate the asymmetries in the H I line profiles we performed two checks. Firstly, we traced how the fitted third-order Gauss-Hermite polynomials deviated from a normal Gaussian distribution. This was done by checking how the h_3 parameter of the fitted Gauss-Hermite polynomial (i.e. equation 2.2) varies around $h_3 = 0$. For an H I line profile that is symmetric, h_3 is expected to be zero. A negative value of the h_3 parameter would signify a H I line profile skewed to the left as opposed to a positive value of h_3 that shows an H I line profile skewed to the right. The average fitted value of the skewness parameter was found to $| h_3 | \sim 0.15$. In Figure 2.10 we present an h_3 map of NGC 1512/1510. The extreme fitted values of $| h_3 |$ occur on the tidal tails of NGC 1512. This might be due to the ongoing interaction of this galaxy with NGC 1510. Furthermore, we note that both of the inner arms have values of h_3 varying significantly from $h_3 = 0$. These regions are traced out by the H I flux density contours overlaid onto this map.

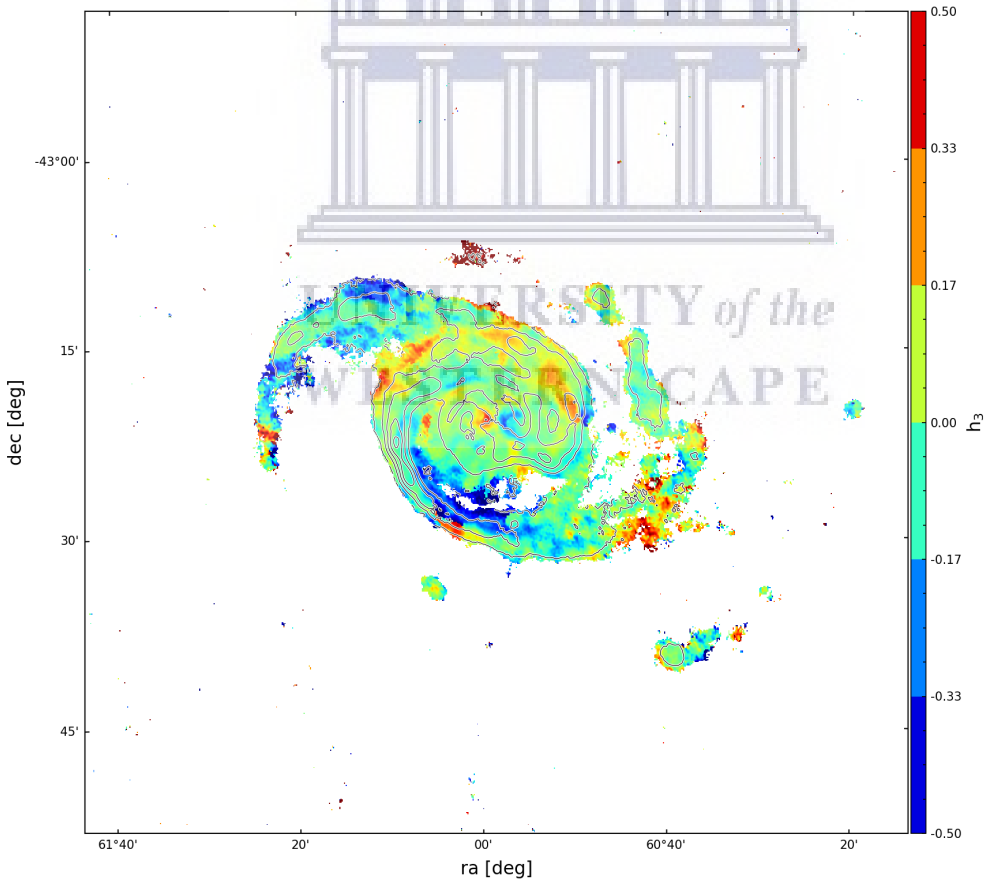

Figure 2.10: NGC 1512/1510 map of fitted h_3 values. Fitted extreme h_3 values are seen on the tidal tails of the galaxy. The overlaid contours are the same as those of the Gauss-Hermite H I total intensity map in Figure 2.4.

Secondly, we adopted the formalism employed by Bok et al. (2019) on their work of whether

http://etd.uwc.ac.za/

galaxy pairs/companions induce asymmetries on the H I spectrum/global profile. For this work, we employed this technique on the H I line profiles rather than the H I spectrum/global profile (i.e. shown in Figure 2.2) as done by them. This method makes use of the H I flux ratio i.e. the H I line profiles were partitioned about the mean velocity of the fitted third-order Gauss-Hermite polynomial. Then, the ratio of the H I flux enclosed (i.e. the area) on each side of the H I line profile was taken. To avoid noise contamination of the resulting ratio, only the points above the 1σ threshold were considered. To calculate the H I flux ratio in each profile we set a criterion to select the left-hand side to the right-hand side or vice-versa. This was done by taking the ratio of the side closest to the systemic velocity (i.e. $v_{sys} = 898.0$ km s^{-1}) to the side furthest. This criterion is shown below:

$$F_{H\,I}\ \ ratio = \begin{cases} \frac{A_{left}}{A_{right}} & \text{if } v_{mean} - v_{sys} > 0 \\ \\ \frac{A_{right}}{A_{left}} & \text{if } v_{mean} - v_{sys} < 0 \end{cases}$$

where A_{left} is taken to be the area of the region to the left of the Gauss-Hermite fitted mean velocity (i.e. the grey region in Figure 2.11 below.) and A_{right} is the area of the region to the right of the Gauss-Hermite fitted mean velocity (i.e. green region in Figure 2.11). This method was considered a more accurate way of probing asymmetries on the H I line profiles of NGC 1512/1510 as it shows in detail how much H I flux is stored on either side of each H I line profile. For symmetric H I line profiles, as one would expect, the H I flux ratio must be one, meaning there is as much flux on the left-hand side as there is on the right-hand side. Figure 2.11 shows selected H I line profiles and their corresponding H I flux ratios. The deviation of the h_3 parameter from zero is shown in the H I flux ratio map of NGC 1512/1510 presented in Figure 2.12. This strongly supports the proposition that galaxy pairs or interacting companions are the primary candidates inducing asymmetries in H I line profiles (Bok et al. (2019)) in galaxies.

UNIVERSITY of the
WESTERN CAPE

http://etd.uwc.ac.za/

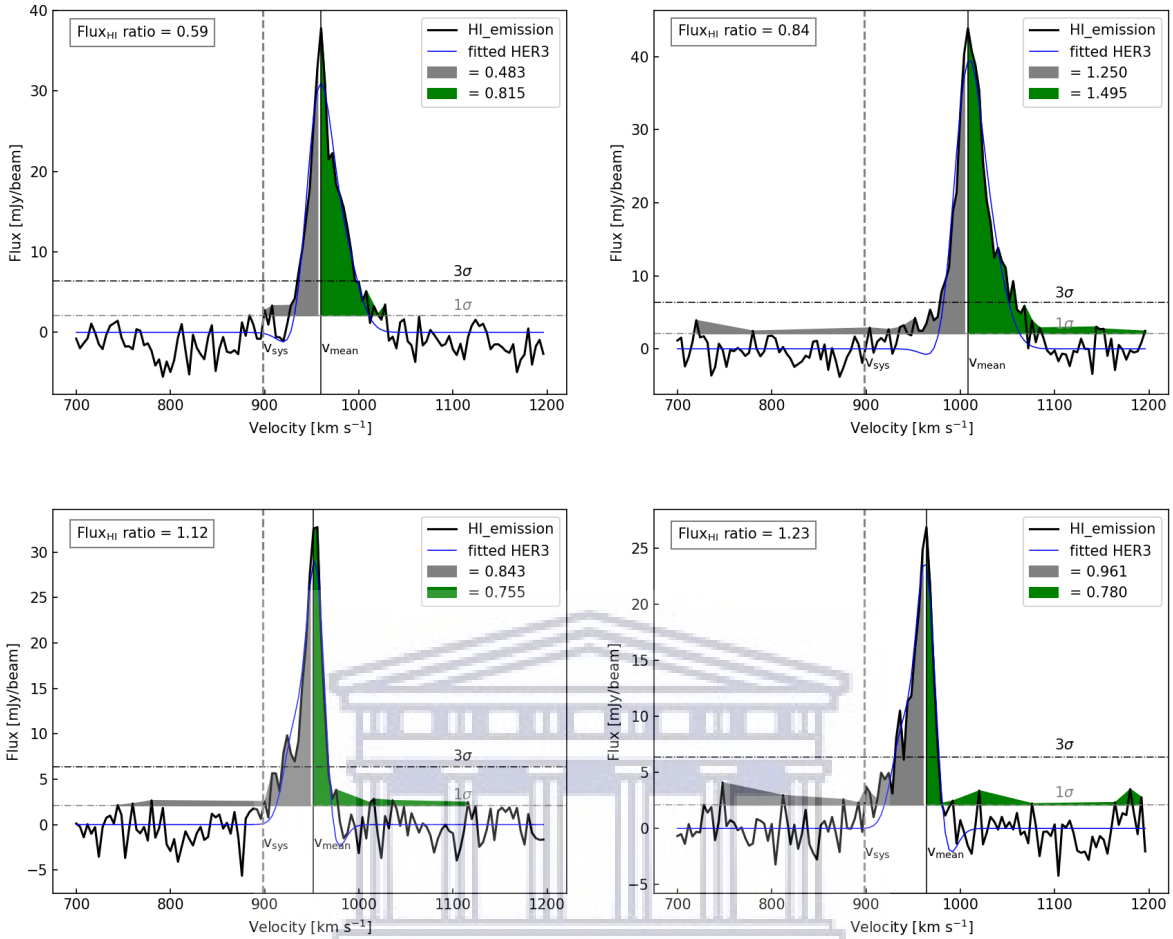

Figure 2.11: Selected H I line profiles of NGC 1512/10 showing levels of asymmetry. Presented on the top right corner of each image is the H I flux ratio calculated from the green and grey regions of the line profiles. The green and grey bars on the legend present the total area stored in the corresponding colored region of the H I line profile.

UNIVERSITY of the WESTERN CAPE

http://etd.uwc.ac.za/

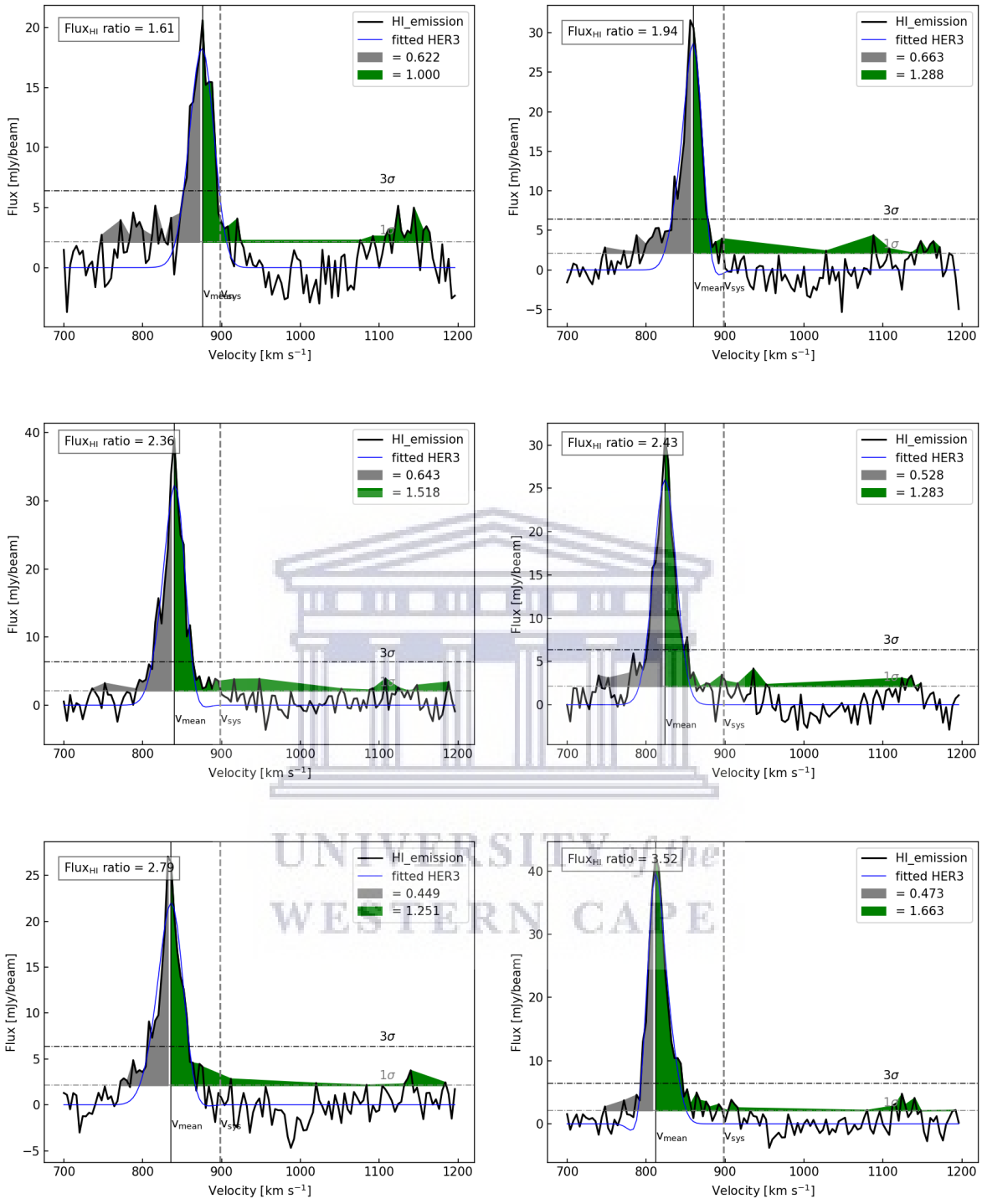

Figure 2.11: Continued

UNIVERSITY of the WESTERN CAPE

http://etd.uwc.ac.za/

Figure 2.12 shows the map of the H I flux ratios of NGC 1512/1510.

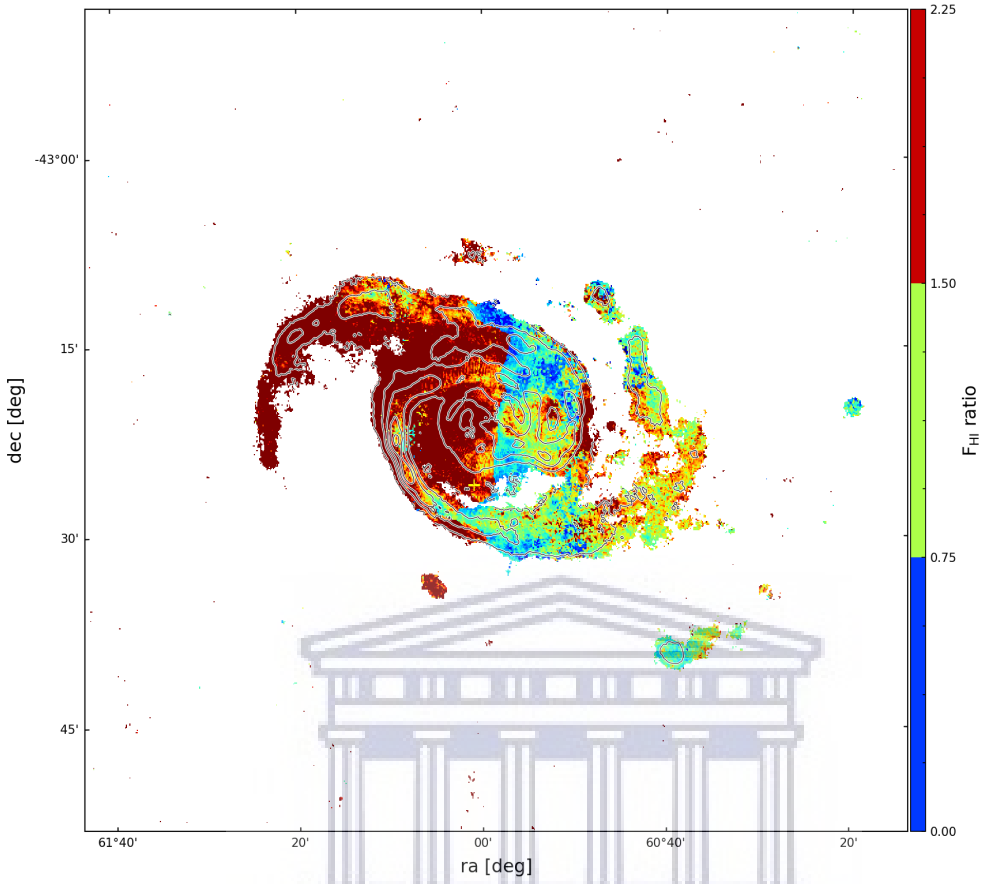

Figure 2.12: The flux ratio map of NGC1512/1510 showing regions of strongly asymmetrical H I line profiles. H I flux density contours from the H I surface density map are overlaid.

Figure 2.10 and 2.12 serve as clear signatures of asymmetries in H I line profiles of the interacting galaxy NGC 1512/1510. As in Bok et al. (2019), we propose that the interacting companion, the blue compact dwarf NGC 1510, is the primary reason for these H I line profile asymmetries. The approaching side of the galaxy is strongly affected by the asymmetries, which might be also due to a gravitational effect by the companion galaxy. For this reason, we propose that the Gauss-Hermite velocity field is of high quality since the parameterization accounts for these asymmetries (i.e. h_3 term (skewness)) (De Blok et al. (2008a); Noordermeer et al. (2007)) in H I line profiles and thus we choose it over the intensity weighted mean velocity field to model the kinematics of the gas around NGC 1512/1510.

UNIVERSITY of the WESTERN CAPE

http://etd.uwc.ac.za/

Chapter 3

H I Kinematics of NGC 1512

The kinematics of a galaxy has major effects on the shape of the H I spectrum. In their recently conducted study on asymmetries of H I profiles, Bok et al. (2019) stated that H I spectra are expected to be symmetric about the systemic velocity of the galaxy (V_{sys}) for disks that are not perturbed. The global profile (Figure 2.2) of NGC 1512/1510 is not symmetric about the systemic velocity. This shows that NGC 1512 has a kinematically complex nature. Thus to model such a kinematically sophisticated system we use the Gauss-Hermite velocity field of NGC 1512/1510 as demonstrated in Figure 2.6 of Chapter 2.

The spectral resolution of $\sim$ 3.5 km s^{-1} of the ATCA H I data cube used for this work allows one to model the gas kinematics of NGC 1512. This chapter is dedicated to discussing the modeling of the rotation curve of the interacting spiral galaxy NGC 1512 using the ATCA data. To model the rotation curve of this galaxy we adopted two approaches: the traditional 2D approach i.e. fitting the 2D velocity field of the galaxy with the tilted-ring model (De Blok et al. (2008a)) and the modern 3D approach i.e. fitting a tilted-ring model to the H I data cube of the galaxy (di Teodoro & Fraternali (2015); Di Teodoro et al. (2016)). The latter i.e. the 3D modeling approach, was used because the 2D modeling routine failed to generate a reliable inclination angle profile of NGC 1512. However, using the 3D modeling routine, a reliable inclination angle profile of NGC 1512 was generated and thus a final rotation curve of the galaxy was achieved. The final rotation curve of NGC 1512 based on the 3D modeling routine is different to the rotation curve of this galaxy generated by Koribalski & López-Sánchez (2009). The difference in the results arises from the different inclination angles used in these studies. This work estimated the inclination angle of NGC 1512 to be $\sim$ 51° by overlaying ellipses onto the WISE 3.4 µm image of NGC 1512 shown in Figure 2.5 of Chapter 2. The 3D modeling routine also favors an inclination angle of $\sim$ 51° for NGC 1512. The study of Koribalski & López-Sánchez (2009) used a constant inclination angle of 35° for the entire H I disc of NGC 1512. The results of the dynamical model based on the 3D modeling approach suggest that the H I disc of NGC 1512 has non-constant inclination angle (see Figure 3.5).

3.1 2D modeling - ROTCUR

The 2D approach of modeling the kinematics of galaxies is primarily based on generating a rotation curve of the galaxy from its velocity field. This is done by fitting the so-called 'tilted-ring model' to the 2D velocity field of the galaxy (Rogstad et al. (1974)). This approach

http://etd.uwc.ac.za/

is however sensitive to several effects such as beam smearing because the velocity field only contains a parameterised subset of the full information of the full H I data cube. a subset of the H I data cube. For this work we fit the tilted-ring model to the Gauss-Hermite velocity field of NGC 1512 presented in Figure 2.6. The 2D approach of modeling the kinematics of galaxies has been applied successfully many times in the past and it is still widely used (De Blok et al. (2008a), Begeman (1989)). For the 2D approach, the GIPSY task ROTCUR (Begeman (1989)) is used in this work. ROTCUR is based on fitting a set of concentric rings onto the 2D velocity field of the galaxy following a non-linear least squares algorithm.

The tilted-ring analysis was first proposed by Rogstad et al. (1974) as a possible explanation to the H I disc of the spiral galaxy M83. This method (i.e. tilted-ring model) decomposes the disc of the galaxy into a series of concentric rings. One of the assumptions of the tilted-ring model is that the disc of the galaxy is dominated by circular motions. This means that the H I gas in the galaxy is assumed to be moving in circular orbits along the concentric rings. This method has proven to be a good approximation in modeling the kinematics of local galaxies as their discs are nearly circular due to a lack of a galactic bar (Schoenmakers et al. (1997)). Each of these rings is determined by a set of six parameters. These parameters are:

- the inclination angle (i) which describes how inclined the H I disc of the galaxy is, with respect to the line of sight.
- the position angle (PA) which is calculated from the north to the semi-major axis of the receding side of the galaxy.
- the dynamical center position of the galaxy usually described as x_c and y_c.
- the systemic (V_{sys}) and the rotation velocity (V_{rot}) of the galaxy in a given concentric ring.

UNIVERSITY of the WESTERN CAPE

The first three bullet points present four parameters of the tilted-ring model that are referred to as geometric parameters and the last two are referred to as kinematic parameters. Each of these parameters is linked directly to the observed line-of-sight velocity of each ring, which is given by the equation 3.1 where the streaming (i.e. non-circular) motions are ignored (De Blok et al. (2008a)):

$$V_{los}(R,\theta) = V_{sys} + V_{rot}(R)cos(\theta)sin(i). \tag{3.1}$$

In this expression V_{los} is the line-of-sight velocity of each ring at a given set of polar coordinates R, and θ. *R* is the radial distance from the kinematic center of the galaxy and θ is the azimuthal angle measured in the plane of the galaxy starting from the major axis (i.e. $\theta = 0^\circ$ for major axis). This angle is directly linked to the inclination angle (*i*) and the position angle (*PA*) of the galaxy by

$$cos(\theta) = \frac{-(x-x_c)sin(PA) + (y-y_c)cos(PA)}{R} \tag{3.2}$$

$$sin(\theta) = \frac{-(x-x_c)cos(PA) + (y-y_c)sin(PA)}{Rcos(i)}, \tag{3.3}$$

where *x* and *y* are the rectangular coordinates on the sky.

http://etd.uwc.ac.za/

After a detailed visual inspection of the H I surface density map of NGC 1512/1510 (see 2.4) we found that the distribution of H I in the disc of NGC 1512 is perturbed beyond a radius of r ∼ 450 arcsec from the center. For this reason, we decided to model the kinematics of the H I disc out to a radius of r ∼ 450 arcsec. The velocity field (in Figure 2.6) of NGC 1512 suggests that beyond this radius, the gas kinematics of this galaxy cannot be reliable due to the disturbed distribution of the H I gas. A total number of 15 rings was used, starting at radius r ∼ 30 arcsec from the galactic center. Each ring was given a width of dR = 30 arcsec. This was selected to be approximately equal to half of the beam size (i.e. the beam major-axis given in table 2.2). A | cos θ | weighting function was used to give more weight to points closer to the major-axis of the galaxy. On the major-axis of the galaxy the line-of-sight velocities are dominated by circular motions (De Blok et al. (2008a); Elson et al. (2010)). The minor axis of the galaxy contains information about the radial motions of the gas. To minimize the effect of points close to the minor axis, we omitted all points within an angle of 10° of semi-minor axis.

3.1.1 Fitting procedure

The traditional way of fitting the tilted-ring model consists of five iterations:

- Iteration 1: all the parameters of the tilted-ring model are varying freely with radius, mainly focusing on the convergence of the dynamical center (i.e. x_c and y_c).
- Iteration 2: the dynamical center parameters are henceforth fixed, given a sensible value has been achieved. This can determined by comparing the achieved value with the optical center of the galaxy. The second iteration focuses on the best-fitted value of the systemic velocity of the galaxy (V_{sys}). The systemic velocity is fixed as well to a sensible value achieved by the tilted-ring algorithm. Because the systemic velocity of a galaxy can be determined from the H I spectrum/profile (i.e. Figure 2.2), this step can be taken as a crucial test to the accuracy of the tilted-ring fitting algorithm i.e ROTCUR. If we find that ROTCUR produces a systemic velocity value in agreement with that determined from the global profile, thus this agreement validates performing a third iteration which fixes the systemic velocity (V_{sys}) and dynamical center positions (i.e. x_c and y_c).
- Iteration 3: the third iteration consists of the dynamical center position and the systemic velocity parameters of the tilted-ring model being fixed to the previous values found in iteration 1 and 2, respectively. In this iteration the inclination angle (i), the position angle (PA) and the rotation velocity parameters of the tilted-ring model vary freely with radius.This iteration fits the position angle (PA)) of the galaxy.
- Iteration 4: the position angle is fixed to its best fit value achieved in the previous iteration. The inclination angle is being fitted in this iteration.
- Iteration 5: the inclination angle of each ring is fixed to the best fitting value found in the previous iteration. In this iteration, the final rotation curve of the galaxy is produced.

For NGC 1512 the tilted-ring model was fitted in an iterative fashion following the traditional way described above (Elson et al. (2016); De Blok et al. (2008a); Swaters et al. (2009)). The first run had all the six parameters of the tilted-ring model varying freely with radius. One

http://etd.uwc.ac.za/

way of obtaining a good model from this dynamical modeling technique is to give it good initial parameters that best describe the H I disc of the galaxy. For this work, to obtain initial estimates of the inclination and position angle of NGC 1512/10, an ellipse was overlaid onto the least surface brightness isophote of the WISE 3.4 μm image of NGC 1512 presented in Figure 2.5. The surface brightness level of the isophote is ∼ 20 mag arcsec^{-2}. The initial estimate of the inclination angle was then calculated as i = cos^{-1}(b/a) from the overlaid ellipse, with *a* and *b* being the major and minor axis of the ellipse respectively. The position angle was calculated from the north to the semi-major axis of the receding side of the galaxy. The GALEX UV center (Koribalski & López-Sánchez (2009)) of the galaxy was adopted as the initial estimate of the dynamical center position (i.e. x_c and y_c). For the systemic velocity the value calculated from the H I spectrum/profile (2.2) was adopted as the initial estimate and finally, an inclination corrected rotation velocity, i.e. $V_{rot} = 0.5W_{20}/\sin(i)$ (di Teodoro & Fraternali (2015)) was used as an initial estimate to the V_{rot} parameter of the tilted-ring model on ROTCUR, where W_{20} is the velocity width at 20% of the peak flux. The results of each iteration of ROTCUR are presented below in figures 3.1, 3.2, 3.3 and 3.4. Table 3.1 contains the initial estimates that were used as inputs in ROTCUR for this work and the work done by Koribalski & López-Sánchez (2009).

Table 3.1: Initial ROTCUR parameters for NGC 1512/10.

Parameter	This work	Koribalski & López-Sánchez (2009)
x_c	-43° 21′ 03″	-43° 21′ 03″
y_c	-43° 24′ 01″	-43° 24′ 01″
V_{rot}	196 km s^{-1}	∼ 150 - 200 km s^{-1}
V_{sys}	898 km s^{-1}	900 km s^{-1}
i	51°	∼ 35°
PA	260°	260°

All the parameters presented in the table above were derived originally from this work except for the center coordinates (i.e. x_c and y_c) that were adopted from Koribalski & López-Sánchez (2009).

UNIVERSITY of the WESTERN CAPE

http://etd.uwc.ac.za/

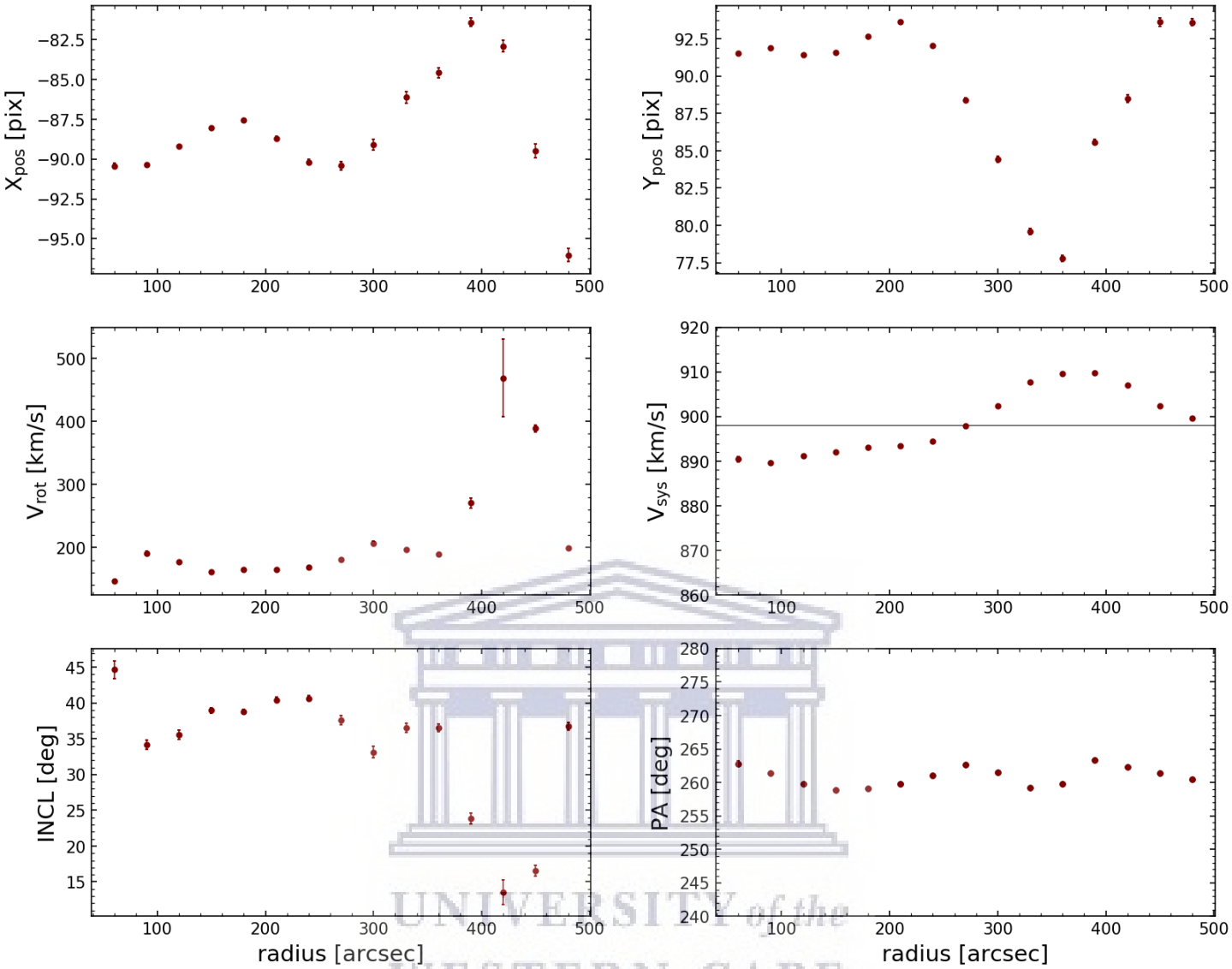

Figure 3.1: Iteration 1: All the parameters of the tilted-ring model varying freely with radius. The top row shows the radial runs of the x and y coordinates (x_c & y_c) which are the dynamical center coordinates of NGC 1512. The middle row shows the results of the rotation velocity (V_{rot}) and the systemic velocity (V_{sys}) after the first run. The horizontal line marks the systemic velocity of NGC 1512 as calculated from the global profile (Figure 2.2). The geometric parameters are presented in the last row, with inclination profile on the left and the position angle on the right. The error bars in each of the six panels represent the least-square errors.

The results for the first run of ROTCUR are shown in Figure 3.1. The dynamical center of the galaxy is converging to values of $x_c \sim$ -90 and $y_c \sim$ 91 in pixel units (according to the GIPSY software). These values were confirmed to correspond to the GALEX UV optical center position given in Table 1.1. For the second iteration, the dynamical center positions of the galaxy were fixed to these values. On the second iteration, the tilted-ring model parameter that is being fit is the systemic velocity (V_{sys}) of the galaxy. The results of the second iteration are presented in Figure 3.2.

UNIVERSITY of the WESTERN CAPE

http://etd.uwc.ac.za/

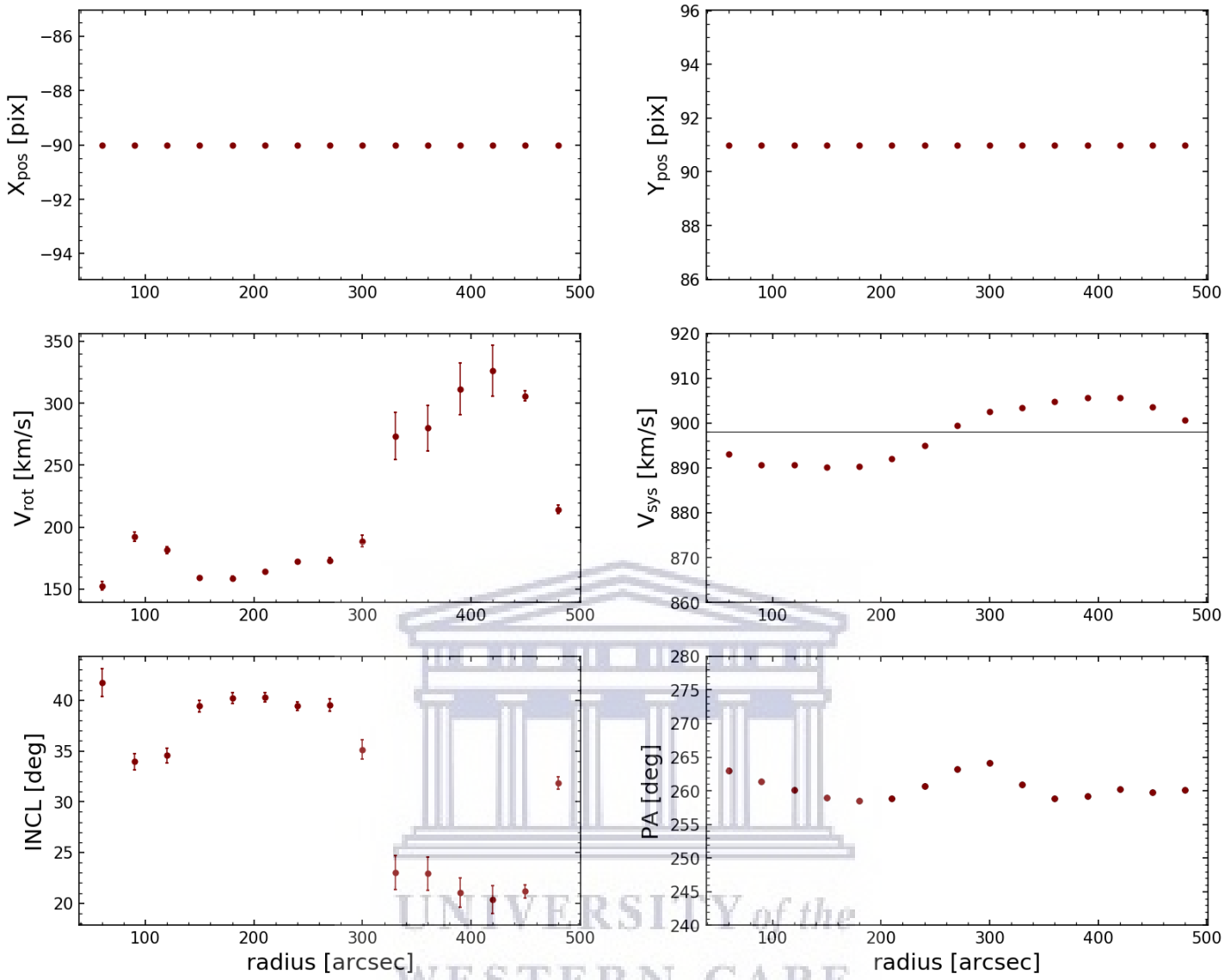

Figure 3.2: Iteration 2: As in Figure 3.1, but with the dynamical centre coordinates in the top row fixed from the first iteration.

The results of the second iteration shown in Figure 3.2 show that the systemic velocity of the galaxy varies around the value of the systemic velocity calculated from the global profile, V_{sys} = 898 km s^{-1}. We also note how the position angle profile is varying mildly around the initial estimate of 260°, with an average scatter of $\leqslant 5°$. The third iteration aimed to get a reliable best-fit value for the position angle, and fixed the systemic velocity to V_{sys} = 898 km s^{-1}.

UNIVERSITY of the WESTERN CAPE

http://etd.uwc.ac.za/

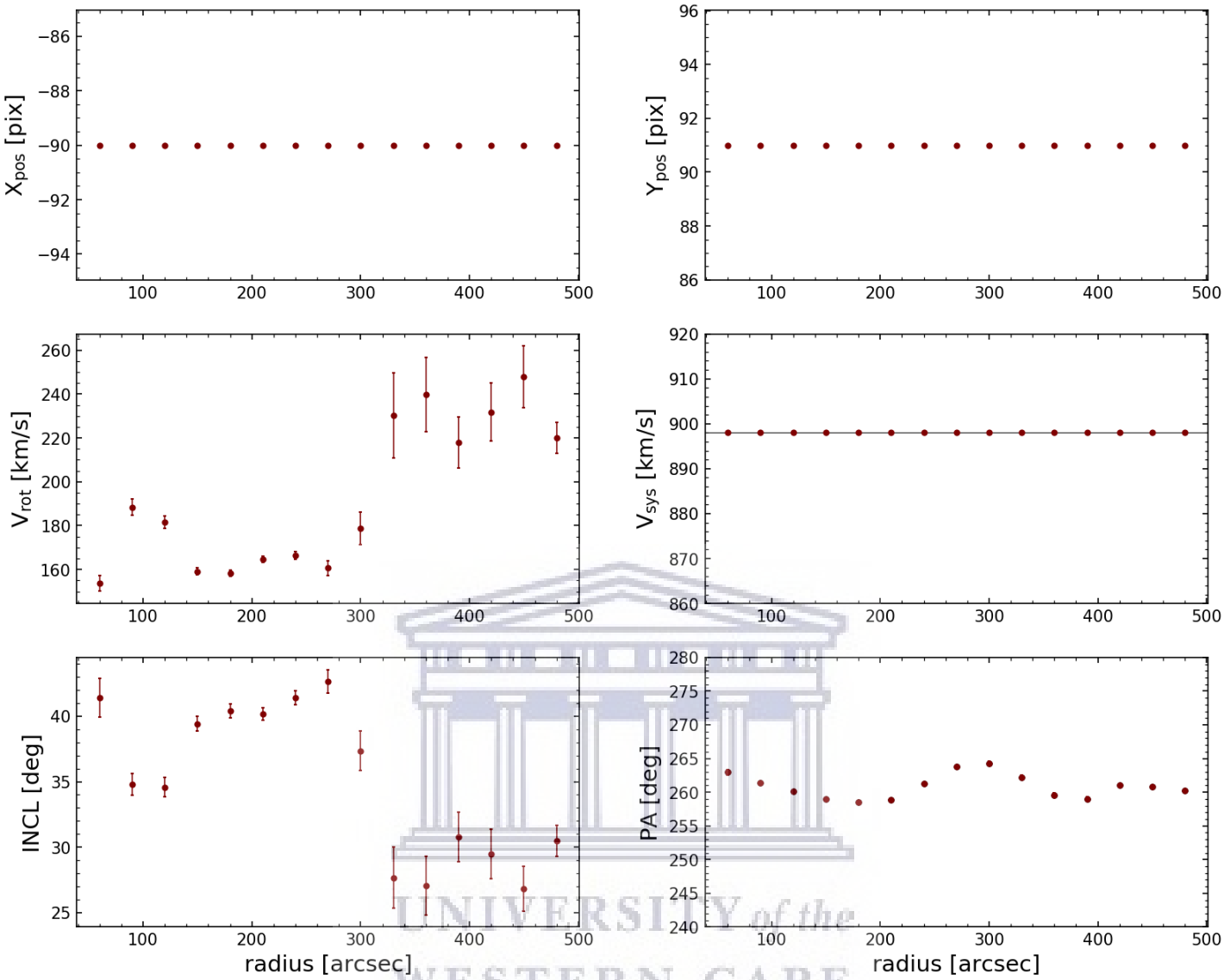

Figure 3.3: Iteration 3: The dynamical center positions and systemic velocity of the galaxy are fixed for the third iteration. The rotation velocity (V_{rot}), inclination and position angle of the galaxy are varying freely with radius in this iteration.

The results of the third iteration of ROTCUR are presented in Figure 3.3. The position angle of the galaxy varies around the initial estimate value of 260°. For the fourth iteration, we fixed the position angle to 260°. The fourth iteration fits the inclination angle parameter of the tilted-ring model. The best-fitting inclination angle results in the final rotation curve of the galaxy.

UNIVERSITY of the WESTERN CAPE

http://etd.uwc.ac.za/

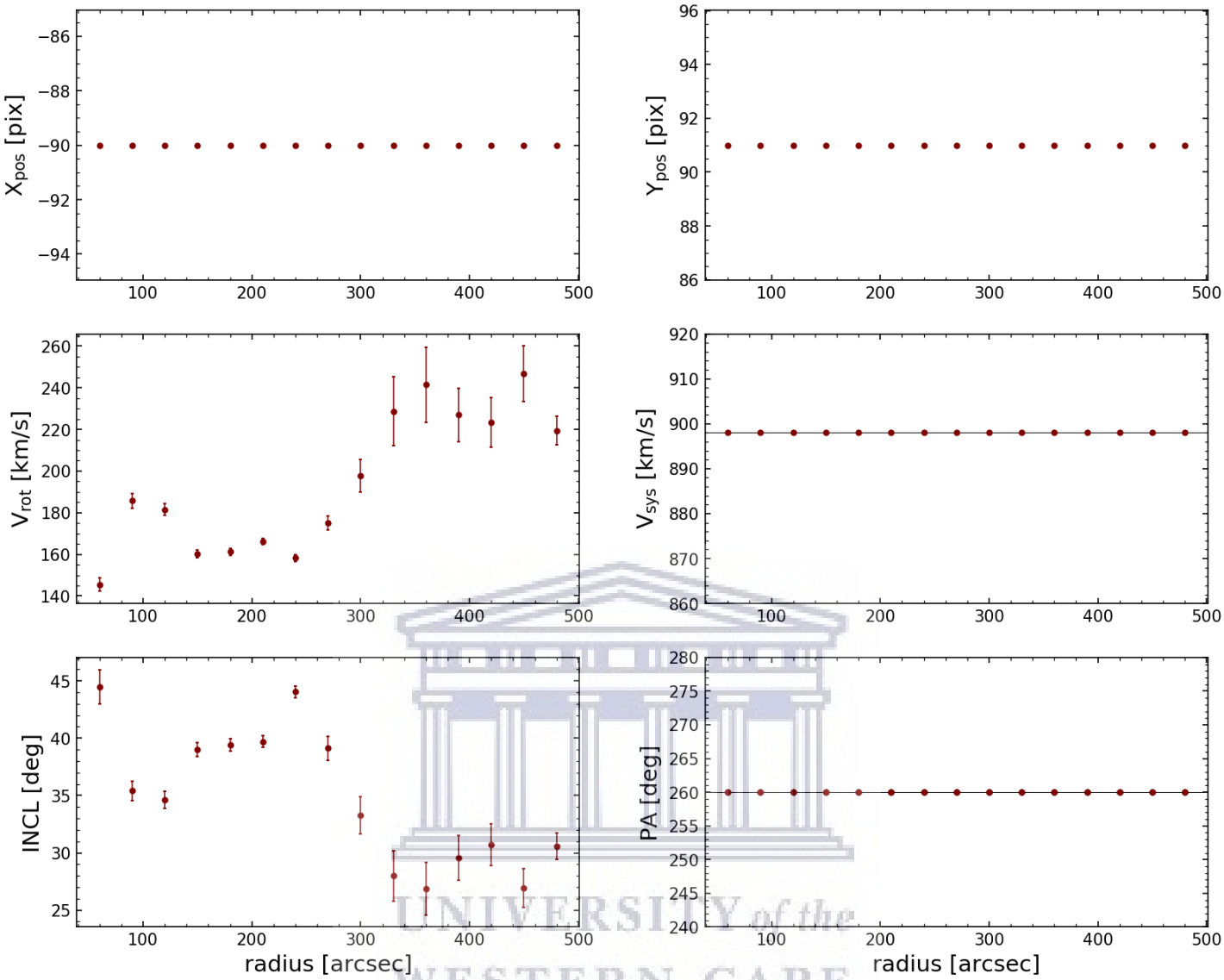

Figure 3.4: Iteration 4: The dynamical center positions, systemic velocity and the position angle parameters of the tilted-ring model are all fixed to the best fitting values. The inclination angle and the rotation velocity of the galaxy are varying freely with the radius.

The results of the fourth iteration are presented in Figure 3.4. The inclination angle of the galaxy changes significantly at r ~ 280 arcsec. At radii that are less than ~ 280 arcsec, the inclination angle of the galaxy averages ~ 40° and beyond r ~ 280 arcsec there is a sudden decline of the inclination angle to i $\lesssim$ 30°. At this radius occurs a large inter-arm region. This is seen clearly on the H I surface density map of NGC 1512/1510 presented in Figure 2.4. This result suggests that the H I disc of NGC 1512 does not have a uniform inclination angle. The non-uniform inclination angle of this galaxy might be resulting from the ongoing interaction of NGC 1512 with the blue compact dwarf galaxy NGC 1510.

The 2D tilted-ring model is only fitted to the velocity field of the galaxy and thus effects arising from the distribution of the H I gas are not accounted for. Noticing that the 2D tilted-ring model of NGC 1512 is affected by the perturbed distribution of the H I gas, we decided to use a modeling routine that would account for the galaxy's gas distribution. One such modeling technique is ^{3D}Barolo (di Teodoro & Fraternali (2015)).

UNIVERSITY of the WESTERN CAPE

http://etd.uwc.ac.za/

The rotation curve of NGC 1512 was produced by Koribalski & López-Sánchez (2009) using H I observations observed with ATCA. In their study, they used the 2D modeling routine, ROTCUR. A final rotation curve was achieved by adopting a constant inclination angle of $\sim 35^{\circ}$ for the entire H I disc of NGC 1512. However, it is not clear how the inclination angle of $\sim 35^{\circ}$ was obtained. The rotation curve of NGC 1512 generated by Koribalski & López-Sánchez (2009) goes out to a radius of r $\sim$ 1200 arcsec. Our results from the 2D tilted ring model suggest that the H I disc has a varying inclination angle with the radius. We also show that the rotation curve of NGC 1512 is less reliable beyond a radius of r $\sim$ 450 arcsec, largely due to the disturbed H I distribution beyond this point. The effect of the disturbed H I distribution in NGC 1512 is especially clear from the modeling with ROTCUR, which gives considerably varied results. We estimate the inclination angle of NGC 1512 by tracing the infrared disc of the galaxy with an ellipse. The inclination angle calculated from the ellipse is greater by 15° than the value used by Koribalski & López-Sánchez (2009). The systemic velocity and the position angle fitted parameters from this work agree well with the values found by Koribalski & López-Sánchez (2009). Also, the dynamical center from our tilted-ring model agrees very well with the values they found. Thus the disagreement between our work and the study of Koribalski & López-Sánchez (2009) arises from the inclination angle of the H I disc of NGC 1512.

http://etd.uwc.ac.za/

3.2 3D modeling - ^{3D}Barolo

The 2D modeling routine i.e. ROTCUR (Begeman (1989)), has been applied successfully to model the rotation curves of galaxies. However, it is often affected by several factors. Such factors are beam smearing, face-on inclination galaxy discs, asymmetric discs e.g. due to warping H I galaxy discs. Beam smearing results from the poor resolution of the telescope which causes the H I emission to be smeared on the adjacent regions (De Blok et al. (2008a)). The other problem which is often a burden to ROTCUR is the degeneracy between the rotation velocity and inclination angle. In Figure 3.4 the drastic change in the inclination angle of NGC 1512 induces a noticeable change in the rotation curve of the galaxy. The degeneracy between these two tilted-ring model parameters makes it impossible to determine one of these parameters separately (Begeman (1989)). Thus, to accommodate such effects we used the ^{3D}Barolo routine.

3.2.1 ^{3D}Barolo algorithm

^{3D}Barolo is a code that takes as an input a full 3D line-emission cube and fits a 3D tilted ring model to it (di Teodoro & Fraternali (2015)). The leading feature of this algorithm is that it creates a mock data cube based on the input. This is achieved by simulating a disc model of the galaxy at first. To seed the gas in the artificial disc model a Monte-Carlo approach is adopted. This is done by using a stochastic function that randomly populates both the spatial and velocity dimension with gas (di Teodoro & Fraternali (2015)). As in ROTCUR, the mock disc is broken down into a series of N concentric rings. The gas in these concentric rings is built on a 6D domain of parameters. Three of these parameters are spatial locations. These can be thought of as cartesian coordinates x, y and z. These spatial coordinates describe the locations of each gas particle in the mock disc. The three remaining parameters are the velocity coordinates i.e. v_x, v_y and v_z. These describe the velocity of each gas particle. The z-component in the velocity space, i.e. v_z, accounts for streaming motions in the mock disc. In the artificial disc model, each ring has radius R and width W.

As with ROTCUR, each of these rings is described by a set of parameters. Six of these parameters are similar to the ones of ROTCUR with additional three parameters, which are velocity dispersion (σ_{gas}), face-on column density (Σ) and scale-height of the gas disc (z_o). After the disc model has been created, the algorithm further convolves it to the same spatial resolution as that of the input line emission cube. This is achieved via a 2D Gaussian representing the point spread function (di Teodoro & Fraternali (2015)).

This set of rings is then projected onto the input 3D line emission cube and a thorough ring-by-ring comparison is done between the artificial disc and the data, starting from the inner-most defined disc and moving outwards. During this comparison at each step, if the model best represents the observations, the algorithm continues to the next ring, if not, the parameters of the model ring are updated until the model best represents the data.

Unlike most of the 2D modeling routines, ^{3D}Barolo is not based on any analytic function. A method of minimizing non-analytic functions by using a multidimensional simplex solver is adopted. This is also called the Nelder-Mead (Nelder & Meadf (1965)) method. The algorithm builds a function based on the initial guesses of the disc parameters provided by the user.

UNIVERSITY of the WESTERN CAPE

http://etd.uwc.ac.za/

This function then is passed to the minimization algorithm. As in ROTCUR, the initial guesses of the parameter can either be global or be specific to each ring. In cases where there are no initial guesses provided, the algorithm automatically estimates the initial parameters for the fit. This is one of the features that make this modeling algorithm extra-ordinary. However, it is strongly advised to provide initial guesses to the algorithm (di Teodoro & Fraternali (2015)).

^{3D}Barolo has lots of other interesting and useful features such as source detection. In a given dataset, ^{3D}Barolo, can identify all the sources and fit to each of them. One puzzling feature of this modeling technique is the automatic regularization of parameters. Unlike in ROTCUR, ^{3D}Barolo automatically fixes the model parameters to the best fitting profile on the second iteration.

The initial estimates that were used for the 3D modeling technique are $\sigma_{\rm disp} = 8$ km s^{-1}, and Z0 $= 35$ arcsec. The initial estimates of these two parameters are not important when modeling the kinematics of galaxies using the 3D modeling technique (di Teodoro & Fraternali (2015)), thus any sensible value can be used as an initial estimate. A total of 15 rings were used and the inner 30 arcsec of the galaxy was ignored. The width of each ring was set to dR $= 30$ arcsec. The weighting function was set to use $|\cos\theta|$ and the function to minimize the residuals between the data and the model was set to use the `chi-squared` (χ^2) function. The `SMOOTH` function was used to mask the cube and the `LOCAL` function was selected for normalization of the model cube. The common parameters between ^{3D}Barolo and `ROTCUR` were set to the ones given in table 3.1.

UNIVERSITY of the
WESTERN CAPE

http://etd.uwc.ac.za/

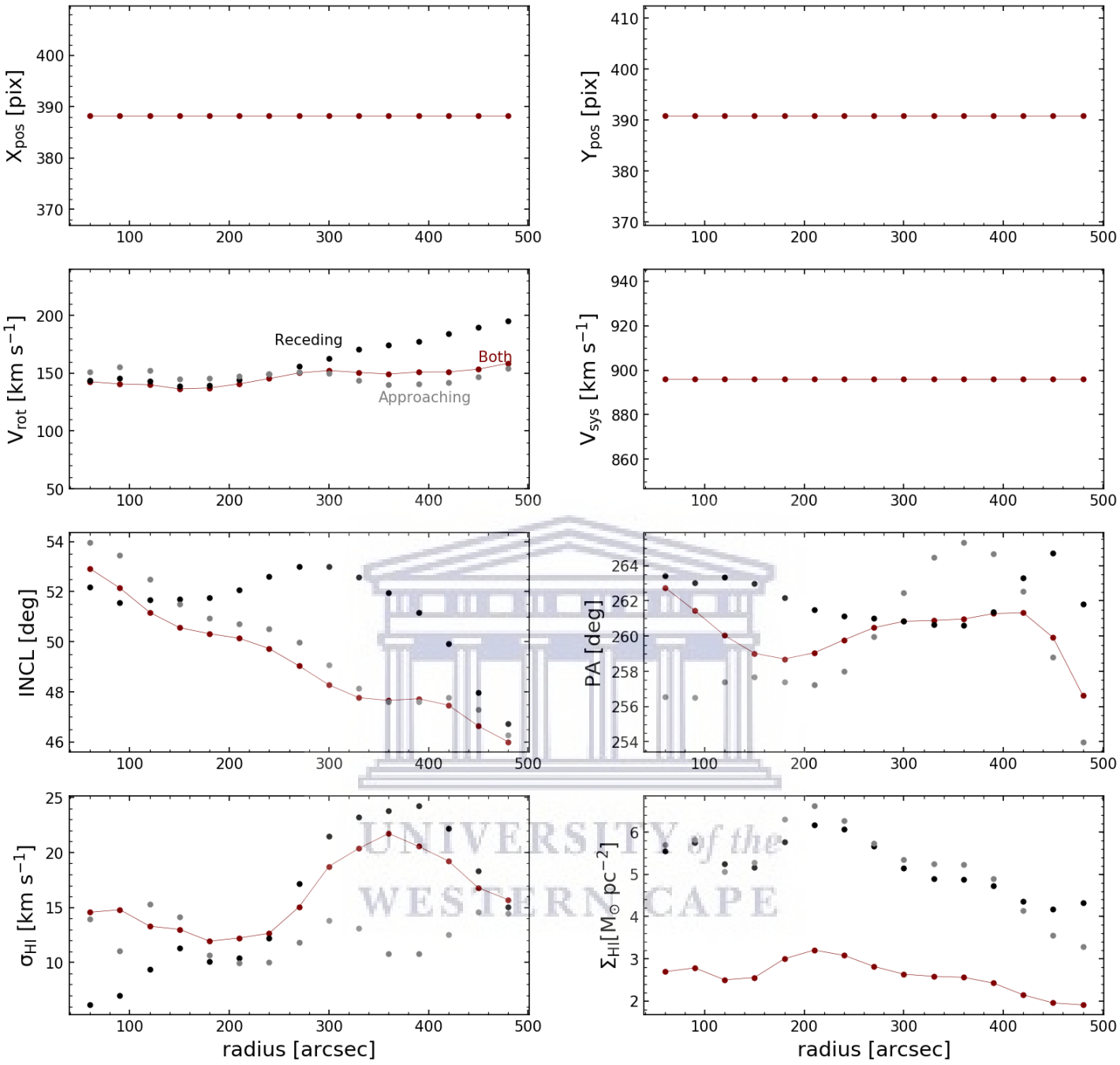

Figure 3.5: The dynamical model of NGC 1512 generated with the 3D modeling technique. The top row shows the dynamical center position of the galaxy in units of pixels. The second row presents the rotation curve (left) and the systemic velocity profile of the NGC 1512. Shown on the third row is the inclination angle (left) and position angle (right). The last row shows the gas dispersion velocity profile (left) and the H I surface density profile (right). The black points represent profiles of the receding side and the grey points represent profiles of the approaching side of the galaxy.

Figure 3.5 presents the results of the dynamical model of NGC 1512 from the second iteration of the 3D modeling technique. The dynamical center position, systemic velocity, and position angle profiles are similar to the results of the 2D modeling routine (Figure 3.4).The results of the 3D modeling routine suggest that the H I disc of NGC 1512 has an inclination angle of $\sim 51^\circ$ which is different from the one that was found by Koribalski & López-Sánchez

http://etd.uwc.ac.za/

(2009). We also modeled each side of the galaxy separately i.e. the receding and the approaching side. The rotation curve of the receding side of NGC 1512 differs at r ~ 300 arcsec from that of the approaching side. The rotation curve of both sides of the galaxy seems to be dominated by the rotation velocities of the approaching side at outer radii. The final rotation curve of NGC 1512 is fairly flat i.e. from the starting to the last measured radial point.

The shape of this rotation curve is different from the typical shape of the rotation curve of spiral galaxies, which usually has a steep rising part at inner radii and a flat behavior to outer radii. However, it is similar to the rotation curves of three spiral galaxies from the sample of galaxies studied by De Blok et al. (2008a). These three galaxies are NGC 2841, NGC 3031 or M81 and NGC 7331. These galaxies also have fairly flat rotation curves with the inner rising part missing. The inclination angle of the receding side of NGC 1512 only differs by ~ 4° from that of the approaching side. The difference is much more noticeable from r ~ 140 arcsec out to r ~ 440 arcsec. This peculiar inclination profile of NGC 1512 for the receding side of the galaxy might be largely due to the ongoing interaction with NGC 1510, which is located at the receding side of the H I disc of NGC 1512 (see Figure 2.6 in Chapter 2).

The position angle of the entire H I disc of NGC 1512 averages to 260°. The two sides of the galaxy have different position angle profiles. There is no significant difference in the radial H I surface density profile of NGC 1512 between the receding and the approaching sides. However, the radial H I surface density profile for both sides of the galaxy is lower by a value of 3 $M_{\odot}$ pc^{-2} to that of both the receding and approaching side of NGC 1512. At this point, it is not clear what may be the real cause of this difference.

UNIVERSITY of the
WESTERN CAPE

http://etd.uwc.ac.za/

3.2.2 Data-model comparison

To test the accuracy of the dynamical model (i.e. Figure 3.5) we compared the model data cube to the ATCA data cube. We first compared the channel maps of the ATCA data cube to those of the model cube produced from the 3D algorithm. This was done by overlaying the contours of the model cube onto the channel maps based on the ATCA data cube. This would show us if the model traces the emission in a convincing way. The data to model comparison through channel maps is presented below in Figure 3.6.

http://etd.uwc.ac.za/

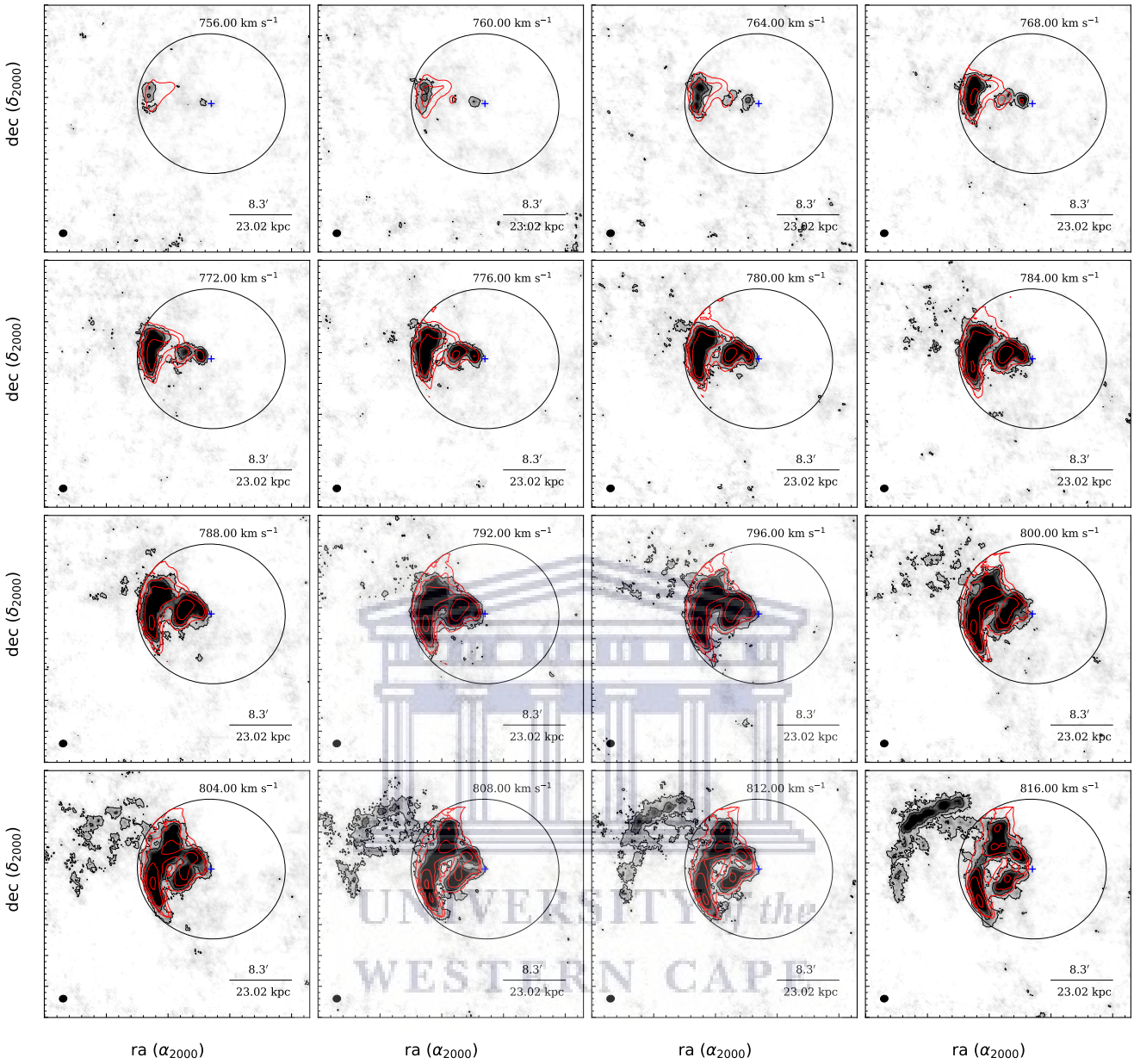

Figure 3.6: Selected H I channel maps of NGC 1512/1510 based on the robust ATCA data cube (greyscale range: –0.02σ to 10σ, where σ = 2.13 mJy/beam). Each channel spans a velocity width of 4 km/s, and the velocity of each channel is shown in the upper right corner of each panel. H I flux density contours representing the data are shown in black at levels of $\sigma 2^n$ and H I flux density contours representing the model are shown in red at levels of $\sigma_{model} 2^n$, where σ_{model} = 0.00625 mJy/beam and n = 1, 2, 3, ...,8. The blue cross in each panel marks the center estimated by the 3D modeling technique. The limit of the model is marked by the black circle. The synthesized beam of size 62.11″ × 55.31″ is shown in black at the bottom left corner of each panel.

UNIVERSITY of the WESTERN CAPE

http://etd.uwc.ac.za/

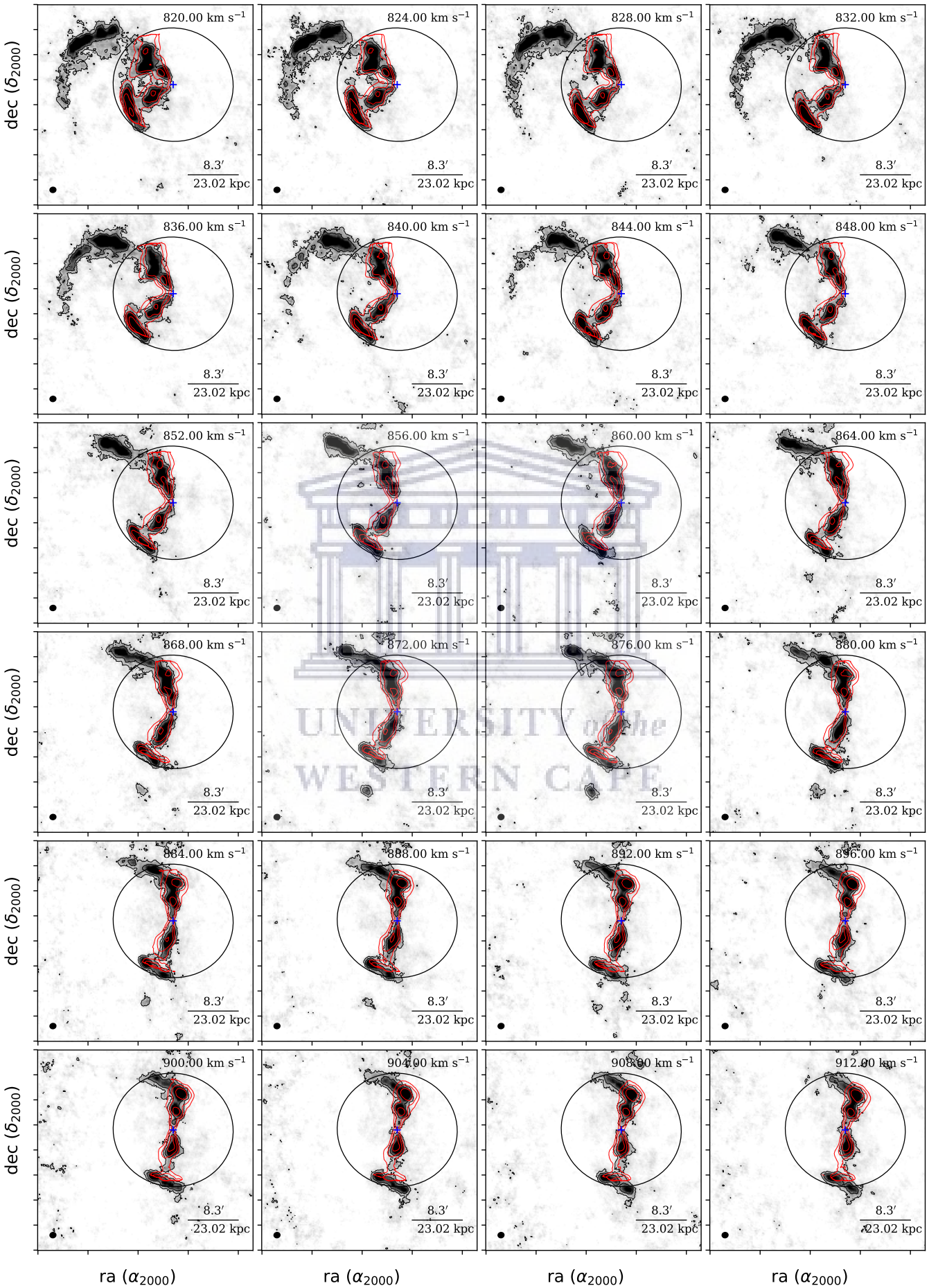

UNIVERSITY of the WESTERN CAPE

http://etd.uwc.ac.za/

Figure 3.6: Continued

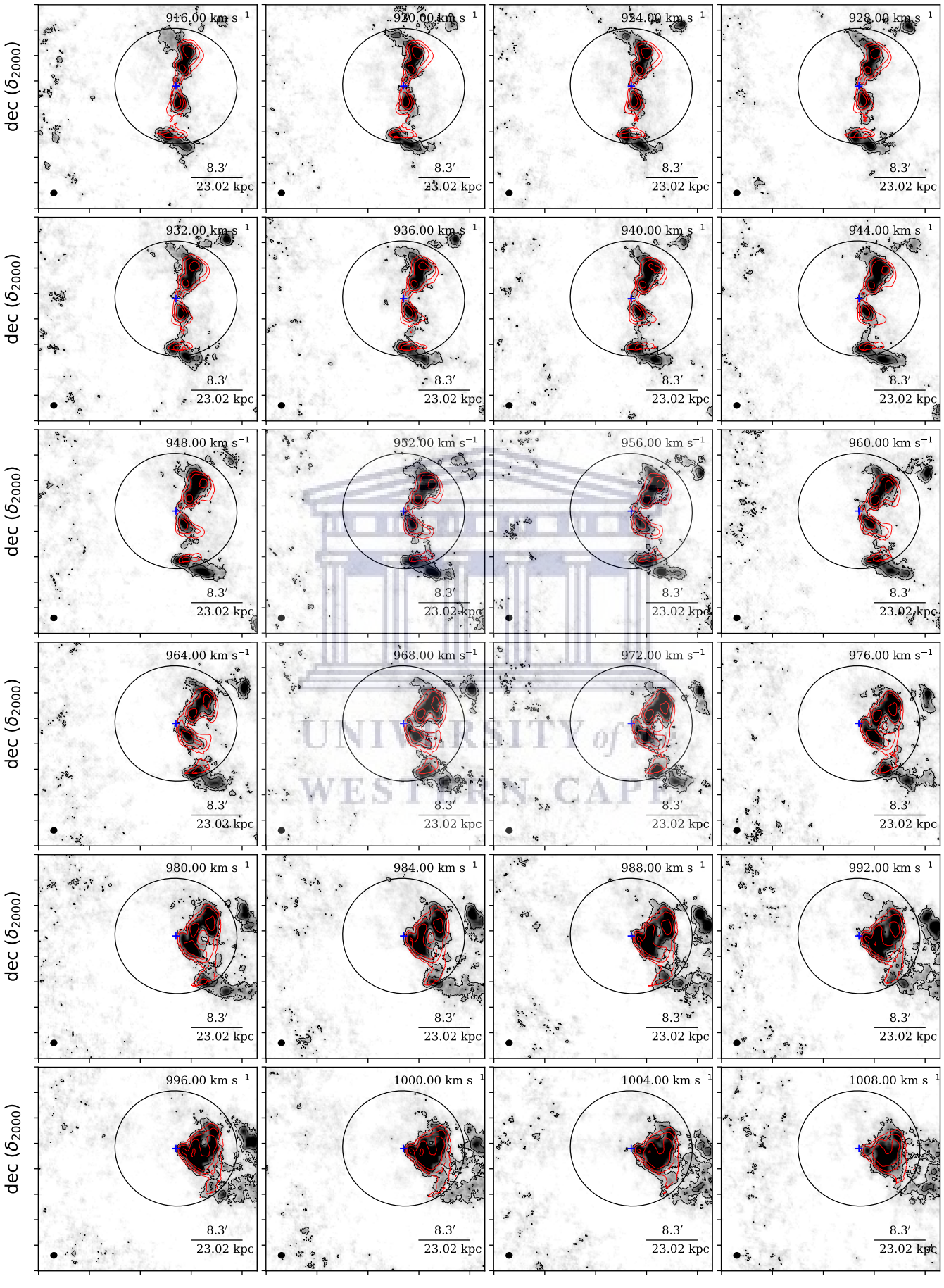

UNIVERSITY of the WESTERN CAPE

http://etd.uwc.ac.za/

Figure 3.6: Continued

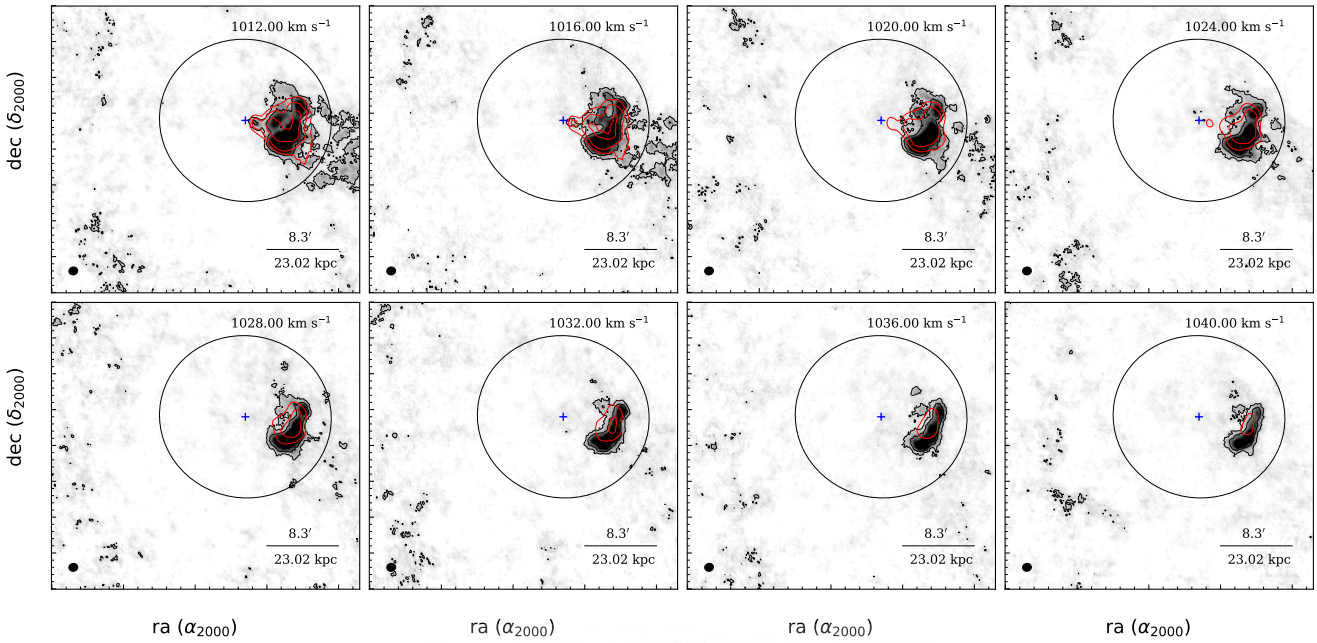

Figure 3.6: Continued

The comparison of the model to data presented in Figure 3.6 shows that the model and the data are in good agreement. This result shows that the dynamical model is reliable. However, the accuracy of results cannot depend on one comparison. Thus, we decided to do a second comparison of the dynamical model to data by comparing the position-velocity (PV) slices of the model cube to those of the ATCA data cube.

We extracted several PV slices from both the model cube and the ATCA data cube at four different angles starting from the fitted position angle (PA = 260°) of the galaxy and moving in steps of 45°. Thus, the PV slices were extracted at angles of 260°, 215°, 170°, and 125°. The PV slices from the ATCA data cube were overlaid with contours of the model cube from the 3D modeling technique. Several PV slices were extracted and compared to make sure that the model cube matches the ATCA data cube very well. Figure 3.7 below is the H I surface density map of NGC 1512/1510 showing the positions at which the PV slices were extracted. The positions of the PV slices are numbered from 1 to 14 and four different colors are used for each angle. The length of each of the PV slices was set to 220 pixels (1100 arcsec) and each PV slice has a width equal to 15 arcsec, which is about a fourth of the beam width (beam width = 62 arcsec).

http://etd.uwc.ac.za/

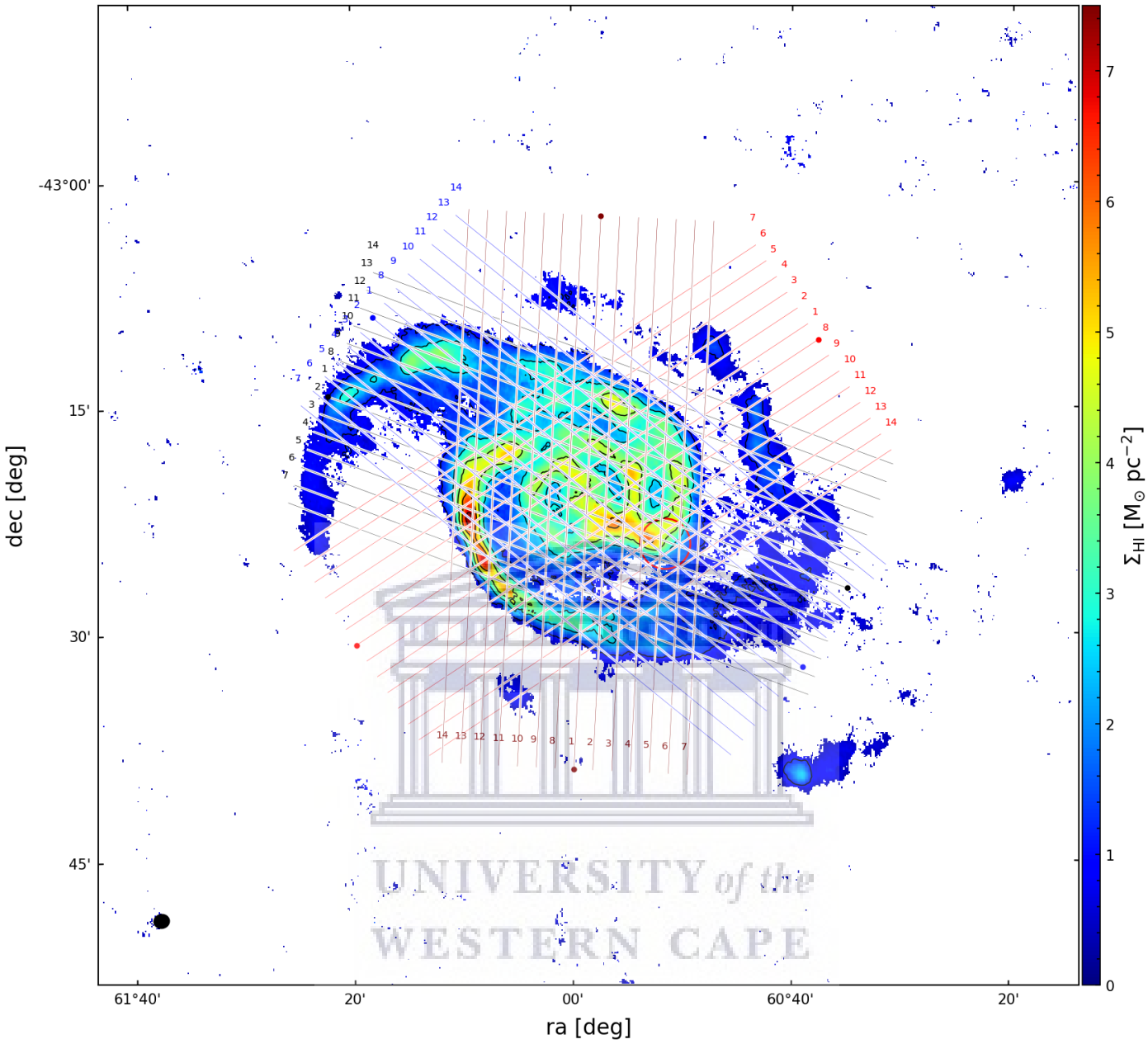

Figure 3.7: H I surface density map of NGC 1512/1510 showing the positions of the PV slices extracted at four different angles. The black color represents all the slices extracted at 260°, red at 215°, maroon at 170°, and blue at 125°. At each angle 14 PV slices were extracted.

Figure 3.8 below presents the comparison of model to data though PV slices.
The comparison of the model cube to the ATCA data cube shown in Figure 3.8 suggests that the model matches the data well. However, we note that in a few PV slices e.g. PV slice 14 at 260° the contours of the model are absent. This is because these PV slices were extracted at positions that are out of the limit of the model (the limit of the model is shown in Figure 3.6). This and the first comparison of the model cube to the ATCA data cube suggest that the dynamical model of NGC 1512 from the 3D technique is reliable.

The final rotation curve of NGC 1512 based on the 3D modeling routine (see Figure 3.5) is fairly straight from the first to the last measured point. This shape of the rotation curve is not suitable to carry out the mass-modeling of NGC 1512. Thus, a measure of the inner rotation

http://etd.uwc.ac.za/

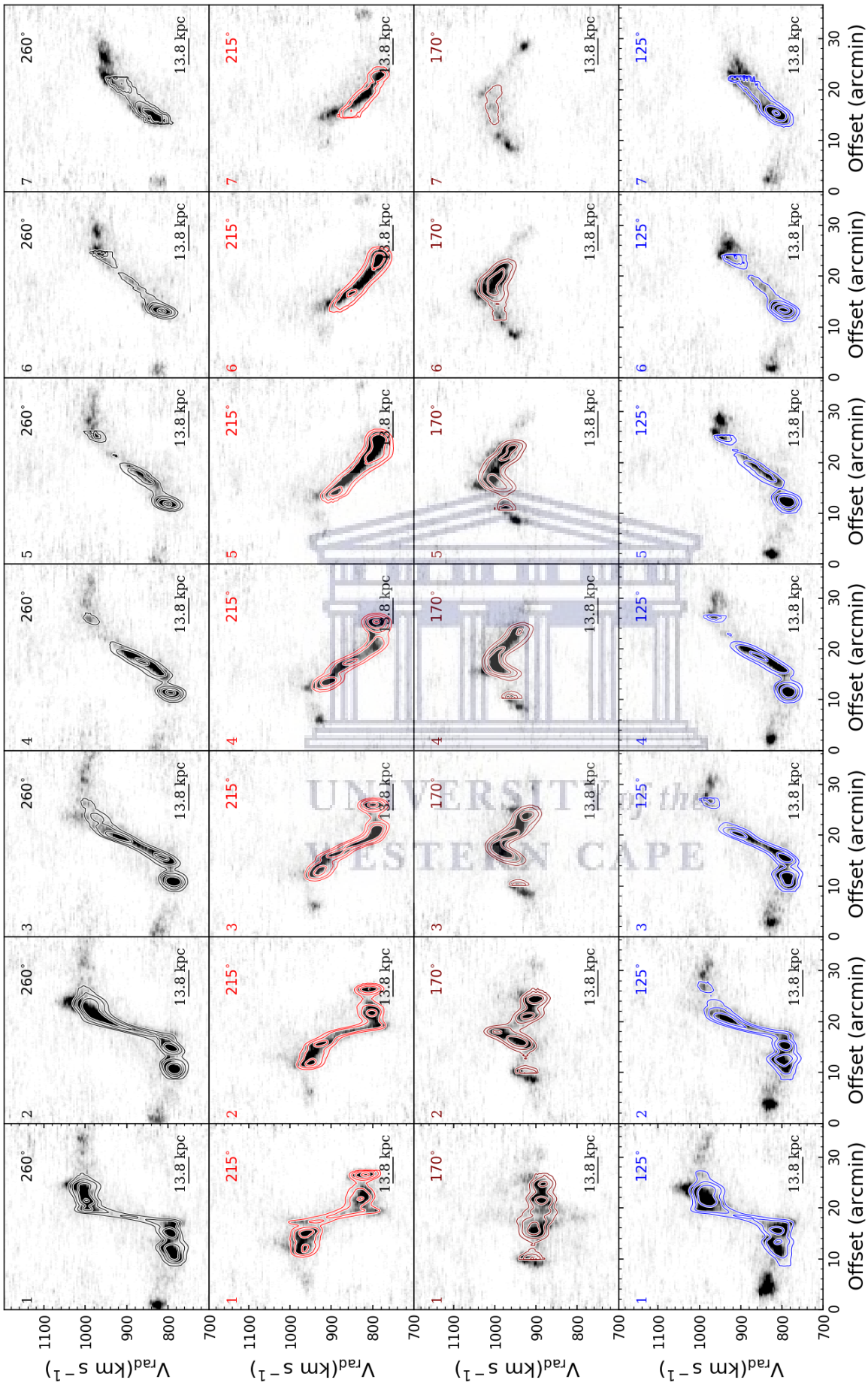

Figure 3.8: The PV slices from the robust-weighted ATCA data cube (greyscale ranges from -0.02σ to 10σ, where σ = 2.13 mJy/beam) overlaid with contours of the model cube generated using the 3D modeling approach. The contour levels are $2^n\sigma_{model}$ where $\sigma_{model} = 0.00625$ mJy/beam is the noise level of the model cube. The numbering and different colors correspond to the ones shown in Figure 3.7 above.

UNIVERSITY of the WESTERN CAPE

http://etd.uwc.ac.za/

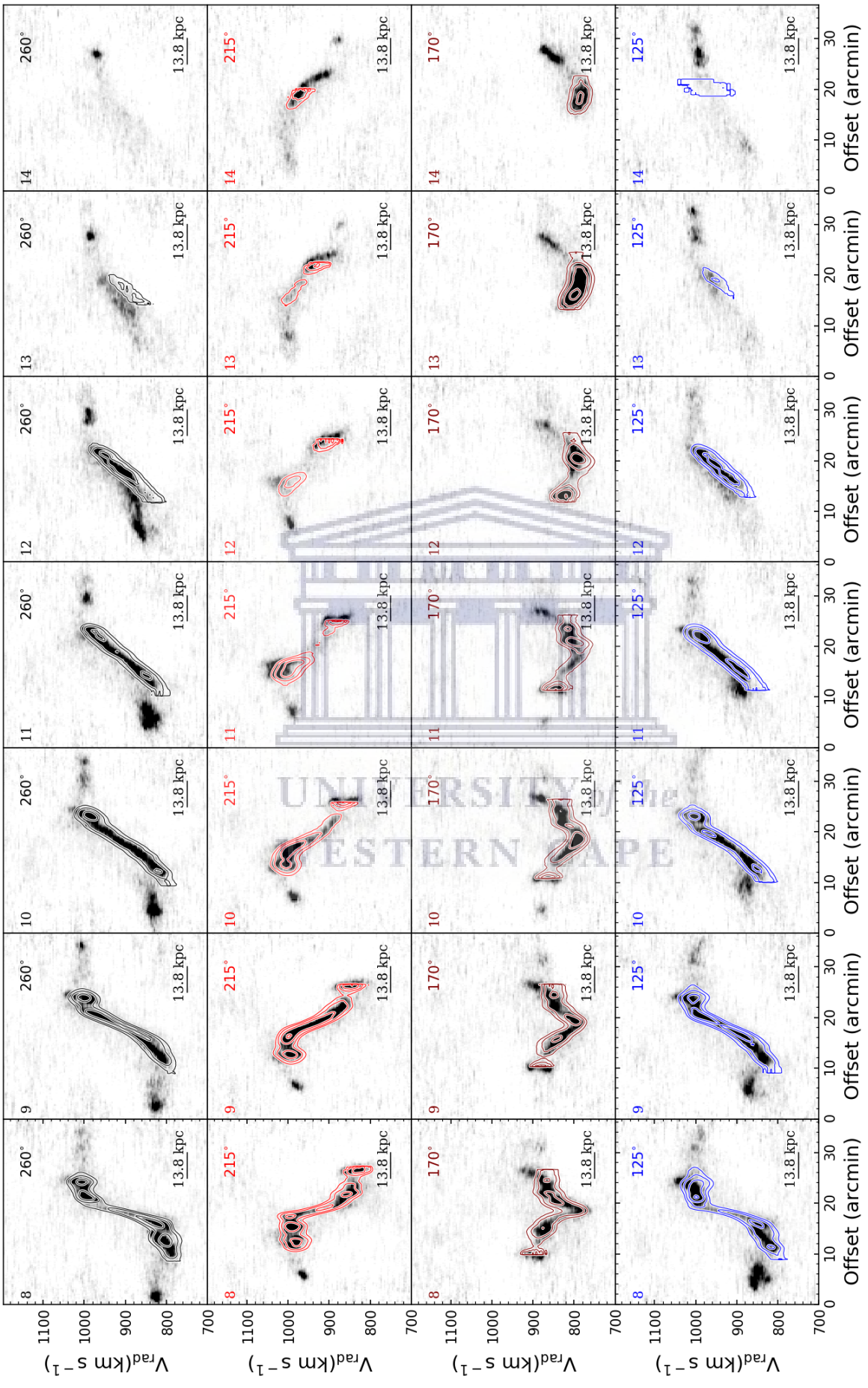

Figure 3.8: Continued

http://etd.uwc.ac.za/

curve is required to achieve a sensible mass-model of NGC 1512. We therefore adopt, in the next section, a new approach of generating such a rotation curve for NGC 1512.

3.2.3 Extracting rotation velocities from PV slice.

The new rotation curve of NGC 1512 was generated from the major-axis PV slice extracted from the ATCA data cube. The idea of generating a new rotation curve of NGC 1512 from the PV slice was to obtain a rotation curve with points at inner radii as already stated above. he major-axis PV slice was extracted at the average of the fitted position angle (260°) of NGC 1512 (see Figure 3.5). Figure 3.9 shows the major-axis PV slice of NGC 1512 based on the ATCA data cube. The position of the major-axis PV slice on the H I surface density map of NGC 1512/1510 is labeled number 1 in Figure 3.7, i.e. it passes through the fitted dynamical center of the galaxy which is (x_c, y_c) = (388.22 pixels, 390.81 pixels) (see Figure 3.5). The width of this PV slice is equal to 15 arcsec and its length is 220 pixels.

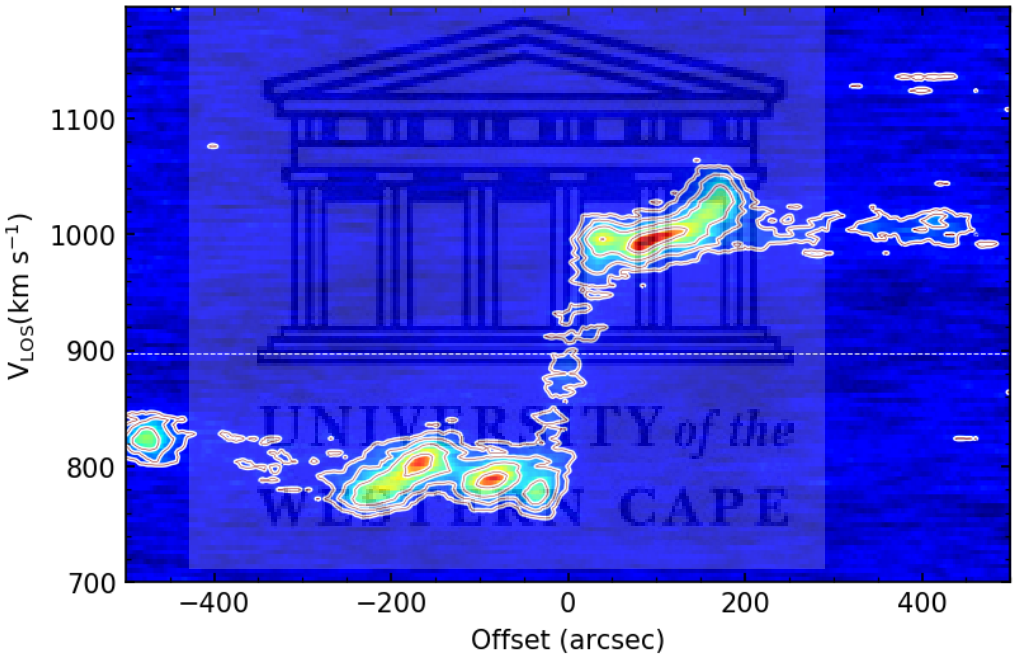

Figure 3.9: The major-axis pv slice as extracted from the ATCA data cube of NGC 1512. The dashed white line marks the systemic velocity of NGC 1512 at V_{sys} = 898 km s^{-1}. The contours levels are at $2^n\sigma$, where n = 0, 1, 2, ..., 8 and σ = 2.13 mJy/beam.

Figure 3.9 shows that the distribution of the H I gas on the receding side is different from that of the approaching side. This might be due to the ongoing interaction of NGC 1512 with NGC 1510. This then would allow us to carry out the mass-model of this galaxy.

The new rotation curve of NGC 1512 was generated by partitioning the major-axis PV slice into the receding and approaching side of the galaxy. The approaching side of the major-axis PV slice was transformed to match the PV slice of the receding side of the galaxy. The average of the two PV slice sides was taken. This was done to achieve a rotation curve of the galaxy that is based on both sides of the major-axis PV slice. A rotation curve based only on

http://etd.uwc.ac.za/

one side would impose uncertainties since the distribution of the H I gas is different on either sides. Figure 3.10 illustrates this process.

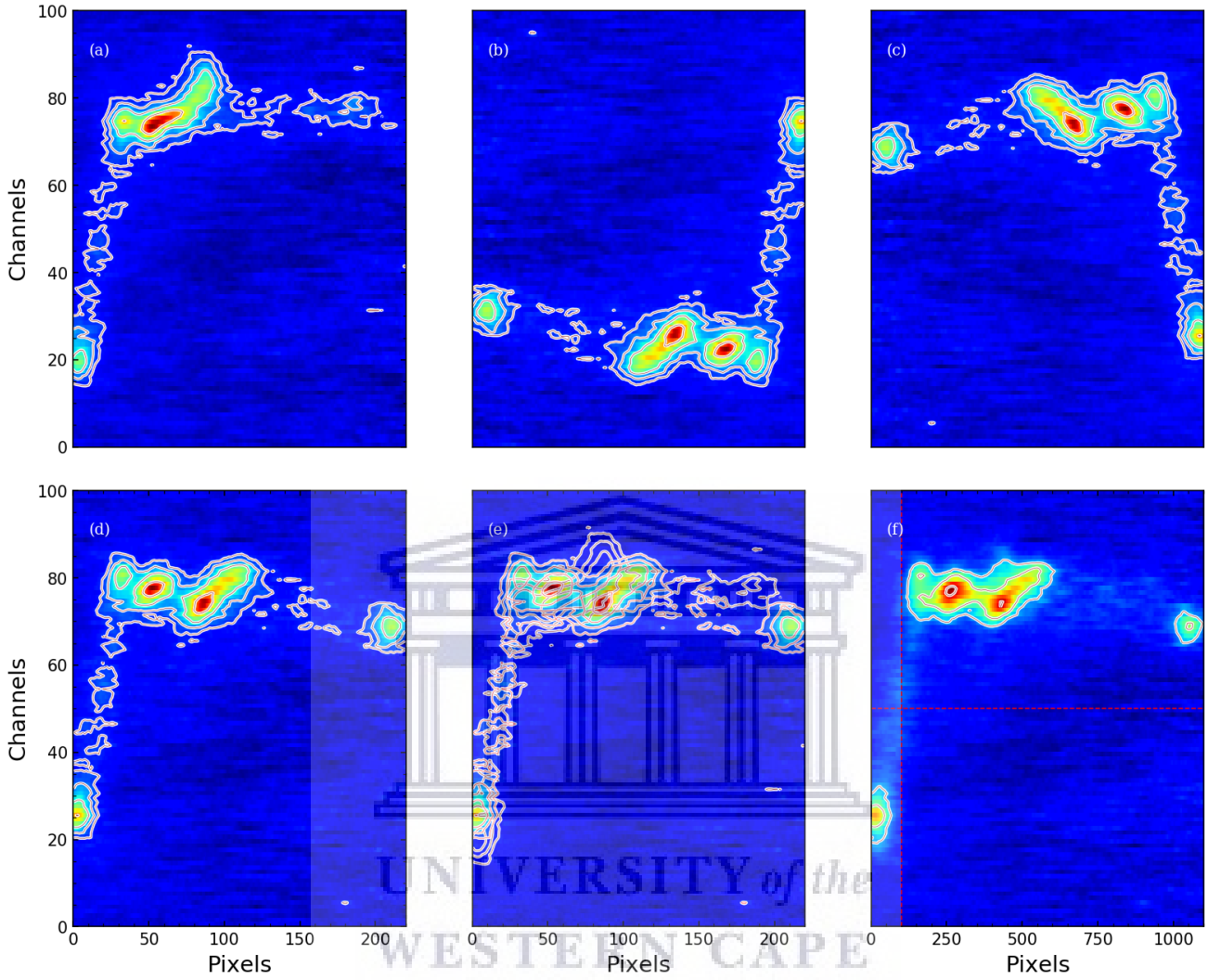

Figure 3.10: The major-axis PV slice of NGC 1512 partitioned into two sides. Panel (a) shows the receding/upper side of the PV slice. Panel (b) shows the approaching/lower side, (c) is the approaching side flipped with respect to the y-axis and in (d) panel (c) flipped again with respect to x-axis. In panel (e) the two sides are overlaid onto each and panel (f) shows the result of the average between the two sides. The vertical dashed red line shown in panel (f) marks the half of the full major-axis PV slice and the horizontal marks the middle channel.

After taking the average of the two sides, the resulting PV slice was convolved with a two-dimensional box to smooth it and also a flux cut at 1.3σ, where $\sigma = 2.13$ mJy beam^{-1} was applied. The smoothed PV slice of NGC 1512 was then binned into regions spanning 6 pixels each. The size of each pixel in the ATCA data cube is 5 arcseconds. So the bins were selected to span a size that is half the beam-size ($\sim$ 30 arcseconds). In each of the bins, the intensity weighted mean velocity was calculated. Figure 3.11 shows the smoothed version of the final PV slice and also the calculated intensity weighted mean velocities.

UNIVERSITY of the WESTERN CAPE

http://etd.uwc.ac.za/

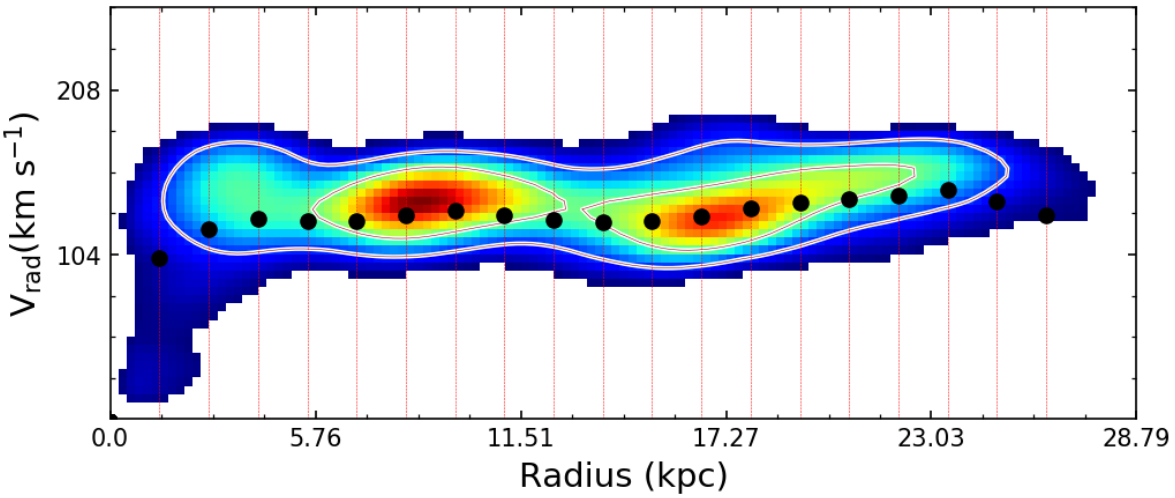

Figure 3.11: The smoothed and flux cut version of panel (f) in Figure 3.10. The black dots present the intensity weighted mean velocities calculated in each bin. The vertical red dotted lines mark the binned regions.

The velocities presented by black dots in Figure 3.11 were then extracted and corrected for inclination angle by dividing each velocity by sin(i) using the average of the fitted inclination angle $\sim 51^{\circ}$. The inclination corrected velocities were taken to be the new rotation curve of the galaxy NGC 1512. The aim of the rotation curve is primarily to carry out the mass-model of NGC 1512. The new rotation curve was parameterized with a polyex curve. As outlined in the work of Giovanelli & Haynes (2002), the polyex function takes the following form,

$$V_{pe}(r) = V_o(1 - e^{-r/r_{pe}})(1 + \alpha r/r_{pe}), \tag{3.4}$$

where V_o is the amplitude of the rotation curve, r_{pe} is the scale length for the inner steep rise of the rotation curve and α is the slope of the outer rotation curve. This parameterization of rotation curves has been used successfully to estimate the inner slope of the rotation curves as set by r_{pe} (Giovanelli & Haynes (2002)). The same formalism was adopted for this work, to smooth out the rotation curve generated from the major-axis PV slice. Figure 3.12 presents the rotation curve of NGC 1512 as extracted from the major-axis PV slice and also the fitted polyex curve to this new rotation curve is shown. We also plot the rotation curve of NGC 1512 based on the 3D modeling technique.

http://etd.uwc.ac.za/

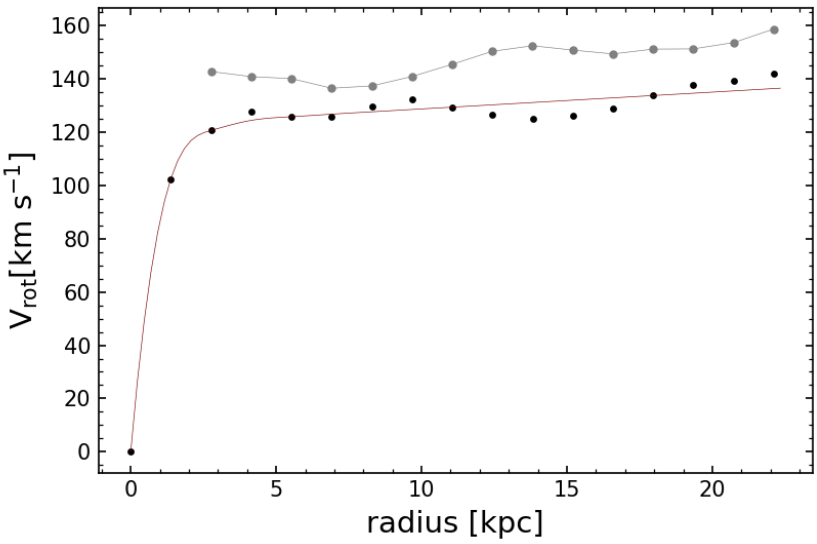

Figure 3.12: The new rotation curve of NGC 1512 as extracted from the major-axis PV slice (black dots) compared to the result of the 3D modeling routine (grey curve) fitted with Polyex curve (maroon curve). The point at (0, 0) was added manually to anchor the lower tail of the Polyex curve.

The new rotation curve of NGC 1512 was taken to be the fitted polyex velocities. The shape of the rotation curve of NGC 1512 generated from the 3D modeling is similar to the outer part of the new rotation curve. However, the new rotation curve of NGC 1512 derived from the major-axis PV slice has lower velocities than the rotation curve generated from the 3D modeling routine. One way to test the accuracy of the new rotation curve we took half difference between the H I spectrum (i.e. Figure 2.2) peak velocities. This difference when corrected for the inclination angle of the galaxy, i.e. by dividing with sin(i), it produces a value of $\sim$ 115.8 km s^{-1}, which matches well with the second data point of the pv-slice rotation curve. This difference might arise from the different techniques that were used to generate these two rotation curves. The new rotation curve has inner points making it suitable for the mass-modeling of NGC 1512. The fitted polyex curve was used as the input into the mass modeling routine. The mass-model of NGC 1512 is discussed in Chapter 4.

UNIVERSITY of the WESTERN CAPE

http://etd.uwc.ac.za/

Chapter 4

Mass distribution

4.1 NGC 1512 mass model

The distribution of dark matter in galaxies is one of the most studied fields in extra-galactic astronomy. There exists a disagreement between observations (Broeils (1992)) and simulations (Navarro et al. (1996)) on the distribution of dark matter in galaxies (see subsection 1.1.3). This is one of the reasons the distribution of dark matter is intensively studied. In this chapter we adopt two dark matter models, the pseudo-isothermal sphere (hereafter ISO) and the Navarro-Frenk and White (hereafter NFW), in modeling the distribution of dark matter in NGC 1512. We compare the results of these models to other galaxy mass models found in literature.

To quantify the amount of dark matter in NGC 1512 a mass model based on the rotation curve presented in Figure 3.5 was carried out. We used the GIPSY task ROTMAS to generate the mass model. ROTMAS is a task that performs a fit of the total velocities to the observed rotation curve of the galaxy. The total velocities are calculated as a quadratic sum of the velocities of all the mass components (e.g. gas, stars and dark matter halo) making up the galaxy and is given as:

UNIVERSITY of the
WESTERN CAPE

$$V_{tot}^2 = \alpha_{gas} V_{gas}^2 + \gamma_d V_d^2 + \gamma_b V_b^2 + V_{halo}^2, \quad (4.1)$$

where V_{gas}, V_d, V_b and V_{halo} are the contributions from the gas component which is assumed to consist of hydrogen (H) and helium (He) gases only, stellar disc, stellar bulge and dark matter halo respectively. V_{halo} for this work is calculated using two dark matter models i.e. ISO and NFW dark matter model (see below for discussion). $\alpha_{gas} = 1.4$ is defined as the scaling factor accounting for He to the gas component of the galaxy as done by De Blok et al. (2008b) and Oh et al. (2008). $\gamma_d = 0.5$ and $\gamma_b = 0.7$ (McGaugh & Schombert (2014)) are the mass-to-light ratios of the disc and bulge respectively, used to convert the observed stellar light into stellar-mass distribution.

The traditional procedure to obtain each of the rotation curves of the gas, stellar disc, stellar bulge and halo components is discussed below.

4.1.1 Gas contribution

The gas component considered for this work is the H I gas only. Using the GIPSY task ELLINT a new radial H I surface density profile was generated from the H I surface density

http://etd.uwc.ac.za/

map of NGC 1512/1510 presented in Figure 2.1.4. The ELLINT task is based on the same formalism as ROTCUR, the input map is broken into a series of concentric rings. The rings were set in a similar way with ROTCUR (see section 3.1 above). A constant position angle of 260° and a constant inclination angle of 51° were used. The optical center of the galaxy given in table 1.1 and distance of 9.5 Mpc were also adopted. In the ELLINT task the H I mass calculated from the H I surface density map was used (i.e. presented on table 2.3).

We note (see Figure 4.1) that the H I surface density profile does not decline exponentially at outer radii. In their work, Swaters et al. (2002) successfully fitted an exponential function onto the radial surface density profile of late-type dwarf galaxies. However, we note that our profile rather portrays a shifted Gaussian distribution. Thus following the work of Martinsson (2011), we fitted successfully a Gaussian function to our H I surface density profile. The fit is shown in Figure 4.1. Hereafter, this is referred to as a Martinsson profile. This parameterization was done to smooth the radial H I surface density profile which in return will produce a smooth rotation velocity for the gas component of NGC 1512. The form for the Martinsson profile is given as:

$$\Sigma_{\mathrm{H\,I}}(r) = \Sigma_{\mathrm{H\,I}}^{max} \exp\left(\frac{(r - r_{\Sigma,max})^2}{2\sigma_{\mathrm{H\,I}}^2}\right), \tag{4.2}$$

where $\Sigma_{\mathrm{H\,I}}^{max}$ is the amplitude of the H I profile, $r_{\Sigma,max}$ is the radius at which the amplitude occurs and $\sigma_{\mathrm{H\,I}}$ is the radial dispersion of the profile. The best fitting parameters are $\Sigma_{\mathrm{H\,I}}^{max}$ = 5.23 $M_\odot$ pc^{-2}, $r_{\Sigma,max}$ = 115.58 $''$ and $\sigma_{\mathrm{H\,I}}$ = 413.87 $''$. Figure 4.1 below shows the radial H I surface density profile of NGC 1512 fitted with a Martinsson profile.

UNIVERSITY of the WESTERN CAPE

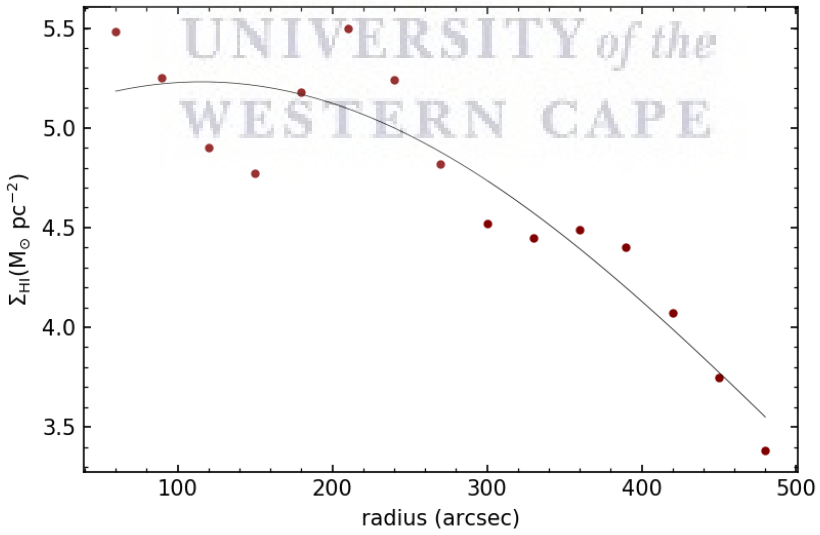

Figure 4.1: The H I surface density as a function of radius based on the H I surface density map of NGC 1512 (filled circles). The solid curve presents a Martinsson profile fit to the data.

The Martinsson profile was used to generate the rotation velocities of the gas component of NGC 1512. The GIPSY task ROTMOD was used to convert the surface density profile into rotation velocities, assuming an infinitely thin disc. The rotation curve of the gas component is presented in Figure 4.2 below.

http://etd.uwc.ac.za/

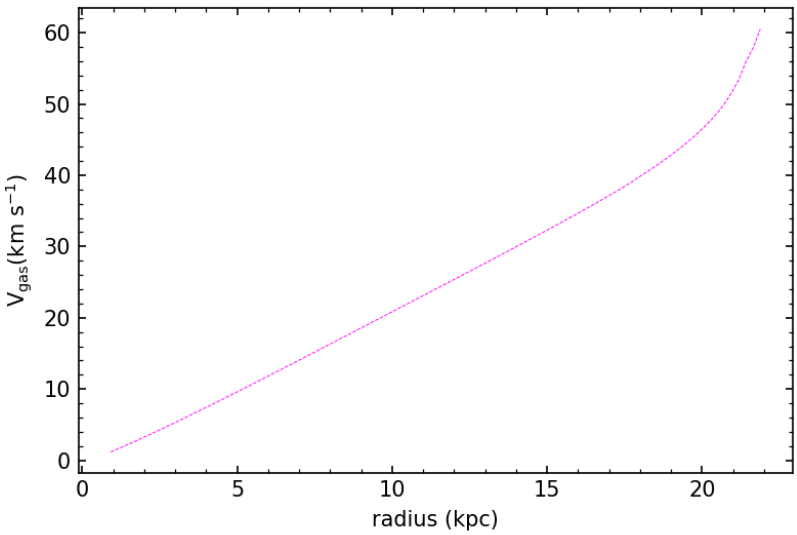

Figure 4.2: The rotation curve of the gas component of NGC 1512 generated using ROTMOD.

4.1.2 Stellar contribution

To quantify the distribution of stellar mass, a WISE 3.4 μm image of NGC 1512 was used. This imaging together with measured 3.4 μm radial surface brightness profiles was kindly provided by Prof T. Jarrett (private communication). The 3.4 μm radial surface brightness profile was given in units of apparent magnitude per square arcseconds (mag/arcsec^2). The stellar component is decomposed into a disc and bulge. Thus, two separate 3.4 μm radial surface brightness profiles, one for disc and the other for bulge, were received. To simplify the process, these were converted to radial surface density profiles in units of solar masses per square parsec ($M_\odot$/pc^2) following the formalism outlined in Cluver et al. (2014). The conversion is summarized below; for further discussions, see Cluver et al. (2014).

The apparent magnitude per square arcseconds (mag/arcsec^2) is converted to the absolute magnitude and then to stellar luminosities in units of solar luminosity per square arcseconds ($L_\odot$/arcsec^2) by:

$$\begin{aligned} M_\odot^{3.4} &= m_\odot^{3.4} - 5\log_{10} D + 5 \\ L_* &= 10^{(W_\odot^{3.4} - M_\odot^{3.4})/2.5}, \end{aligned} \tag{4.3}$$

where $W_\odot^{3.4} = 3.24$ (Cluver et al. (2014)), $D = 9.5 \times 10^6$ pc, is the distance of the galaxy, $M_\odot^{3.4}$ and $m_\odot^{3.4}$ respectively its absolute and apparent magnitudes.

Lastly, the radial surface density in units of solar masses per square arcseconds $M_\odot$/arcsec^2 is calculated as follows:

$$\Sigma_* = (M/L) \times L_*, \tag{4.4}$$

where M/L is the mass-to-light ratio. For the disc, M/L = 0.5 was adopted and for the bulge, M/L = 0.7 was used (McGaugh & Schombert (2014)).

http://etd.uwc.ac.za/

Using the fact that each pixel of the WISE 1 image corresponds to 0.9972″, which is equivalent to a physical size of 45.93 pc at the distance D = 9.5 × 10^6 pc to the galaxy, the surface density profile was converted to units of solar masses per square parsec ($M_\odot/pc^2$). Figure 4.3 presents the radial 3.4 μm surface brightness and the surface density profile for NGC 1512.

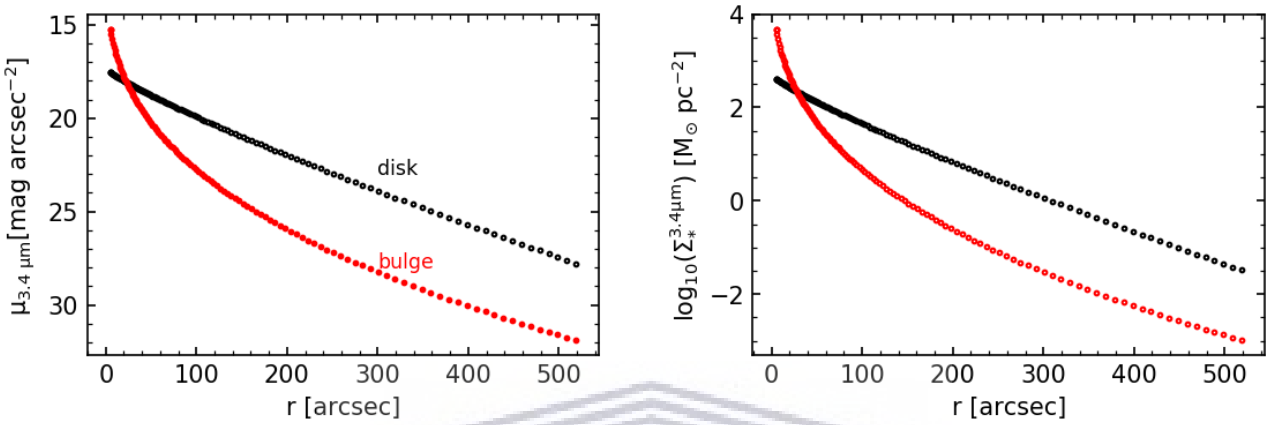

Figure 4.3: The radial surface brightness profile (left) and surface density profile (right) of the spiral galaxy NGC 1512 from WISE1 3.4 μm photometry.

From the 3.4 μm radial surface density profiles, the mass contained in both the bulge and the disc components of NGC 1512 was calculated. This is done through the following equation:

$$\frac{M_*}{M_\odot} = \int_{r_{min}}^{r_{max}} 2\pi \cdot \Sigma_*^{3.4\mu m} \cdot R \cdot dR, \tag{4.5}$$

where $\Sigma_*^{3.4\mu m}$ is the radial surface density profile of both the disc and the bulge and R is the radius, and r_{min} and r_{max} are 5″ and 518.67″ respectively. The mass of the disc of NGC 1512 found by integrating the black profile in Figure 4.3 is $M_{disc} = 1.19 \times 10^{10}$ $M_\odot$ and the mass of the bulge found is $M_{bulge} = 5.59 \times 10^9$ $M_\odot$.

As with the H I radial surface density profile, the disc and the bulge surface density profiles were used to generate the rotation velocities of these two components of NGC 1512. This was done using the GIPSY task ROTMOD. A sech-squared law was assumed for both the disc and the bulge. Figure 4.4 below presents the rotation velocities of the disc and the bulge components of NGC 1512.

UNIVERSITY of the WESTERN CAPE

http://etd.uwc.ac.za/

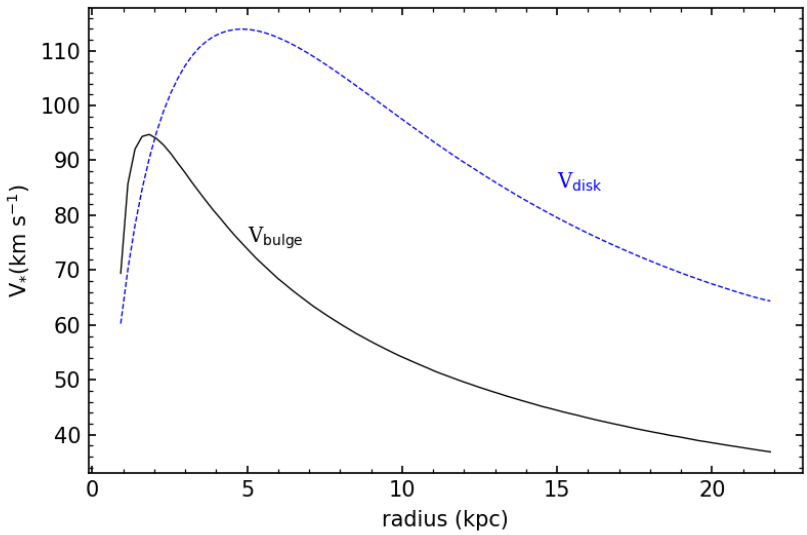

Figure 4.4: The rotation velocities of the stellar disc and stellar bulge components of NGC 1512 as generated from the GIPSY task ROTMOD.

4.1.3 Dark matter contribution

Dark matter halo models are used to account for the contribution of the dark matter in the total mass budget of a galaxy. The primary idea is that the contribution of the baryons i.e. stars and gas, is not enough to account for the observed rotation velocities (Navarro et al. (1996), Navarro et al. (1997)). Thus, dark matter is held responsible for the difference, hence the term 'residual velocities' (Oh et al. (2008)). This work adopts the two well-tested dark matter models: the ΛCDM NFW cusp-dominated and the ISO core-dominated dark matter halo. The two models were used to see which one recovers the observed rotation velocities of NGC 1512 better. The outline of the two models is given below.

NFW dark matter model

Numerical simulations of the hierarchical growth of structure in a Lambda-CDM are used study the distribution of dark matter in galaxies (Navarro et al. (1996), Springel et al. (2008)). This cuspy density distribution is called the 'universal density profile'. The NFW density profile is given in the form:

$$\rho_{NFW}(r) = \frac{\rho_i}{(R/R_s)(1+R/R_s)^2}, \tag{4.6}$$

where ρ_i is the called the critical density given by: $\rho_i = \frac{3H^2}{8\pi G}$, with H the Hubble constant and G the gravitational constant. R_s is the characteristic radius of the dark matter halo. The rotational velocities corresponding to the dark matter halo are given as:

$$V_{NFW}(R) = V_{200}\sqrt{\frac{\ln(1+cx) - cx/(1+cx)}{x[\ln(1+c) - c/(1+c)]}}, \tag{4.7}$$

where c is the concentration parameter given by: $c = R_{200}/R_s$. R_{200} is the radius at which

http://etd.uwc.ac.za/

the halo density is 200 times greater than the critical density of the universe with V_{200} being the velocity occurring at that radius. x is given by: $x = R/R_{200}$.

ISO dark matter model

The ISO dark matter halo model is motivated by observations. This model suggests a constant density on the core of the galaxy (Oh et al. (2008), De Blok et al. (2008a)). In other terms this is described as follows: $\rho_{iso} \propto R^{o}$ towards the center of the galaxy and $\rho_{ISO} \propto R^{-2}$ in the outskirts of the galaxy. The ISO density profile is described by:

$$\rho_{iso}(r) = \frac{\rho_o}{1 + (R/R_c)^2}, \tag{4.8}$$

where ρ_o and R_c are respectively the central density and the core radius of the dark matter halo. The rotation velocities following this density profile are given as:

$$V_{iso}(R) = \sqrt{4\pi G \rho_o R_c^2 \left[1 - \frac{R_c}{R} tan^{-1}(\frac{R}{R_c})\right]}. \tag{4.9}$$

4.1.4 Mass model results

To model the dark matter content of NGC 1512 we made use of the GIPSY package ROTMAS. This routine takes as input the gas velocities, and the stellar velocities comprised of disc and bulge velocities. Then it performs a fit with either NFW or ISO halo model depending on the user's choice. For this work, both halo models were used. In the Figure 4.5 we present all the rotation curves of the mass components found in NGC 1512 without fitting any halo model.

UNIVERSITY of the WESTERN CAPE

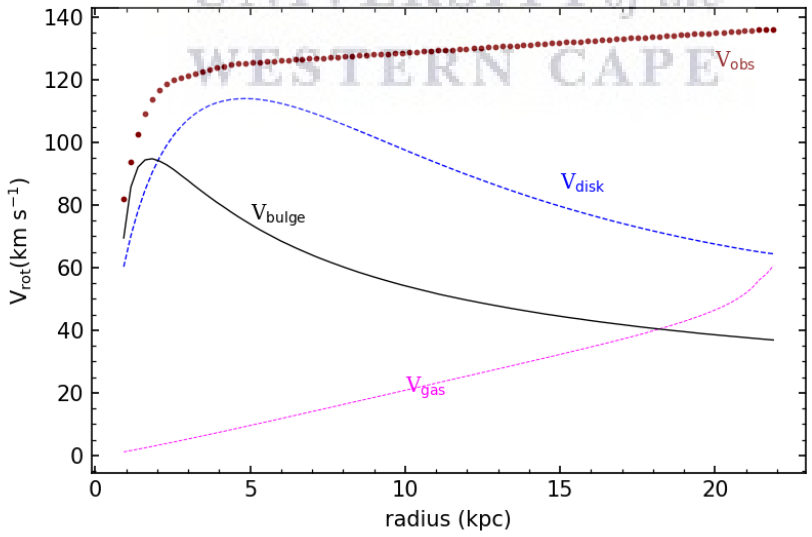

Figure 4.5: The rotation curves for all the mass components of NGC 1512. Each rotation curve is labelled according to the corresponding mass component.

Figure 4.6 presents the best fit case of the ISO halo model. On the best fit case the mass-to-light ratio of the disc and that of the bulge component of the galaxy i.e. γ_{disc} and γ_{bulge} vary

http://etd.uwc.ac.za/

freely. The mass-to-light ratio of the gas component is fixed to $\alpha_{gas} = 1.4$. The best-fitting parameters are quoted in table 4.1.

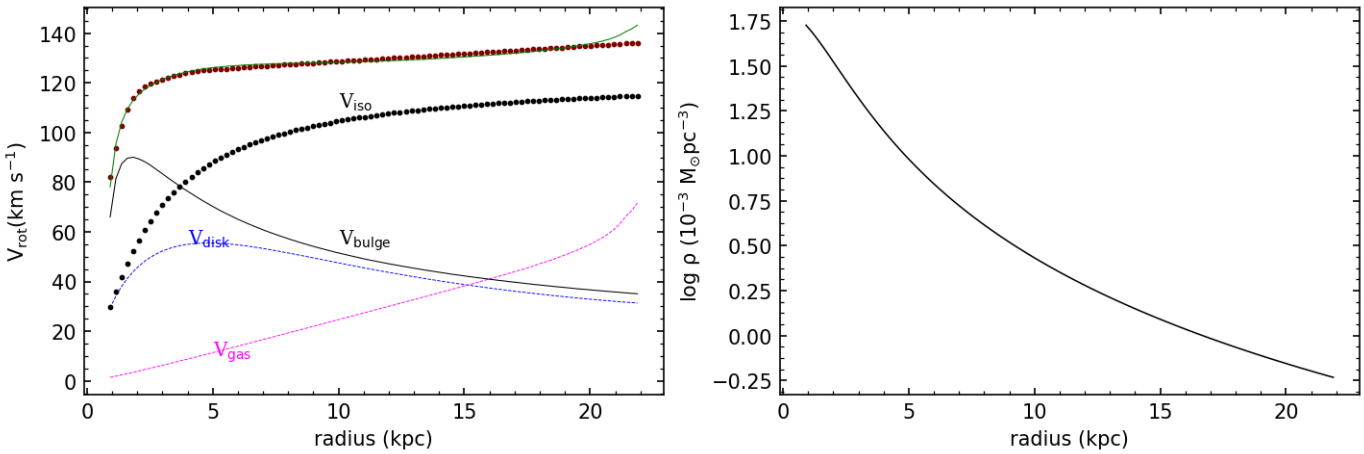

Figure 4.6: The best fit case of NGC 1512 using the ISO halo model. The rotation velocities are labelled according to their corresponding mass components (left). The green curve shows the total velocities through equation 4.1 and the maroon dotted curve shows the observed rotation curve of NGC 1512. Presented on the right is the density distribution following equation 4.8 for the ISO best fit case.

The total velocities from the best fit model match very well with the observed rotation curve with a reduced chi-square (χ^2_{red}) value of 2.45 (see table 4.1). One can also note that the bulge is dominant over the dark matter halo of NGC 1512 out to a radius of r $\sim$ 4 kpc. For the ISO halo model, two more fits were performed. One is where there is no contribution from the gas, stars, and bulge (referred to as the minimum disc case) and the second one is the fixed disc case where the mass-to-light ratios of the stellar bulge and stellar disc are fixed to values of 0.7 and 0.5 respectively. Figure 4.7 presents the fit obtained when a minimum disc case was assumed for NGC 1512.

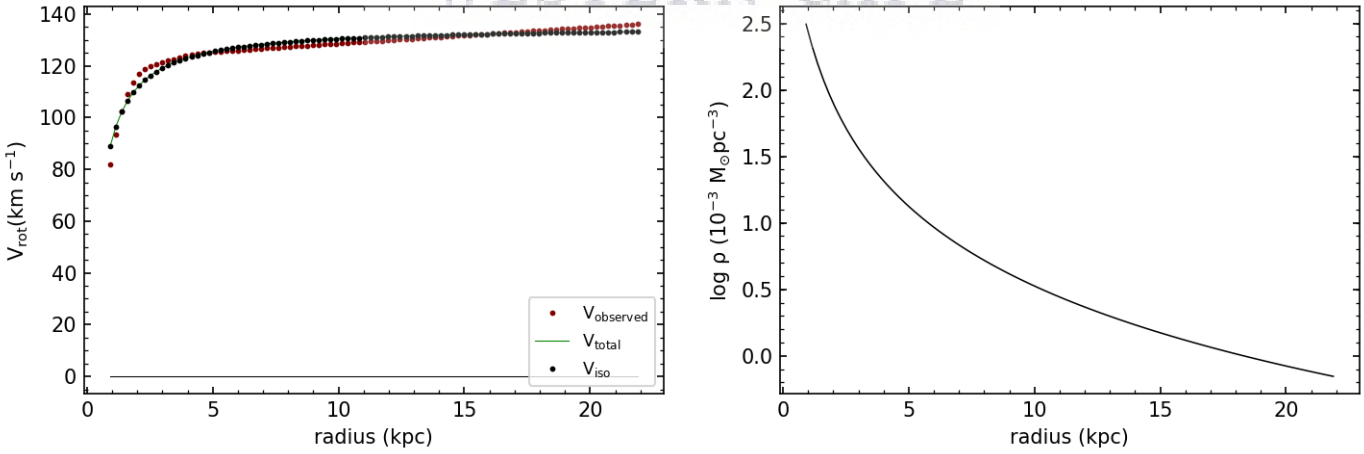

Figure 4.7: The results of the mass model of NGC 1512 based on the assumption of total no contribution from the baryons. The black dotted curve presents the ISO dark matter halo velocities, the green curve is the total velocities and the maroon dotted curve is the observed rotation velocities of NGC 1512. Presented on the right is the density distribution based on the minimum disc case.

Figure 4.7 shows that the total velocities are made up of the dark matter halo velocities

http://etd.uwc.ac.za/

only i.e. the black dotted curve matched the green curve at all radii. However, the reduced chi-square value for this case ($\chi^2_{red} = 3.51$) is greater than that of the best fit scenario. This suggests that the contribution of the baryons is needed to achieve a better mass model of NGC 1512. The following case is the fixed disc model. This case fixes the mass-to-light ratio of the disc and bulge to values of 0.5 and 0.7 respectively and only fits the core density and the core radius.

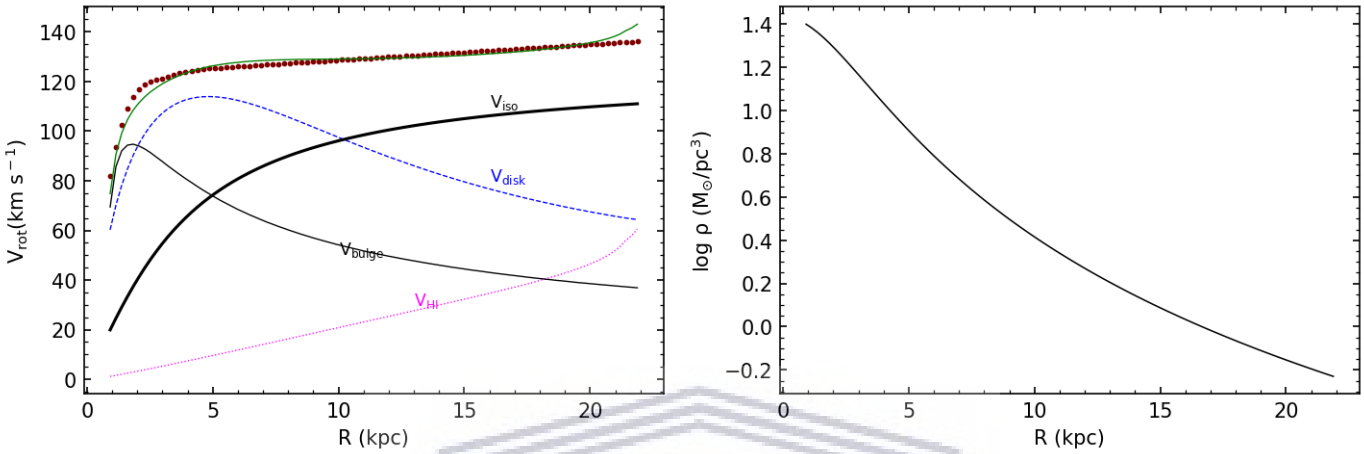

Figure 4.8: The results of the mass model of NGC 1512 assuming the fixed disc case. The curves have the same interpretation as in Figure 4.6. On the right is the density distribution based on the fixed disc case.

The fixed disc case also recovers the observed rotation velocities of NGC 1512 achieving a reduced chi-square value of $\chi^2_{red} = 4.45$. The best fit case suggests that the stellar bulge component favors a higher mass-to-light ratio than 0.7, with the stellar disc component favoring a lower value than 0.5.

Using the NFW halo model the three cases discussed above i.e. the best fit case, minimum disc case, and the fixed disc case were also modelled. The best fit case of the NFW halo model has $\gamma_{\rm disc}$ and $\gamma_{\rm bulge}$, r_{200}, and c as varying parameters. Figure 4.9 presents the best fit case of the mass model of NGC 1512 using the NFW halo model.

UNIVERSITY of the WESTERN CAPE

http://etd.uwc.ac.za/

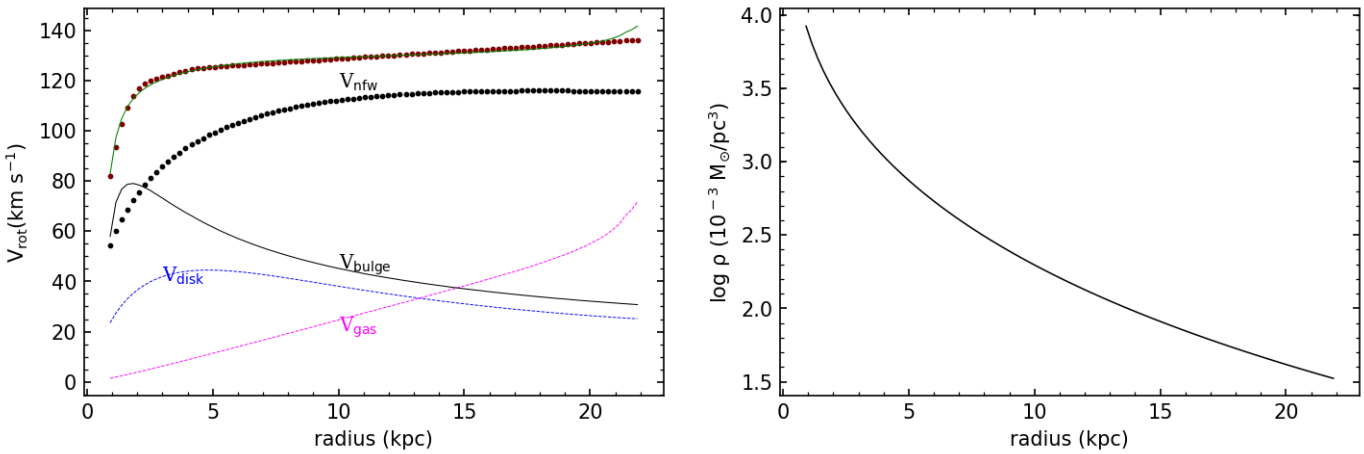

Figure 4.9: The best fit case of NGC 1512 using the NFW halo model. The curves are similar to those presented in Figure 4.6. Presented on the right is the density distribution of NGC 1512 based on the best fit case of the NFW halo model.

In Figure 4.9 the total velocities match very well with the observed rotation curve of NGC 1512. The mass in the bulge dominates the gravitational potential out to r ~ 3 kpc. Beyond this point the dynamics are dominated by the dark matter halo. For both the NFW and ISO halo models, we note how the best fit model suggests a lower mass-to-light ratio of the stellar disc component. Figure 4.10 shows the results of the mass model of NGC 1512 when assuming a minimum disc case using the NFW halo model.

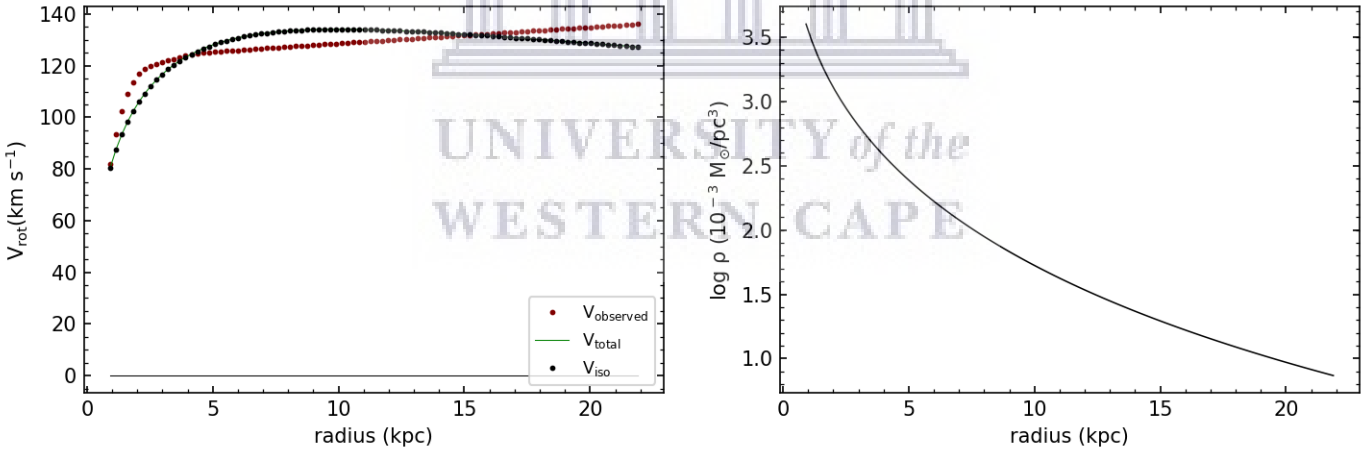

Figure 4.10: The minimum disc scenario of the NFW halo fit shown on the left, with density distribution on the right. The black dotted curve presents the NFW dark matter halo velocities, the green curve presents the total velocities and the maroon dotted points presents the observed rotation velocities of NGC 1512.

The minimum disc case shown in Figure 4.10 suggests that the baryonic matter is of larger dynamical importance than the dark matter mass. This is the case for both dark matter halo models i.e. ISO (see Figure 4.7) and NFW. However, the ISO halo model performs better, with $\chi^2_{\rm red} = 3.51$, than the NFW halo model which achieves a reduced chi-square value of $\chi^2_{\rm red} = 26.74$.

UNIVERSITY of the WESTERN CAPE

http://etd.uwc.ac.za/

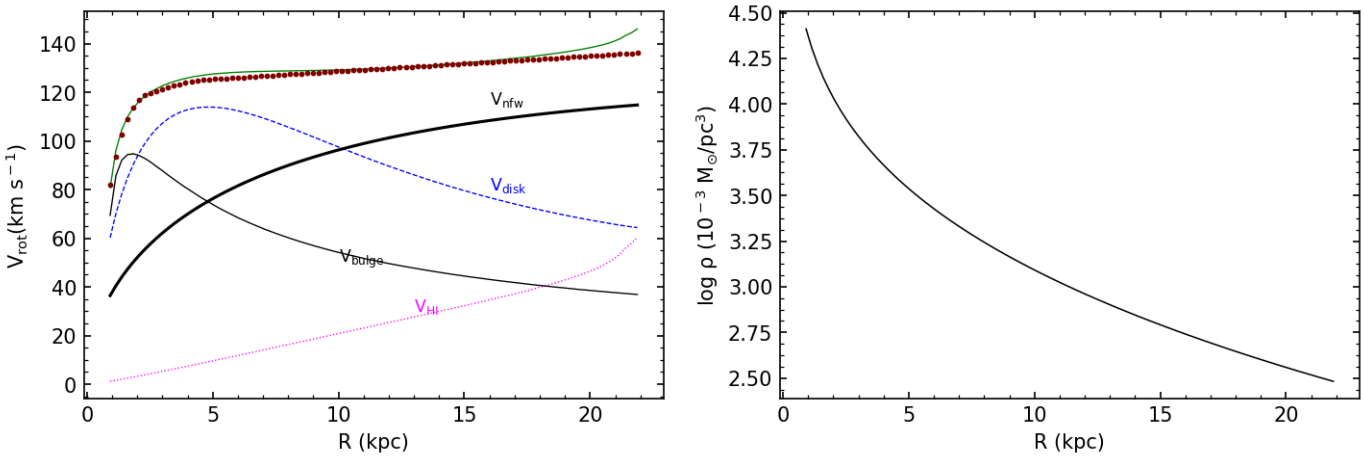

Figure 4.11: The fixed disc scenario based on the NFW halo model shown on the left, with density distribution on the right. The green curve shows the total velocities based on equation 4.1 and the maroon filled points present the observed rotation curve of NGC 1512.

Figure 4.11 presents the fixed disc scenario based on the NFW halo model. The observed rotation curve of NGC 1512 is recovered well by the total velocities. However, at outer radii ($R > 17$ kpc) there is a noticeable deviation. This is announced by the gravitational potential from the contribution of the gas component of the galaxy.

For all the cases (i.e. best fit case, minimum disc case, and the fixed disc case) presented above we determine the ratio of the dark matter mass to the baryonic mass. This ratio compares the amount of dark matter mass to the of the baryons (i.e. stars and gas) in a galaxy. This is done through the equation:

$$\frac{M_{halo}}{M_{baryons}} = \sqrt{\frac{V_{obs}^2 - V_*^2 - \alpha V_{HI}^2}{\alpha V_{HI}^2 + V_*^2}}, \tag{4.10}$$

where V_{obs} and V_{HI} are the last measured points of the observed rotation curve and the gas rotation curve respectively. V_* is calculated as the quadratic sum of the bulge and disc components as:

$$V_*^2 = \gamma_d V_d^2 + \gamma_b V_b^2, \tag{4.11}$$

where γ_d and γ_b are the taken to be the fitted mass-to-light ratios of the stellar disc and bulge,respectively, for each case.

Table 4.1 below quotes all the fitted parameters of the six models above and the calculated dark matter mass to baryonic mass ratios.

UNIVERSITY of the WESTERN CAPE

http://etd.uwc.ac.za/

Table 4.1: Dark matter parameters of NGC 1512

ISO halo model						
Model	$M_{halo}/M_{baryons}$ (1)	γ_{disc} (2)	γ_{bulge} (3)	R_c (4)	ρ_o (5)	χ^2_{red} (6)
Best-fit	1.14	0.23±0.09	0.90±0.04	2.11±0.61	63.50±35.82	2.45
Minimum-disc	—	0.0	0.0	0.48±0.01	1456.43±74.27	3.51
Fixed-disc	0.9	0.5	0.7	3.26	27.14	4.45
NFW halo model						
Model	$M_{halo}/M_{baryons}$ (7)	γ_{disc} (8)	γ_{bulge} (9)	c (10)	r_{200} (11)	χ^2_{red} (12)
Best-fit	1.18	0.15±0.05	0.69±0.02	8.64±0.87	72.44±0.80	1.52
Minimum-disc	—	0.0	0.0	15.67±0.44	72.78±0.60	26.74
Fixed-disc	1.13	0.5	0.7	6.89	156.0	5.69

Column Notes. Columns 1 and 7 present the ratio of the halo mass to baryonic mass. Columns 2, 3, 8 and 9 are the fitted mass-to-light ratios of the disc and bulge respectively for the ISO and NFW halo models. Column 4 is the core-radius in kpc. Column 5 is the core-density in 10^{-3} $M_\odot$ pc^{-3} and Column 6 and 12 present the reduced chi-square value for each model. Column 10 is the concentration parameter and column 11 is the virial radius in kpc.

The dynamical mass of NGC 1512 was calculated from the mass model results. To calculate the dynamical mass of the galaxy within a certain radius we equate the centripetal and gravitational forces as follows:

UNIVERSITY of the WESTERN CAPE

$$\begin{aligned} F_c &= F_g \\ \frac{mV(r)^2}{r} &= \frac{GM(<r)m}{r^2} \\ M(<r)_{dyn} &= \frac{V(r)^2 r}{G}, \end{aligned} \tag{4.12}$$

where V is taken to be the outermost point of the observed rotation velocity (V = 136.11 km s^{-1}). r = 21.88 kpc is the outermost radius point and G is the gravitational constant. For NGC 1512 a dynamical mass of $M_{dyn} = 9.43\times 10^{10}$ $M_\odot$ was calculated.

4.1.5 Mass model results comparisons

The results of the mass model of NGC 1512 were compared to the literature mass model results. For the ISO halo model, the fitted values of the core-radius (R_c) and the core-density (ρ_o) were compared to literature values for all the three cases i.e. minimum disc, fixed disc,

http://etd.uwc.ac.za/

and the best fit. The fitted values of these parameters for all the three cases of the ISO halo model seemed to fall within the range of the values that were found by De Blok et al. (2008a), Korsaga et al. (2019), Oh et al. (2015), Swaters et al. (2009). Figure 4.12 shows these comparisons.

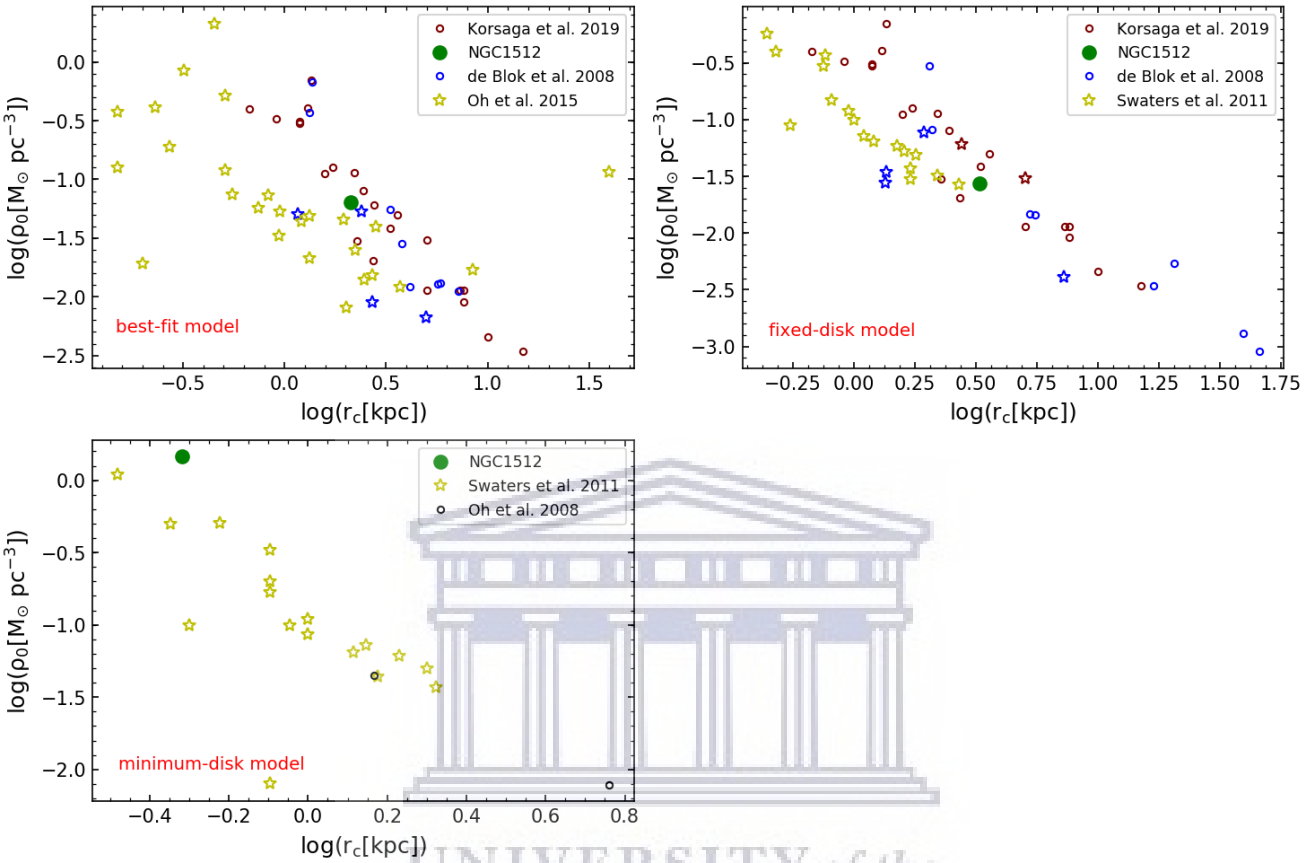

Figure 4.12: The comparison of the best fit values of R_c and ρ_o for all the three cases based on the ISO halo model. Every open star symbol in this Figure presents a dwarf galaxy i.e. the maroon stars are dwarfs galaxies in the sample used in Korsaga et al. (2019).

In the top left-top panel of Figure 4.12, NGC 1512 lies within the trend of the galaxies found in the literature. The sample of galaxies used by Korsaga et al. (2019) contains 29 spiral and 2 irregular galaxies. De Blok et al. (2008a) used 19 THINGS galaxies, comprising of dwarf and spiral galaxies. Oh et al. (2015) used a sample of dwarf galaxies from LITTLE THINGS. NGC 1512 lies close to one of the intermediate compact dwarf galaxies from the sample used in De Blok et al. (2008a). In this panel we note the clear separation of dwarf galaxies from spirals, with the exception of a few galaxies. NGC 1512 lies closely to the spiral galaxies.

The fixed disc model is presented on the top right panel of Figure 4.12. Again, in this panel there is a distinct separation of the dwarf galaxies to the spirals with the exception of about three dwarf galaxies mixing with the spirals. NGC 1512 is an intermediate dense spiral galaxy with an average core-radius. The intermediate density of NGC 1512 results from the gravitational potential from the baryons being dominant only at inner radii. This behavior makes NGC 1512 to have similar dark matter properties to two spiral galaxies from the sample used in Korsaga et al. (2019).

UNIVERSITY of the WESTERN CAPE

http://etd.uwc.ac.za/

The minimum disc case is presented on the bottom panel of Figure 4.12. For this case we note that when there is no contribution from the baryons, NGC 1512 is best described by a dark matter halo that is highly dense and more compact. This again highlights the importance of baryons to the gravitational potential at inner radii. The two galaxies from Oh et al. (2008) are IC 2574 and NGC 2366, both dwarf galaxies. Throughout this chapter, we use the value of $H_o = 75$ km/s/Mpc for the Hubble constant

We also carried the same comparison for the NFW halo model fitted dark matter parameters c and V_{200}. The latter is defined as $V_{200} = R_{200}h$, with $h = H_o/100$. Thus the fitted values of R_{200} presented in table 4.1 were converted to V_{200} using this expression. Also, for the NFW halo model the fitted parameters of NGC 1512 are well within the values found from the literature. For the best fit case, NGC 1512 portrays similar behavior to that of a dwarf galaxy from the sample used in De Blok et al. (2008a). Only one dwarf galaxy from the sample of De Blok et al. (2008a) produced reliable (i.e. physical) dark matter halo parameters using the NFW model.

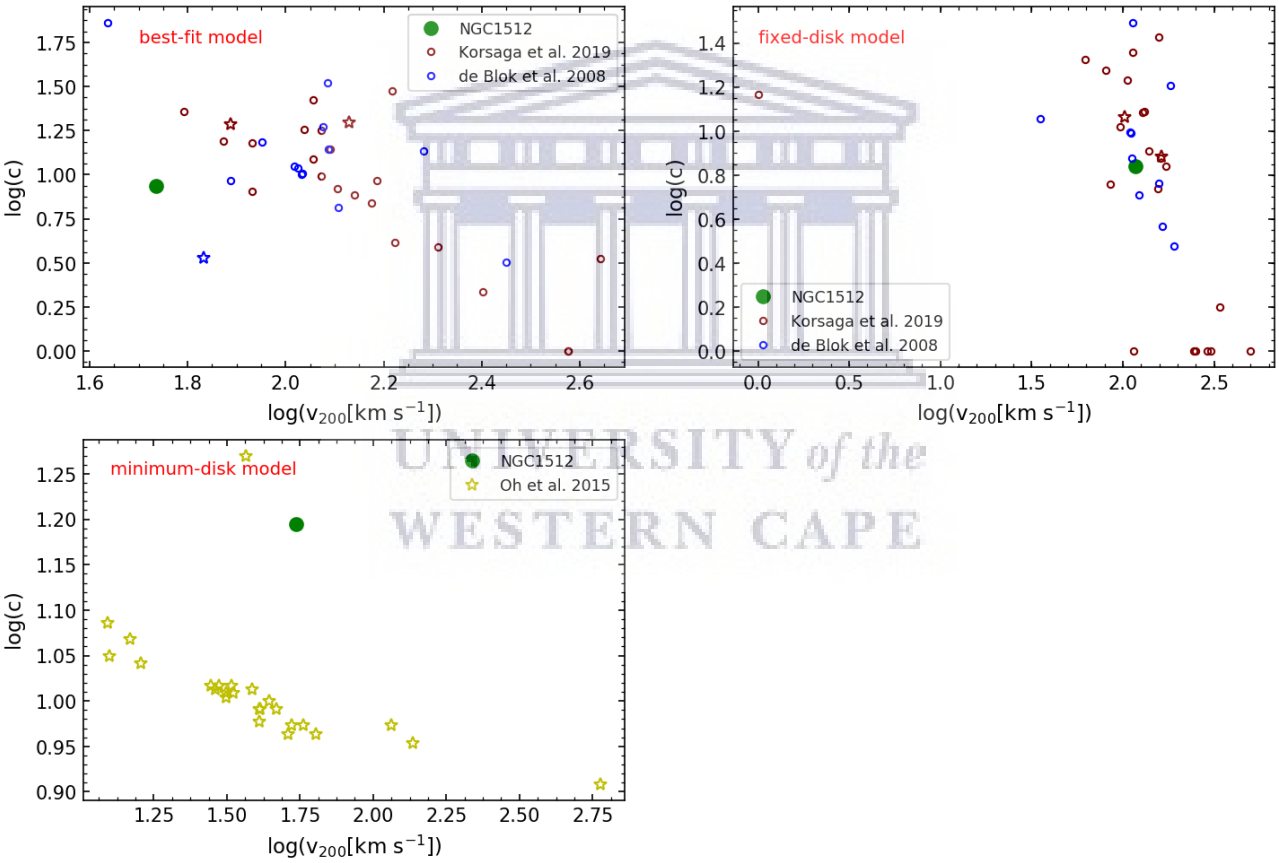

Figure 4.13: The comparison of the best fit values of c and v_{200} for all the three cases based on the NFW halo model. Every open star symbol in this Figure presents a dwarf galaxy i.e. the maroon stars are dwarfs galaxies in the sample used in Korsaga et al. (2019).

The top left panel of Figure 4.13 presents the best fit model based on the NFW halo model. NGC 1512 sits near the only dwarf galaxy from De Blok et al. (2008a), which could be an indication that NGC 1512 behaves like a dwarf galaxy in the velocity-concentration parameter space. This behaviour might result from the dominance of the dark matter halo velocities from r ~ 3 kpc till the last measured point (see Figure 4.9).

UNIVERSITY of the WESTERN CAPE

http://etd.uwc.ac.za/

The fixed disc case is presented on the top right panel of Figure 4.13. NGC 1512 has similar dark matter properties as those of the spiral galaxies from the literature.

Lastly, the minimum disc case is shown on the bottom panel of Figure 4.13. For this case NGC 1512 does not seem to have halo parameters matching any of the dwarf galaxies from Oh et al. (2015). NGC 1512 has a large concentration parameter making it clearly separated from the dwarf galaxies taken from Oh et al. (2015). This again signifies that baryons are of larger importance to the gravitational dynamics of this galaxy.

In this work the mass model of NGC 1512 was measured out to a radius of r = 21.88 kpc. The mass stored within this radius i.e. the dynamical mass was found to be $M_{dyn} = 9.43 \times 10^{10}$. Two well-tested dark matter halo models (the observation based pseudo-isothermal sphere (ISO) and the simulation based Navarro-Frenk and White (NFW) halo models) were used to investigate the distribution of the dark matter in NGC 1512. We further assumed three scenarios for the mass-to-light ratios of the stellar disc and stellar bulge, which are:

- the best fit case scenario - all the parameters of the halo model are left to vary freely, except for the gas scaling factor α_{gas}.
- the fixed disc case - the mass-to-light ratio of the stellar disc (γ_{disc}) and that of the stellar bulge (γ_{bulge}) are fixed to 0.5 and 0.7, respectively.
- and lastly the minimum disc case - where we fixed the gas scaling factor α_{gas}, (γ_{disc}), and (γ_{bulge}) to zero.

The maximum disc case was not modelled because the stellar bulge velocities are at maximum already. The chi-squared value of the best fit case for the NFW halo model is less than that of the ISO halo model. Thus the best fit case of the NGC 1512 is best described by the NFW halo model. From the minimum disc cases based on both halo models we learned that dark matter alone cannot account for the gravitational potential of NGC 1512, thus both halo models suggest that baryons are of significant importance.

UNIVERSITY of the WESTERN CAPE

http://etd.uwc.ac.za/

Chapter 5

5.1 Summary

The main aim of this work was to generate a new dynamical model of the nearby (D = 9.5 Mpc) interacting spiral galaxy NGC 1512/1510, from which the distribution of the dark matter in the halo can be inferred. With the knowledge that neutral hydrogen is one of the best tracers of kinematics in galaxies, this work used H I line observations from ATCA. The high spectral resolution of this dataset allows us to study the H I kinematics of NGC 1512 with great precision. This data is complemented with 3.4 μm WISE photometry to probe the contribution of the stellar component on the total rotation curve. The main steps followed to achieve all the above work are listed below:

- The H I data products of NGC 1512/1510 (i.e. H I surface density map, velocity field, and H I global profile) were generated. To account for the effects of noise from the data, the ATCA H I data cube was parameterized with a third-order Gauss-Hermite polynomial (HER 3) i.e. a third-order Gauss-Hermite polynomial was fitted to each H I line profile in the cube. To fit the third-order Gauss-Hermite polynomial a criterion of selecting three consecutive channels with a maximum flux value $\geqslant 3\sigma$ was implemented. The H I surface density map of NGC 1512/1510 (Figure 2.4) was generated by calculating the area enclosed in each fitted Gauss-Hermite polynomial at a given spatial position. Assuming a distance of 9.5 Mpc for the NGC 1512/1510, an H I mass of $M_{H\,I} = 7.16\times10^9$ $M_\odot$ was calculated from the H I surface density map. The velocity field (Figure 2.6) was produced by taking the fitted mean velocity of the Gauss-Hermite polynomial at a given spatial position. An intensity weighted mean velocity field (or the moment 1 map presented in Figure 2.7) of NGC 1512/1510 was also generated using the traditional technique (see Walter et al. (2008) for a detailed discussion). To generate the H I global profile (Figure 2.2) the sum of all the H I flux above 3σ in the cube was taken. Through equation 2.1 the systemic velocity of $V_{sys} = 898$ km s^{-1} was calculated from the H I global profile of NGC 1512/1510.

- The Gauss-Hermite velocity field (Figure 2.6) of NGC 1512/1520 was compared to the intensity weighted mean velocity field (presented in Figure 2.7). This was done to investigate which of the two maps truly portrays the kinematic information of the interacting system. This comparison was done by subtracting the Gauss-Hermite velocity field from the intensity weighted mean map. The resulting residual velocity map shows regions where the two maps differ, and we noted differences of up to ~ 40 km s^{-1}. The

http://etd.uwc.ac.za/

Gauss-Hermite velocity field was chosen over the intensity weighted mean velocity field. This is because the Gauss-Hermite velocity field is less affected by the adverse effects such as noise due to the parameterization. Thus the Gauss-Hermite velocity field was used to model the rotation curve of NGC 1512.

- To generate the rotation curve of NGC 1512 a tilted-ring model was fitted to the Gauss-Hermite velocity field of NGC 1512. This was done using a 2-dimensional (2D) modeling technique through the GIPSY task ROTCUR. To get the initial estimate of the inclination angle of NGC 1512 we overlaid an ellipse that traces the infrared disk of the galaxy onto the WISE 3.4μm infrared image. From the ellipse, an inclination angle of i $\sim 51^{\circ}$ was found. This inclination angle is different from the one used by Koribalski & López-Sánchez (2009) and Buta (1988) which is i $\sim 35^{\circ}$. In their work Buta (1988) claimed that the inclination angle of NGC 1512/1510 could not be accurately estimated because of the resolution of the optical data they used. We also estimated the position angle from the infrared imaging, and a value of PA $\sim 260^{\circ}$ was found. The GALEX UV center position estimates (α = -43° 21′ 03″, δ = -43° 24′ 01″) of the galaxy were used as initial inputs into the 2D modeling routine. The systemic velocity (V_{sys} = 898 km s^{-1}) was taken from the H I global profile. Despite multiple attempts, we noted that the 2D modeling routine i.e. ROTCUR could not achieve a realistic inclination profile (see fig 3.4) for NGC 1512. Thus a dynamical model of NGC 1512 could not be generated using the 2D modeling routine.

- We therefore used a 3-dimensional modeling routine to generate a dynamical model of NGC 1512 using the ^{3d}Barolo software package. Unlike ROTCUR, which fits fits a 2D tilted-ring model to the velocity field of the galaxy which is just a sub-dataset of the H I data cube, ^{3d}Barolo fits a 3D tilted ring model to the full H I data cube of the galaxy. The same initial estimates that were used for ROTCUR were also used for the 3D modeling routine. With this technique, a dynamical model of NGC 1512 was generated (Figure 3.5). The rotation curve of NGC 1512 based on the 3D modeling routine is flat at all radii (i.e. starting from r = 30″ to 480″). An inclination angle of i $\sim 51^{\circ}$ was determined. The new dynamical model was compared to the ATCA H I data cube and was found to agree well.

- The new model was then used to generate a mass model for NGC 1512. The total velocities in the galaxy are taken to be the quadratic sum of the velocities of gas, stars and dark matter halo (see equation 4.1). The H I surface density map of NGC 1512 was used generate an H I radial surface density profile. This was done by using the GIPSY task ELLINT. Then, the H I radial surface density profile was converted into velocities of the gas component using GIPSY task ROTMOD. The velocities of the stars were derived in a similar manner from the WISE 3.4 μm stellar radial surface density profiles presented in 4.3. To account for the dark matter velocities we used two dark matter halo distribution models: the pseudo-isothermal sphere (ISO) and the Navarro-Frenk and White model. However, a sensible fit of the total velocities (equation 4.1) to the observed rotation curve (Figure 3.5) of NGC 1512 was not obtained. This is because the rotation curve of NGC 1512 based on the 3D modeling technique is flat at all radii.

- Thus, we decided to generate a new rotation curve that has inner points. The new rotation curve was generated from the major-axis position-velocity (PV) slice (3.9). The major-axis PV-slice was partitioned into two sides, the receding and the approaching side. Then, we took the average of the two sides (Figure 3.10). The resulting PV-slice

http://etd.uwc.ac.za/

was binned into regions spanning 6 pixels (i.e. 30″). Then, through equation 2.4 an intensity weighted mean velocity was calculated for each bin (see Figure 3.11). The velocities calculated for each bin were taken to be the new rotation curve of NGC 1512. The new rotation curve was parameterized with a polyex fit. A sensible mass model of NGC 1512 was generated with the new rotation curve. The mass model results were compared with results of mass models of other galaxies from the literature. The fitted halo parameters for NGC 1512 appear to be physical and well within the range of other galaxy parameters.

In conclusion, a new dynamical model of NGC 1512 was generated in this work, which in turn allowed us to quantify the amount of dark matter within this galaxy. This was achieved by generating a dynamical model that agrees well with the data through the 3D modeling routine.

5.2 Conclusions

Having done a thorough kinematic study of NGC 1512, from this work we have learned that the average inclination angle of this galaxy is greater compared to that initially used by Koribalski & López-Sánchez (2009). In this study, this was proven first by estimating the inclination angle of NGC 1512 from its infrared image. Again, running the 3D modeling technique in its automatic mode produced the same average inclination angle. The attempts made to generate a new rotation curve of NGC 1512 have further proven that the distribution of H I in this galaxy is a non-trivial one. This further shows that the ongoing interaction of NGC 1512 with NGC 1510 has had a major impact on the distribution of H I gas. This is strongly supported by the study of asymmetries carried out in this work. Bok et al. (2019) also claimed that galaxy interactions are a possible explanation for asymmetries found in the gas.

Thus the ongoing interaction of NGC 1512 with NGC 1510 holds more information about the distribution of H I in this galaxy system. This makes the NGC 1512/1510 system even more interesting, i.e. studies about gas accretion between the two galaxies could give useful insights into the current H I distribution. These studies could possibly explain the origin of the inter-arm regions seen on the H I surface density map (see Figure 2.4) of NGC 1512. Thus, there is still more that can be done to understand the complex nature of the distribution of the H I in NGC 1512.

Despite the sophisticated nature of NGC 1512, we carried out a mass model of this galaxy based on its rotation curve (see Figure 3.12). Even though we modeled successfully the distribution of the mass in NGC 1512, one needs to pay extra attention to the stellar bulge component of this galaxy as in the inner radius regime it produces large velocities. From the results of the mass model, we have learned that the dark matter halo mass in NGC 1512 is dominant over the baryonic mass. This is measured by the $M_{halo}/M_{baryons}$ parameter (see table 4.1). Furthermore, the results show that the best performing dark matter halo model is the NFW model. This further reveals that the dark matter distribution of NGC 1512 is in favor with the ΛCDM hierarchical simulations (Navarro et al. (1997)).

UNIVERSITY of the WESTERN CAPE

http://etd.uwc.ac.za/

5.3 Future prospects

A list of possible future extensions for this work is presented below:

- For this work, only one galaxy was studied. To better test this methodology, it is essential to move to a larger sample size and apply it to a sample of nearby galaxies and study their different H I properties.
- We could also use galaxy simulations, such as those in SIMBA (Davé et al. (2019)) to test out the models applied in this work. Simulations offer larger samples of galaxies than the current H I surveys e.g. THINGS (Walter et al. (2008)). Thus, this would allow us to test our models on even larger samples. One other key feature of galaxy simulations is that most of the information about galaxies is readily known, hence they provide a good platform to test models.
- Finally, it would be interesting to apply the same methods to MeerKAT (the precursor to the Square Kilometer Array, SKA) data. The upcoming MeerKAT H I surveys such as Looking At the Distant Universe with MeerKAT Array (LADUMA) and MeerKAT H I Observations of Nearby Galactic Objects - Observing Southern Emitters (MHONGOOSE) will provide H I data with high quality resolution. This and MeerKAT radio telescope being sensitive, will enable good modeling of galaxies.

UNIVERSITY of the
WESTERN CAPE

http://etd.uwc.ac.za/

Bibliography

Begeman K. G., 1989, , 223, 47

Bok J., Blyth S. L., Gilbank D. G., Elson E. C., 2019, Monthly Notices of the Royal Astronomical Society, 484, 582

Bosma A., 1981, , 86, 1825

Broeils A. H., 1992, , 256, 19

Buta R., 1988, , 66, 233

Carignan C., Beaulieu S., 1989, , 347, 760

Carignan C., Freeman K. C., 1987, in . p. 684

Cluver M. E., et al., 2014, , 782, 90

Côté S., Carignan C., Freeman K. C., 2000, , 120, 3027

Davé R., Anglés-Alcázar D., Narayanan D., Li Q., Rafieferantsoa M. H., Appleby S., 2019, Monthly Notices of the Royal Astronomical Society, 486, 2827–2849

De Blok W. J. G., Mcgaugh S. S., Van Def Hulst J. M., 1996, 283, 18

De Blok W. J. G., Walter F., Brinks E., Trachternach C., Oh S. H., Kennicutt R. C., 2008a, Astronomical Journal, 136, 2648

De Blok W. J., Walter F., Brinks E., Trachternach C., Oh S. H., Kennicutt R. C., 2008b, Astronomical Journal, 136, 2648

Di Teodoro E. M., Fraternali F., Miller S. H., 2016, Astronomy and Astrophysics, 594

Dubinski J., Carlberg R. G., 1991, , 378, 496

Efstathiou G., Sutherland W. J., Maddox S. J., 1990, , 348, 705

Einasto J., 2009 (arXiv:0901.0632)

Elson E. C., de Blok W. J. G., Kraan-Korteweg R. C., 2010, Monthly Notices of the Royal Astronomical Society

Elson E. C., Blyth S. L., Baker A. J., 2016, Monthly Notices of the Royal Astronomical Society, 460, 4366

Fraternali F., Oosterloo T., Sancisi R., 2004, , 424, 485

UNIVERSITY of the WESTERN CAPE

http://etd.uwc.ac.za/

Freeman K. C., 1970, , 160, 811

Giovanelli R., Haynes M. P., 2002, Astrophys. J., 571, L107

Hack T.-P., 2013 (arXiv:1306.3074)

Hawarden T. G. 1979, Astronomy and Astrophysics, p. 43

Hayashi E., Navarro J. F., Springel V., 2007, Monthly Notices of the Royal Astronomical Society, 377, 50–62

Houjun Mo Frank van den Bosch S. W., 2010, Galaxy Formation and Evolution, 1 edn. Cambridge University Press, http://gen.lib.rus.ec/book/index.php?md5=78e5d4591602a221c4f4b1a158a5ed8c

Koribalski B. S., López-Sánchez R., 2009, Monthly Notices of the Royal Astronomical Society, 400, 1749–1767

Korsaga M., Epinat B., Amram P., Carignan C., Adamczyk P., Sorgho A., 2019, Monthly Notices of the Royal Astronomical Society, 490, 2977–3024

Krajnović D., Cappellari M., de Zeeuw P. T., Copin Y., 2006, , 366, 787

López-Sánchez R., Westmeier T., Esteban C., Koribalski B. S., 2015, Monthly Notices of the Royal Astronomical Society, 450, 3381

Martinsson T., 2011, PhD thesis

McGaugh S. S., Schombert J. M., 2014, , 148, 77

Navarro J. F., Frenk C. S., White S. D. M., 1996, , 462, 563

Navarro J. F., Frenk C. S., White S. D. M., 1997, , 490, 493

Nelder J. A., Meadf R., 1965, A simplex method for function minimization. https://doi.org/10.1093/comjnl/7.4.308

Nielsen J. T., Guffanti A., Sarkar S., 2016, Scientific Reports, 6

Noordermeer E., Van Der Hulst J. M., Sancisi R., Swaters R. S., Van Albada T. S., 2007, Monthly Notices of the Royal Astronomical Society, 376, 1513

Oh S. H., De Blok W. J. G., Walter F., Brinks E., Kennicutt R. C., 2008, Astronomical Journal, 136, 2761

Oh S.-H., et al., 2015, , 149, 180

Planck-Collaboration et al., 2018 (arXiv:1807.06209)

Rezaei Z., 2020, Canadian Journal of Physics, 98, 210–216

Rogstad D. H., Lockhart I. A., Wright M. C. H., 1974, , 193, 309

Rubin V. C., 1983, Scientific American, 248, 1

Rubin V. C., Ford W. K. J., Thonnard N., 1980, 238, 471

UNIVERSITY of the WESTERN CAPE

http://etd.uwc.ac.za/

Schoenmakers R. H. M., Franx M., de Zeeuw P. T., 1997, Monthly Notices of the Royal Astronomical Society, 292, 349

Scott D., 2018 (arXiv:1804.01318)

Sofue Y., Rubin V., 2001, , 39, 137

Sofue Y., Tutui Y., Honma M., Tomita A., Takamiya T., Koda J., Takeda Y.,

Sofue Y., Tutui Y., Honma M., Tomita A., Takamiya T., Koda J., Takeda Y.,

Spekkens K., Sellwood J. A., 2007, , 664, 204

Springel V., et al., 2008, , 391, 1685

Swaters R., 1998 (arXiv:astro-ph/9811010)

Swaters R. A., van Albada T. S., van der Hulst J. M., Sancisi R., 2002, , 390, 829

Swaters R. A., Sancisi R., Albada T. S. V., Hulst J. M. V. D., 2009, 892, 871

Swaters R. A., Sancisi R., van Albada T. S., van der Hulst J. M., 2011, The Astrophysical Journal, 729, 118

Walter F., Brinks E., de Blok W. J. G., Bigiel F., Kennicutt Robert C. J., Thornley M. D., Leroy A., 2008, , 136, 2563

Warner P. J., Wright M. C. H., Baldwin J. E., 1973, , 163, 163

de Vaucouleurs G., de Vaucouleurs A., Corwin Herold G. J., Buta R. J., Paturel G., Fouque P., 1991,

di Teodoro E. M., Fraternali F., 2015, Monthly Notices of the Royal Astronomical Society, 451, 3021

van Der Marel R. O., Franx M., 1993,] 1993ApJ...407..525V, p. 43

UNIVERSITY of the WESTERN CAPE

http://etd.uwc.ac.za/